The role of innate immunity in pancreatic cancer progression and treatment

Lee Sheng Yang

Downing College

Cancer Research UK Cambridge Institute

University of Cambridge

This thesis is submitted for the degree of

Doctor of Philosophy

September 2022

DECLARATION

This thesis is the result of my own work and includes nothing which is the outcome of work done in collaboration except as declared in the Preface and specified in the text. I further state that no substantial part of my thesis has already been submitted, or, is being concurrently submitted for any such degree, diploma or other qualification at the University of Cambridge or any other University or similar institution except as declared in the Preface and specified in the text. It does not exceed the prescribed 60,000 word limit for the Clinical Medicine and Clinical Veterinary Medicine Degree Committee.

ABSTRACT

The role of innate immunity in pancreatic cancer progression and treatment

Lee Sheng Yang

Immune cells are highly abundant in the tumour microenvironment of pancreatic ductal adenocarcinoma (PDAC) and they significantly influence the entire process of PDAC tumourigenesis. While the anti-tumour response is typically mediated by adaptive immunity, cells of the innate immune system can significantly influence this anti-tumour response and in some cases dictate response to treatment. This thesis presents work on two projects – the first project is focussed on characterizing the immunomodulatory effects of gemcitabine in combination with an Ataxia Telangiectasia and Rad3-related (ATR) inhibitor (Gem/ATRi) in pancreatic cancer, whereas the second project describes the pro-tumourigenic role of type 2 innate lymphoid cells (ILC2s) in PDAC.

In chapter 3, Gem/ATRi showed preclinical efficacy in the 'T cell high' 2838c3 tumour model and induced dendritic cell (DC) activation in both the tumour and draining lymph node (LN). This was associated with a substantial depletion of all intratumoural DC subsets in the tumour and a selective depletion of LN-resident DCs in the dLN. Gem/ATRi similarly caused a depletion of intratumoural $CD8^+$ T cells, but of the remaining population there was a decrease in the proportion of exhausted cells along with an increased proportion of proliferating cells. Experiments using the 'T cell low' 6419c5 tumour model revealed that cDC1 in these tumours were dysfunctional and unresponsive to stimulation compared to those in 2838c3 tumours.

In chapter 4, I demonstrated the pro-tumourigenic role of ILC2s in PDAC and investigated mechanisms that potentially underlie this observation. ILC2 deletion significantly extended the survival of 2838c3-bearing mice and altered the intratumoural immune infiltrate. Attempts to pinpoint the mechanism(s) underlying the pro-tumourigenic role of ILC2s (i.e. IL-33, IL-13, eosinophils, NK cells and the ILC2-OX40L-Treg axis) did not yield any positive results, although it is clear that they modulate tumour growth via an effect on adaptive immunity. Further experiments involving $CD8^+$ T cell depletion in ILC2-deficient mice revealed that ILC2s influence tumour growth via both $CD8^+$ T cell-dependent and independent mechanisms. Finally, the impact of ILC2 deletion on PDAC tumour growth was found to be dependent on tumour cell-intrinsic factors, possibly on those that dictate the strength of the baseline anti-tumour $CD8^+$ T cell response.

ACKNOWLEDGEMENTS

I'd like to thank Professor Duncan Jodrell and Dr Frances Richards for giving me the opportunity to do a PhD at the CRUK CI. Thank you for always being patient with me and providing all the guidance and resources I needed to get started on my project. Thank you to all the Jodrell lab members, past and present, who were always supportive and happy to provide advice and answer any questions that I had. Special thanks to Vincenzo and Hannah – we started on this journey together and I'm grateful for your help and companionship throughout these past four years.

I'd also like to thank Dr Tim Halim for providing excellent supervision and support throughout the past two years, not only in terms of research direction but also with technical help (all those hours spent doing mouse surgery!). Massive thank you to all Halim lab members for creating such a fun and collaborative lab environment to work in, it's been a pleasure to be part of this team and I deeply cherish the camaraderie we shared in this period of time. I'm especially grateful to Shaun. who has been a treasured friend from when we first started our PhDs. From sharing lunch breaks to sharing an office in our final months of PhD, thank you for your companionship and for being someone who I can share joys and hardships with.

I have been very lucky to work in an institute with state-of-the-art facilities and resources, and have benefitted greatly from the expertise of the numerous core facilities present in CRUK CI. Thank you also to Cancer Research UK and the Cambridge Commonwealth, European and International Trust for making this research possible.

Outside of the lab, I'm grateful to all the friends I've met during my time in Cambridge. Thank you to the Cambridge University Ballet Club, especially to Ellie for your wonderful ballet classes - these weekly classes have given me much-needed respite during the busiest times of my PhD. Finally, I'm grateful to my family for being there for me all this time. To my parents, whose love and support have carried me to where I am today.

TABLE OF CONTENTS

ABBREVIATIONS

5-FU	Fluorouracil
aCD40	Agonistic anti-CD40 antibody
AOM/DSS	Azoxymethane/dextran sodium sulfate
APC	Antigen-presenting cell
apCAF	Antigen-presenting cancer-associated fibroblasts
ATM	Ataxia Telangiectasia Mutated
ATR	Ataxia Telangiectasia and Rad3-related
bDC	$CD103^+$ $CD11b^+$ 'barilla' DC
cDC1	$CD103^+$ $CD11b^-$ type 1 conventional DC
cDC2	$CD103^-$ $CD11b^+$ type 2 conventional DC
CDNs	Cyclic dinucleotides
CDP	Common dendritic cell progenitor
cGAMP	Cyclic GMP-AMP
cGAS	Cyclic GMP-AMP synthase
CILP	Common innate lymphoid progenitor
cKO	Conditional knock-out
CMP	Common myeloid progenitor
CRC	Colorectal cancer
CSF1R	Colony-stimulating factor-1 receptor
DAMPs	Damage-associated molecular patterns
DC	Dendritic cell
DMXAA	5,6-dimethylxanthenone-4-acetic acid
DQ-OVA	DQ Ovalbumin
DSB	Double-strand break
DT	Diphtheria toxin
ECM	Extracellular matrix
EMT	Epithelial-to-mesenchymal transition
FACS	Fluorescence-activated cell sorting
Flt3L	Fms-related tyrosine kinase 3 ligand
FOLFIRINOX	Folinic acid, fluorouracil, irinotecan and oxaliplatin
G-CSF	Granulocyte-colony stimulating factor
GA, Gem/ATRi	Combination of gemcitabine and ATR inhibition
GEMM	Genetically modified mouse model
GM-CSF	Granulocyte-macrophage colony-stimulating factor
H&E	Haematoxylin & eosin
HSC	Haematopoietic stem cell
iCAF	Inflammatory cancer-associated fibroblasts
ICD	Immunogenic cell death
ICPI	Immune checkpoint inhibitor
iDC	Inflammatory DC
IFN	Interferon
ILC	Innate lymphoid cell

IP	Intra-peritoneal
IRF	Interferon regulatory factor
KPC	*Kras*$^{LSL-G12D/+}$*Trp53*$^{LSL-R172H/+}$*Pdx1*$^{Cre/+}$ transgenic PDAC mouse model
LN	Lymph node
LTi	Lymphoid tissue-inducer cells
MDSC	Myeloid-derived suppressor cells
MHC	Major histocompatibility complex
MMR	Mismatch repair
MoDC	Monocyte-derived DC
myCAF	Myofibroblastic cancer-associated fibroblasts
NET	Neutrophil extracellular trap
NF-κB	Nuclear factor-kappa B
OG	Oral gavage
PanINs	Pancreatic intraepithelial neoplasia
PBMCs	Peripheral blood mononuclear cells
PDAC	Pancreatic ductal adenocarcinoma
pDC	Plasmacytoid DC
PGE_2	Prostaglandin E2
pIC	Polyinosinic–polycytidylic acid sodium salt
pLN	Pancreatic lymph node
RIG-I	Retinoic acid-inducible gene-I
RLR	Retinoic acid-inducible gene-I-like receptors
RT	Room temperature
SqCC	Squamous cell carcinoma
STING	Stimulator of interferon genes
T1IFN	Type 1 interferon
TAM	Tumour-associated macrophages
TBK1	TANK-binding kinase 1
TGF-β	Transforming growth factor-β
Th cells	$CD4^+$ T helper cells
TLR	Toll-like receptor
TMB	Tumour mutational burden
TME	Tumour microenvironment
TNF-α	Tumour necrosis factor-α
Tr-1 cells	T regulatory type 1 cells
Treg	Regulatory T cells
VEGF	Vascular endothelial growth factor
WAT	White adipose tissue
WT	Wild-type
αSMA	Alpha smooth muscle actin

CHAPTER ONE: Introduction to Pancreatic Ductal Adenocarcinoma (PDAC)

1.1. PDAC biology

Among the many subtypes of pancreatic cancer, pancreatic ductal adenocarcinoma (PDAC) is the most common and makes up for greater than 90% of all cases[1]. Although PDAC has a relatively low incidence compared to other cancers, it is one of the most aggressive solid malignancies, being the fourth leading cause of cancer-related deaths in the US[2] and projected to rise to the second leading cause in 2030[3]. Common risk factors for pancreatic cancer include smoking, obesity and excessive alcohol consumption, and approximately 10% of PDAC cases are hereditary. For example, individuals with germline mutations in genes such as *BRCA2, CDKN2A* and *STK11* are known to be much more susceptible to developing PDAC during their lifetime[4].

In contrast to the steady increase in survival rates for most cancers, PDAC patients currently have an estimated 5-year survival rate of only 10% and this has barely improved in the past 40 years[5]. There are many reasons for such poor prognosis, including the aggressive nature of PDAC, patients frequently being diagnosed at late stages and cancer drug resistance. One of the major factors contributing to the late diagnosis of PDAC is the vague (and in some cases, the absence of) symptoms associated with the disease such as weight loss, abdominal pain and diabetes mellitus[6]. As a result, a vast majority of patients present with locally advanced or metastatic disease and are ineligible for surgery. Surgical resection is potentially curative, but for the 10-20% of patients who have operable disease, approximately 80% will eventually relapse and succumb to metastatic disease[7]. For patients with locally advanced or metastatic disease, the current standard of care is systemic chemotherapy. Gemcitabine monotherapy was the standard of care for patients with metastatic PDAC from 1997[8], until the introduction of FOLFIRINOX (a combination of folinic acid, fluorouracil (5-FU), irinotecan and oxaliplatin)[9] and gemcitabine in combination with nab-paclitaxel[10]. Although these combination therapies offer improved survival benefit compared to gemcitabine alone in patients with advanced disease, patient median overall survival remains relatively low (6.8 months for gemcitabine monotherapy versus 8.7 for gemcitabine-nab-paclitaxel and 11.1 for FOLFIRINOX). Additionally, these combination regimens are associated with substantial toxicity and are

reserved only for patients with better performance status. There is therefore a clear need for more efficacious therapies.

Thus far two models of PDAC evolution have been proposed - in 2000, Hruban and colleagues proposed the stepwise progression model of PDAC[11]. In this landmark publication, the authors posit that pancreatic intraepithelial neoplasia (PanINs) of increasing grade (showing higher levels of dysplasia) were associated with greater accumulation of genetic alterations. For example, activating mutations in *KRAS* can be found in PanINs of all stages, whereas inactivating mutations of tumour suppressor genes such as *TP53* and *CDKN2A* are typically only found in more advanced PanINs, suggesting that these mutations appear later in the evolution of pancreatic lesions. It was then widely accepted that PDAC develops progressively via stepwise, independent accumulation of genetic alterations, and progression from the earliest mutation to metastatic disease has been estimated to require almost two decades[12]. In 2016, Notta and colleagues challenged this hypothesis using whole genome sequencing data from 107 human PDAC samples[13]. Analysis of DNA copy number and chromosomal rearrangements showed that 65% of these tumours harboured at least one chromothripsis event, and these large-scale chromosomal rearrangement events can result in the inactivation of multiple tumour suppressor genes at a time. These findings challenge the stepwise progression model as the simultaneous acquisition of multiple key genetic alterations in a single event could thus result in a sudden acceleration of tumour progression. Regardless of the evolution kinetics, it is clear that PDAC initiation and progression is strongly driven by genetic alterations. As mentioned previously, *KRAS* mutations occur at the earliest stages of PDAC tumourigenesis. Greater than 90% of PDAC cases harbour an activating *KRAS* mutation[14], the majority of these being *KRAS* G12D point mutations[15]. The G12D mutation impairs the hydrolysis of KRAS-bound GTP, thus extending the duration of KRAS signalling and leads to aberrant stimulation of the RAF-MEK-ERK axis (along with other associated pathways) that promote cell proliferation and survival[16]. Both the high mutation frequency and early activation of KRAS suggest that oncogenic RAS signalling is the principal driver of PDAC. *TP53* inactivating mutations are present in approximately 70% of cases[14], and these often occur at the DNA binding domain which abrogate its ability to bind to DNA as a transcription factor. This not only leads to loss of its function as a tumour suppressor (e.g. regulation of cell cycle arrest, apoptosis, senescence etc.) but also confer various novel

functions which may be pro-tumourigenic. This gain-of-function is mediated by protein-protein interactions of the mutant p53 protein with a vast range of other proteins, and the pro-tumourigenic effects of these interactions span from tumour cell chemoresistance to immune evasion[17–19]. Although the tumour suppressor gene *CDKN2A* is only mutated in approximately 30% of cases[20], p16 signalling is abrogated in greater than 90% of PDAC given that it is often transcriptionally silenced via hypermethylation of its promoter[21]. As p16 is an inhibitor of cyclin-dependent kinase (CDK) 4/6, p16 loss results in dysregulation at the G1/S cell cycle border. *SMAD4* is mutated in approximately half of all PDAC cases, and it is a transcription factor that mediates TGF-β-induced cell cycle arrest and apoptosis[22]. In addition to these four main driver genes, there are many other genes mutated at lower prevalence that can be clustered into 12 canonical cell signalling pathways, each of which is altered in 67% to 100% of PDAC cases[23]. In the past decade, multiple independent reports have attempted to classify PDAC into different molecular subtypes based on their genomic, transcriptomic and proteomic profiles – these studies have shed light on the heterogeneity of genomic alterations observed in PDAC and identified distinct profiles that have predictive value in terms of clinical outcome and therapy response[24–26].

1.2. The PDAC tumour microenvironment

The PDAC tumour microenvironment (TME) is a highly complex ecosystem comprised of many different cell types (e.g. cancer cells, stromal cells, immune cells etc.) all embedded within a dense extracellular matrix (ECM). From the earliest stages of tumourigenesis, PDAC cancer cells are capable of subverting their local niche to exert significant structural, cellular and molecular changes that promote their survival and proliferation. Throughout the entire process of PDAC initiation, growth and metastasis, cancer cells have a dynamic and reciprocal relationship with their surrounding stromal and immune counterparts; understanding these complex interactions have been the focus of much research in the past two decades and is key to finding novel therapies that disrupt these pro-tumourigenic signalling networks.

Perhaps the most distinctive feature of human PDAC is the abundance of stroma and the extensive desmoplasia due to ECM deposition by cancer-associated fibroblasts (CAFs), particularly of type I, III and IV collagens[27]. Given that CAFs are the most abundant cell type in the PDAC TME, there has been a lot of interest in characterizing CAF heterogeneity and

potentially targeting CAFs for therapeutic benefit[28,29]. Three CAF subtypes have been described in PDAC via single-cell RNA sequencing, namely inflammatory CAFs (iCAFs), myofibroblastic CAFs (myCAFs) and antigen-presenting CAFs (apCAFs)[30]. As its name suggests, iCAFs secrete a wide range of cytokines and chemokines such as interleukin (IL)-1, IL-6, and CXCL12 that influence immune cell infiltration and function within the TME. Many of these iCAF-derived cytokines and chemokines have been shown to promote immunosuppression in PDAC. For example, CAF-derived CXCL12 has been shown to form a coating on cancer cells, and ligation to its receptor (CXCR4) on T cells mediates T cell exclusion from cancer cell nests[31,32]. Consequently, CXCR4 inhibition in preclinical models promotes intratumoural T cell infiltration and renders PDAC susceptible to anti-PD-L1 checkpoint blockade[31], with potentially the same effect in human PDAC[33]. On the other hand, myCAFs are mainly associated with ECM deposition and have garnered substantial attention due to their capacity to suppress PDAC growth[34,35]. Although the mechanism(s) underlying the anti-tumourigenic function of myCAFs is currently unknown, depletion of αSMA$^+$ myCAFs in a preclinical model of PDAC led to invasive and undifferentiated tumours that decreased survival. A similar mechanism might be true in humans as low αSMA staining in PDAC of untreated patients correlates with decreased overall survival[35]. It is currently difficult to formulate therapeutic strategies that exploit the anti-tumour function of myCAFs as there is a lack of understanding of the underlying mechanism, although it might be possible to increase the myCAF to iCAF ratio to achieve therapeutic benefit given the plasticity between these two populations[36]. Unlike iCAFs and myCAFs, apCAFs have a mesothelial origin and express high levels of MHC-II which allow them to directly engage and activate naïve CD4$^+$ T cells. However, they do not express any co-stimulatory molecules (e.g. CD80 and CD86) that are necessary to induce full T cell activation – this causes them to drive the differentiation of naïve CD4$^+$ T cells into regulatory T cells (Tregs) to potentially have a negative impact on anti-tumour immunity[30,37]. Historically, stroma-targeting strategies in PDAC have been fraught with difficulties – examples that have failed late stage clinical trials include the use of pegylated recombinant human hyaluronidase 20 (PEGPH20) to enhance intratumoural chemotherapy perfusion[38,39], blocking vascular endothelial growth factor (VEGF)-mediated tumour angiogenesis[40,41] and CAF depletion via Hedgehog inhibitors[42,43]. Although no stroma-targeting agents have shown therapeutic benefit in the clinic thus far, major advancements in the understanding of PDAC stroma have been made in the past few years; this will hopefully allow us to think about

stroma targeting in a more nuanced way (e.g. selective targeting of CAF subpopulations, patient selection based on stroma profile etc.) to pave the way for the next generation of stroma-targeting therapeutics[44].

Next to CAFs, immune cells make up the second largest population in the PDAC TME. PDAC is historically considered to be immunologically 'cold', and many factors have been shown to contribute to this immunosuppressive TME - these include the recruitment of regulatory immune cells (such as myeloid-derived suppressor cells (MDSCs) and tumour-associated macrophages (TAMs)), the production of immunoregulatory cytokines, chemokines and metabolites within the TME, and the desmoplastic stroma[45]. TAMs constitute the most abundant immune cell type in the PDAC TME[46]. TAMs in PDAC are programmed to suppress anti-tumour immunity, and TAM density correlates with decreased overall survival in PDAC patients[47]. TAMs in PDAC are derived from a mixed population of pancreas-resident macrophages (which originate from embryonic progenitors) and circulating monocytes (derived from haematopoietic stem cells). These two TAM populations have distinct transcriptional profiles and they influence the TME in different ways. Specifically, embryonically-derived macrophages were shown to express higher levels of proteins involved in ECM deposition and remodelling whereas monocyte-derived TAMs were more associated with regulating TME immunosuppression[48,49]. TAMs also have different polarization and activation states[50] – although the bulk TAM population is generally immunosuppressive, they can be 're-polarized' to acquire anti-tumour function by therapeutic agents (such as agonistic anti-CD40 (aCD40) antibody)[51]. Thus far, several approaches have been developed to deplete and/or re-polarize intratumoural TAMs in PDAC, the most prominent of which is via colony-stimulating factor-1 receptor (CSF1R) inhibition. The combination of CSF1R and checkpoint blockade showed impressive activity in multiple preclinical models of PDAC[52,53], but unfortunately these results have not translated well into the clinic[54,55].

The immunosuppressive role of MDSCs in PDAC has long been known but it was not until a decade ago that two articles simultaneously showed the mechanism of MDSC recruitment in PDAC[56,57]. In these two papers, the authors showed that oncogenic activation of Kras (*Kras*^{G12D}) in pancreatic ductal epithelial cells drives granulocyte-macrophage colony-stimulating factor (GM-CSF) production in PanINs. GM-CSF-mediated recruitment of MDSCs into early

pancreatic lesions then leads to suppression of $CD8^+$ T cell-mediated anti-tumour immunity[56,57]. Four years later, CXCR2-mediated recruitment of neutrophils and MDSCs was similarly shown to antagonize $CD8^+$ T cell-mediated immunity in PDAC[58,59]. In these studies, CXCR2 blockade (via genetic ablation or pharmacological inhibition) abolished metastasis, slowed primary tumour growth and increased T cell infiltration in preclinical models of PDAC. Given the importance of MDSC-dependent immunosuppression in the PDAC TME, multiple novel therapeutic strategies have since been developed to disrupt MDSC recruitment into the tumour. For example, CXCR2 inhibitors have shown great efficacy in preclinical models and a small molecule inhibitor (SX-682) is currently undergoing clinical trials in combination with PD-1 blockade[60]. CD11b agonism has emerged as another potential mechanism of reducing intratumoural myeloid cell recruitment (in addition to promoting M1 macrophage polarization and cDC1 recruitment)[61], and it is currently undergoing clinical trials in combination with PD-1 blockade[62].

Dendritic cells (DCs) are professional antigen-presenting cells (APCs) which play a key role in the initiation of antigen-specific adaptive immunity. They directly engage with naïve T cells via major histocompatibility complex (MHC) molecules and provide activation signals through co-stimulation (i.e. CD80 and CD86) and pro-inflammatory cytokine production (e.g. IL-12). Their proper functioning is important in the initiation and maintenance of $CD8^+$ T cell-driven anti-tumour immunity, and intratumoural $CD103^+$ $CD11b^-$ type 1 conventional DC (cDC1) infiltration in human PDAC correlates with extended survival[63]. However, there is accumulating evidence in preclinical mouse models and patients to suggest that DC function is systemically impaired in PDAC-bearing hosts[64]. In 2010, Tjomsland and colleagues showed a lower frequency of circulating DCs in PDAC patients compared to healthy volunteers, and these DCs had a dysfunctional semi-mature phenotype due to exposure to elevated PGE_2 plasma levels[65]. cDC1s require the transcription factor IRF8 during development, but tumour-derived granulocyte-colony stimulating factor (G-CSF) can act to suppress IRF8 expression in DC progenitors within the bone marrow, leading to impaired cDC1 development and a decrease in systemic cDC1 numbers[66]. Increased serum levels of IL-6 have also been associated with systemic cDC1 apoptosis and suppression in mouse models of PDAC[67]. Intratumoural DCs consist of a heterogeneous population that exert opposing effects on anti-tumour immunity, but the DC population as a whole is pro-tumourigenic as systemic DC

depletion slows pancreatic tumour growth[68]. This is likely due to the large proportion (~80%) of pro-tumourigenic CD103$^-$ CD11b$^+$ cDC2s within the tumour that promote the differentiation of immunosuppressive IL-10$^+$ IL-17$^+$ Tr-1 cells[68]. There are many mechanisms through which intratumoural DCs may acquire an immunosuppressive phenotype, for example through exposure to various metabolites and cytokines or direct cell-cell interaction with Tregs[69,70]. CD11b$^+$ DCs have been shown to not only suppress anti-tumour immunity at the primary PDAC tumour, but also accumulate at metastatic sites to establish an immunosuppressive microenvironment that is conducive to metastatic seeding[71]. Given the importance of cDC1s in CD8$^+$ T cell-mediated anti-tumour immunity, therapeutic strategies have been developed to expand and activate cDC1 in PDAC. Fms-related tyrosine kinase 3 ligand (Flt3L) is a growth factor that plays a key role in cDC development, and repeated injections of Flt3L increases cDC1 infiltration in both PanINs and established PDAC tumours[67,72]. When co-administered with another agent that can induce DC activation (e.g. agonistic aCD40 antibody, STING agonists or radiotherapy), greater cDC1 infiltration can be achieved along with increased CD8$^+$ T cell infiltration and tumour regression[67,72]. More recently, PD-1 blockade was shown to activate type 2 innate lymphoid cells (ILC2s) in a mouse model of PDAC, leading to increased production of CCL5 which recruits intratumoural cDC1[73]. CD40 engagement on DCs leads to activation of the nuclear factor-kappa B (NF-κB) pathway, which is an important step in the maturation process of cDC1s and essential for their anti-tumour function[74,75]. The use of agonistic aCD40 antibody in PDAC has been studied extensively by the Vonderheide lab over the past decade and phase I clinical trials have shown remarkable safety and efficacy in combination with chemotherapy and PD-1 blockade[51,76–82]. However, a recently completed phase 2 trial did not show any benefit of adding aCD40 to chemotherapy and PD-1 blockade, suggesting that more work needs to be done to better understand the mechanism of action of aCD40[83]. An introduction to other DC subsets and the potential use of chemotherapy to activate DCs will be further discussed in chapter 3.

In addition to myeloid-dependent immunosuppression, lymphoid immune cells have also been shown to antagonize CD8$^+$ T cell-dependent anti-tumour immunity in PDAC. Specifically, Foxp3-expressing Tregs play an essential role in maintaining self-tolerance in homeostasis, but their immunosuppressive capabilities are co-opted during tumourigenesis to suppress anti-tumour immunity[84]. High intratumoural Treg density is associated with a poor prognosis

in most solid tumours, and PDAC is no exception - a meta-analysis encompassing sixteen studies with 1791 PDAC patients revealed that high levels of $Foxp3^+$ Treg infiltration correlates with decreased overall survival[85]. Historically, Tregs were considered to be a homogenous, pro-tumourigenic population and many mechanisms of Treg-mediated suppression of anti-tumour immune responses have been proposed. However, the role of Tregs in PDAC is not straightforward as research using preclinical models of PDAC have shown contrasting roles for Tregs. In 2017, the Bar-Sagi lab showed that intratumoural Tregs engage with dendritic cells to impart a tolerogenic phenotype, leading to decreased co-stimulatory molecule expression and impaired $CD8^+$ T cell activation[70]. Consequently, Treg depletion in an orthotopic PDAC model decreased tumour burden, a phenotype that was dependent on IFNγ-producing $CD8^+$ T cells. This was not the first demonstration of the pro-tumourigenic role of Tregs in PDAC, as a previous study has shown that inhibiting intratumoural Treg recruitment via CCR5 inhibition decreased tumour growth in a subcutaneous syngeneic PDAC model[86]. In 2020, an article published by the Pasca di Magliano lab challenged these findings, showing that Treg depletion in early disease using an autochthonous model of PDAC accelerated neoplastic progression[87]. This effect was attributed to the disruption of cross-talk between Tregs and CAFs – Tregs are a key source of TGF-β ligands in the TME, and their depletion led to reprogramming of the CAF population with loss of tumour-restraining αSMA^+ myCAFs and an increase in CCR1 ligand-producing iCAFs. This discrepancy observed in Treg function may be due to multiple factors - for example, results obtained with different PDAC mouse models (autochthonous, orthotopically-implanted or subcutaneously-implanted tumours) cannot be directly compared as the TME (and consequently, the role of Tregs in said TME) varies significantly between models. It is also clear that the timing of Treg depletion is key – in KPC mice, Treg depletion accelerated PanIN progression in early disease but it had no effect in established tumours[87]. Lastly, systemic Treg depletion using $Foxp3^{DTR}$ mice is known to cause widespread inflammation, and the length of Treg depletion was different between different studies, ranging from 7-21 days[70,87]. These findings were likely confounded by a combination of these factors, and more studies are needed to clarify the role of Tregs in human PDAC, especially in advanced disease when therapeutic intervention is often initiated.

$CD4^+$ T helper (Th) cells are also present in the PDAC TME, and it is known that Th17 cells and its associated cytokine IL-17A has a pro-tumourigenic role in PDAC. Oncogenic activation of

Kras (*Kras*^{G12D}) in pancreatic ductal epithelial cells promotes the recruitment of IL-17A-producing Th17 and γδT cells into PanIN lesions[88]. Kras activation in epithelial cells also induces the expression of IL-17 receptor A (IL-17RA) in these cells (which is otherwise minimally expressed under normal conditions), allowing these transformed cells to respond to IL-17A. IL-17A signalling in pancreatic cancer cells upregulates NF-κB and MAPK signalling and modulates cancer cell stemness by upregulating expression of the stem cell markers DCLK1 and ALDH1A1[89]. IL-17A also recruits neutrophils into the TME and promotes neutrophil extracellular trap (NET) formation which negatively impacts $CD8^+$ T cell function[90]. Intratumoural $CD11b^+$ $CD103^-$ cDC2 have also been shown to contribute to this axis by producing high levels of IL-23 and TGF-β, both of which are known to contribute to the differentiation and maintenance of Th17 cells[68]. In addition to its effects on cancer and immune cells, IL-17A is also known to have an impact on the transcriptional profile of CAFs. In the absence of IL-17A, CAFs expressed higher levels of T cell-recruiting chemokines and Th1-skewing cytokines, and this was associated with increased intratumoural $CD8^+$ T cell infiltration[91]. Genes associated with ECM remodelling were also differentially expressed in the absence of IL-17A, whereby collagen deposition in the IL-17A-deficient setting is more orientated to form soft nests around tumour cells (rather than compact, stiff capsules) – this difference in intratumoural ECM scaffolding potentially has an impact on tumour cell motility and immune cell infiltration[92]. Given the pro-tumourigenic roles of IL-17A, overexpression of IL-17A in the pancreas dramatically accelerates PanIN initiation and progression in mouse models of PDAC, whereas pharmacological inhibition of IL-17A signalling reduces PanIN burden, pancreatic fibrosis and CAF accumulation[72,88]. IL-17A neutralization also decreases ERK, STAT3 and EGFR signalling in transformed epithelial cells due to loss of IL-17RA activation in these cells[72,89]. IL-17A neutralization also promotes $CD8^+$ T cell-mediated anti-tumour immunity, leading to an increase in the number of activated $CD8^+$ T cells which are localized in closer proximity to tumour cells – consequently, tumours depleted of IL-17A were rendered susceptible to checkpoint blockade[90]. Given the established pro-tumourigenic effects of IL-17A in PDAC, it is intriguing that anti-IL-17 agents have not been evaluated in PDAC clinical trials, especially considering the pre-existing approved use of anti-IL-17 biologics for autoimmune diseases.

Innate lymphoid cells (ILCs) are a relatively novel group of immune cells, and they can be broadly classified into three subsets (ILC1, ILC2 and ILC3) that mirror the T helper cell response in terms of transcription factor expression and cytokine production[93]. While first characterized for their roles in infection and autoimmunity in barrier tissues, they are now known to be present in PDAC tumours and have important roles in modulating the anti-tumour response[73,94,95]. An introduction to ILCs and their roles in cancer will be further discussed in chapter 4.

1.3. $CD8^+$ T cell-mediated anti-tumour immunity in PDAC

PDAC tumours are generally thought of as immunologically 'cold' and devoid of $CD8^+$ T cells, but transcriptomic and histopathologic analyses of primary human PDAC samples have shown substantial interpatient heterogeneity in intratumoural $CD8^+$ T cell infiltration (**Figure 1.1**)[26,96,97]. Although bulk intratumoural immune signatures do not have any prognostic value[26,97], increased density of T cells (especially $CD8^+$ T cells) significantly correlates with extended survival in PDAC patients[85,96,98,99]. There is also significant inter-and intra-patient heterogeneity in the spatial distribution of intratumoural $CD8^+$ T cells – however, $CD8^+$ T cells generally do not co-localize with tumour cells but rather are present at a much higher density in the tumour margin[96]. Given the positive prognostic value of $CD8^+$ T cells, many currently emerging therapies are developed with the aim to increase intratumoural $CD8^+$ T cell infiltration and activation, especially given the potential synergy with immune checkpoint inhibitors (ICPI) which have shown impressive efficacy in other cancers.

ICPI has revolutionised cancer treatment since its introduction in 2011 for patients with metastatic melanoma[100]. These antibodies bind to regulatory proteins (such as CTLA-4 and PD-1) to inhibit the activation of immune checkpoints and block physiological suppression associated with these negative feedback pathways. ICPI monotherapy has shown efficacy in some cancer types but has failed to provide clinical benefit in PDAC[101], with the exception of mismatch-repair (MMR)-deficient tumours that account for less than 2% of all PDAC tumours[102]. As clinical response to ICPI has been correlated with the abundance of pre-existing intratumoural $CD8^+$ T cells in melanoma, lung and bladder cancer, it has been hypothesized that the lack of response to ICPI in PDAC is due to the paucity of intratumoural $CD8^+$ T cells in these tumours[103–105].

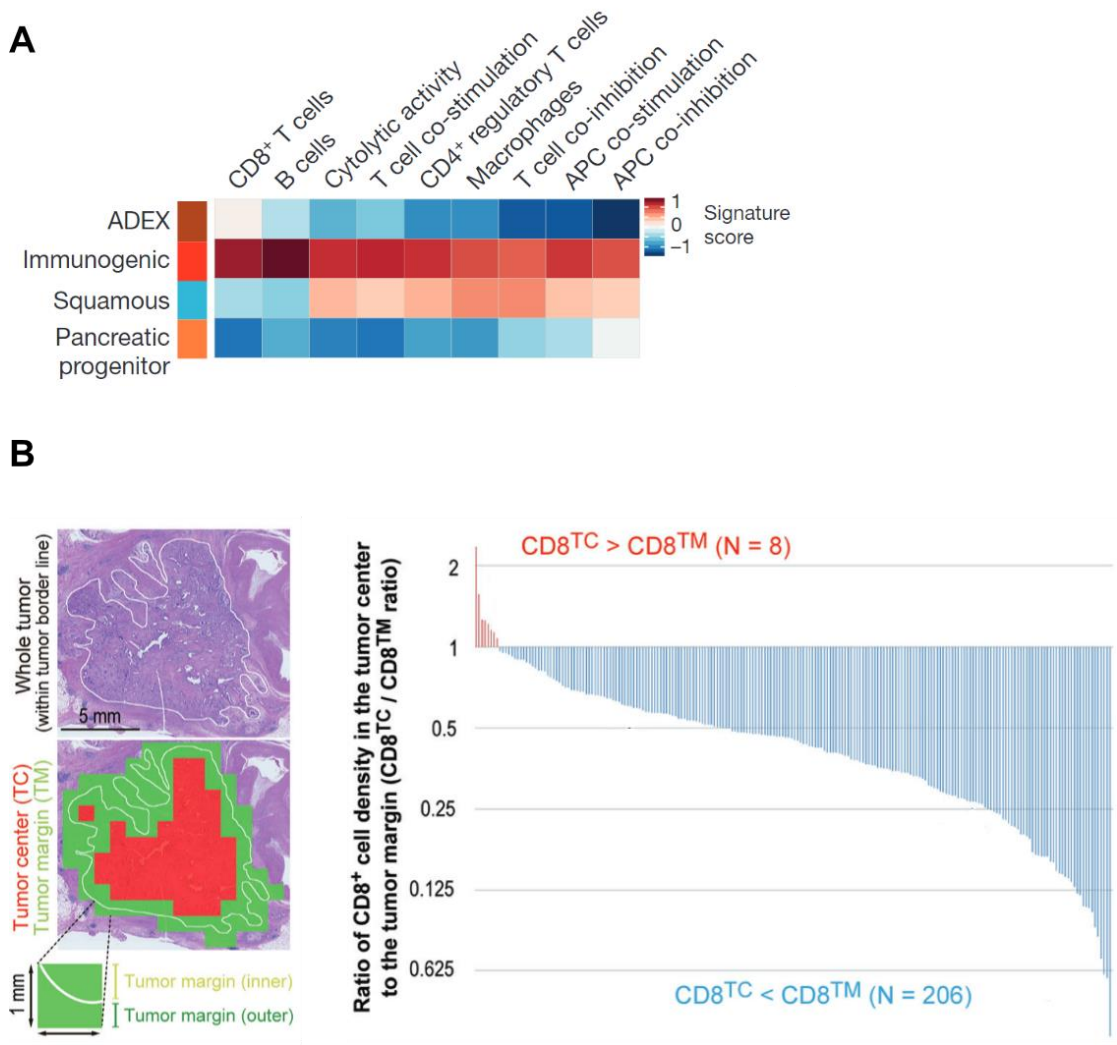

Figure 1.1. Heterogeneity of CD8⁺ T cell-dependent anti-tumour immunity in human PDAC. (A) RNA-seq of bulk PDAC tumours in Bailey et al (2016) revealed four distinct transcriptomic subtypes, including an immunogenic subtype that is highly enriched in CD8⁺ T cell gene signatures. (B, left) Tumour-infiltrating CD8⁺ T cells can be localized to the tumour centre or tumour margin. (B, right) Ratio of CD8⁺ T cell density in the tumour centre to that in the tumour margin in 214 PDAC samples, with a trend towards lower CD8⁺ T cell density within the tumour core. Figure A from Bailey et al (2016)[26]; figure B from Masugi et al (2019)[96].

Another factor that may contribute to ICPI responsiveness is the tumour mutational burden (TMB) – the TMB is a measure of genetic mutations per megabase (Mb) harboured by tumour cells, and higher TMB levels strongly correlate with response to ICPI across many different cancer types[106–108]. Genetic mutations are the source of tumour-specific neoantigens, and the presence of immunogenic neoantigens is a critical determinant of baseline anti-tumour immunity and response to ICPI[109]. As PDAC tumours generally have a low TMB[110], this has led

to the hypothesis that the lack of immunogenic neoantigens in PDAC precludes a productive $CD8^+$ T cell-driven anti-tumour response. However, there is evidence to suggest otherwise - while PDAC harbours significantly fewer predicted neoantigens compared to TMB-high cancers such as melanoma, PDAC samples analysed in the Cancer Genome Atlas (TGCA) and International Cancer Genome Consortium (ICGC) dataset were found to express up to four thousand potential neoantigens, including neoantigens arising from KRAS codon 12 mutations commonly found in PDAC[111]. It is likely that no one factor is responsible for the paucity of $CD8^+$ T cell response in PDAC, but rather many factors collectively contribute to prevent cancer immunosurveillance. This is reflected in the consensus that combination therapies that simultaneously target different facets of PDAC biology will likely be necessary to bring about meaningful benefit to PDAC patients.

1.4. Mouse models of PDAC

Many mouse models of PDAC have been developed over the past 2 decades to facilitate preclinical research in this field – these include genetically modified mouse models (GEMMs) that develop autochthonous PDAC tumours and transplantable tumour models in which PDAC cancer cells are injected into the host. Among PDAC GEMMs, the KPC mouse model ($Kras^{LSL-G12D/+}Trp53^{LSL-R172H/+}Pdx1^{Cre/+}$) is considered to represent the human condition most closely[112]. In this model, mutant KRAS and p53 protein is expressed in all cells which express PDX1, a transcription factor expressed by pancreatic progenitors during embryonic development[113]. These mice start to develop PanIN lesions at 8–10 weeks of age and these lesions rapidly progress into invasive PDAC at 14–16 weeks of age. However, given that PDX1 is also expressed by cells in the developing foregut and epidermis, KPC mice also tend to develop other forms of neoplasms such as gastric/intestinal papillomas and keratoacanthomas of the anal and oral mucosae[114,115]. An alternative strategy to target the expression of mutant KRAS and p53 to the pancreas involves expressing Cre recombinase under PTF1a, a transcription factor expressed by pancreatic progenitors later in embryonic development compared to PDX1[116]. Consequently, non-pancreatic tumours are less commonly found in $Kras^{LSL-G12D/+}Trp53^{LSL-R172H/+}Ptf1a^{Cre/+}$ mice. Over the course of PDAC progression, KPC mice develop clinical signs reminiscent of human PDAC such as cachexia, signs of biliary and small bowel obstruction and haemorrhagic ascites leading to abdominal distension. The pattern of metastatic spread in KPC mice is also similar to human PDAC,

whereby metastases are commonly found in the lung, liver and/or peritoneum. KPC tumours have a desmoplastic stroma (although not to the extent observed in human PDAC), appear well-differentiated and have a high degree of genomic instability[112]. KPC mice also reliably recapitulate the immunological features of human PDAC – established tumours are dominated by immunosuppressive myeloid cells (MDSCs and macrophages) while T cells, B cells and DCs are scarcely present[117]. Similar to human PDAC, KPC mice marginally respond to gemcitabine monotherapy and do not respond to ICPI[31,118]. To study the effects of other genetic alterations commonly found in human PDAC, a wide range of other GEMMs harbouring mutations in genes such *as Ink4a, Notch1, Notch2, Smad4* and *Tgfbr2* have also been developed[119]. Transplantable PDAC models include allografts that utilize cell lines derived from autochthonous PDAC tumours (usually of KPC background) or xenografts using cell lines derived from human PDAC tumours. Cancer cells may be injected into the host either subcutaneously in the mouse flank or orthotopically into the pancreas, and it is well known that these two implantation sites yield tumours with different growth rates, immune infiltrate and preclinical response to therapy[72,73,120–122]. While both models have their advantages and disadvantages, orthotopic tumours are generally considered more representative of the human condition.

Most of the experiments presented in this thesis were performed using the murine 2838c3 allograft model. This cell line is part of a library of clonal cell lines generated in Ben Stanger's lab (University of Pennsylvania), and it was derived via limiting dilution from pancreatic tumours in $Kras^{G12D}Trp53^{R172H}Pdx1^{Cre/+}Rosa26^{YFP/YFP}$ (KPCY) mice on a C57BL/6 background[123]. 2838c3 is a 'T cell high' clone, indicating its propensity to give rise to tumours that have a relatively high T cell infiltrate compared to other clones in the library. We have also obtained 'T cell intermediate' and 'T cell low' clones from the Stanger lab, which form tumours that have lower levels of T cell infiltration. Notably, the level of T cell infiltration in these tumours correlates with responsiveness to a combined chemo-immunotherapy regimen consisting of gemcitabine, nab-paclitaxel, anti-CD40 agonist, anti-CTLA-4, and anti-PD-1[123]. Using these cell lines therefore opens up the possibility of correlating phenotypes observed in my experiments with T cell infiltration status or responsiveness to therapy.

1.5. Thesis outline

When I started my PhD in October 2018, I focussed on my first project to characterize the immunomodulatory effects of gemcitabine in combination with the Ataxia Telangiectasia and Rad3-related (ATR) inhibitor, AZD6738, in pancreatic cancer under the supervision of Professor Duncan Jodrell. In October 2020, I started my second project to investigate the role of ILC2s in pancreatic cancer, under the guidance of Dr Tim Halim. As pancreatic cancer was the unifying theme between both projects, I've provided a general introduction to pancreatic cancer in chapter 1. Project-specific introduction and aims will be provided in chapter 3 and 4, along with results and discussion of each project. Chapter 5 rounds up the thesis with a summary of both projects.

Chapter 1: Introduction

Chapter 2: Materials and methods

Chapter 3: The immunomodulatory effects of Gem/ATRi in PDAC

Chapter 4: The pro-tumourigenic role of ILC2s in PDAC

Chapter 5: Conclusion

CHAPTER TWO: Materials and methods

2.1. Cell culture and chemicals

Murine *Kras^{G12D}Trp53^{R172H}Pdx1$^{Cre/+}$Rosa26$^{YFP/YFP}$* (KPCY)-derived cell lines 2838c3, 6419c5 and 6620c1 were kindly gifted by Ben Stanger (University of Pennsylvania). The murine K8484 cell line was established from KPC mice on a mixed 129/SvJae/C57BL/6 background[124]. All murine KPC cells were cultured in Dulbecco's Modified Eagles Medium (DMEM; ThermoFisherScientific, 41966029) supplemented with 5% FBS (ThermoFisherScientific, 10270106). Human MIA PaCa-2 pancreatic cancer cells, 293T cells (both cultured in DMEM + 10% FBS) and murine 4T1 breast cancer cells (cultured in RPMI-1640 medium (ThermoFisherScientific, 21875034) + 10% FBS)) were purchased from ATCC. KPC-derived T69a PDAC organoids[125] were kindly provided by Giulia Biffi (University of Cambridge) and cultured in Advanced DMEM/F12 (ThermoFisherScientific, 12634028) supplemented with 1X GlutaMAX (ThermoFisherScientific, 35050038), 10 mM HEPES (ThermoFisherScientific, 15630080), 1X B-27 supplement (ThermoFisherScientific, 17504044), 1.25 mM N-Acetyl-L-cysteine (Sigma, A9165), 10 nM Gastrin I (Bio-Techne, 3006), 50 ng/ml mouse EGF recombinant protein (ThermoFisherScientific, PMG8043), 10% RSPO1-conditioned media (prepared in-house), 100 ng/ml recombinant murine noggin (PeproTech, 250-38), 100 ng/ml recombinant human FGF-10 (PeproTech, 100-26) and 10 mM nicotinamide (Sigma, N0636). All cell lines were subjected to regular STR fingerprinting and mycoplasma testing performed by the CRUK-CI Research Instrumentation and Cell Services Core Facility. Gemcitabine hydrochloride (Gem; Tocris Bioscience, 3259), AZD6738 (ATRi; kindly provided by AstraZeneca) and DMXAA (InvivoGen, tlrl-dmx) were dissolved in DMSO (Sigma, D2438). When used *in vitro*, gemcitabine was used at 15 nM, AZD6738 at 215 nM and DMXAA at 10 µg/ml. Polyinosinic–polycytidylic acid sodium salt (poly-I:C, pIC; Sigma, P1530) was dissolved in PBS and used at 10 µg/ml. DMSO was used at a final concentration of 0.2% in all *in vitro* experiments.

2.2. Culture of bone marrow-derived dendritic cells (BMDCs)

Bone marrow-derived dendritic cells (BMDCs) were cultured as described in Mayer et al (2014)[126]. Briefly, 15 million bone marrow cells from mouse femur and tibia were cultured in 10 ml RPMI-1640 supplemented with 10% FBS, 50 µg/ml Penicillin/Streptomycin (ThermoFisherScientific, 15070063), 50 µM 2-mercaptoethanol (Sigma, M3148), 200 ng/ml

recombinant murine Flt3L (PeproTech, 250-31L) and 2 ng/ml recombinant murine GM-CSF (PeproTech, 315-03) for 9 days. Non-adherent cells were then harvested and 3 million cells re-plated in 10ml fresh media. On day 14, non-adherent cells were harvested for downstream analysis. BMDCs +/- 2838c3 tumour cells (4:1 ratio) were cultured in 96-well plates with either DMSO, Gem/ATRi or poly-I:C at indicated concentrations.

2.3. Generation of 2838c3-OVA tumour cells

The pMIG-cytoOVA-IRES-tdTomato plasmid was kindly gifted by Maike de la Roche (University of Cambridge). pMIG-cytoOVA-IRES-tdTomato retroviruses were produced by co-transfecting pMIG-cytoOVA-IRES-tdTomato and pCL-Eco[127] (Addgene, 12371) into 293T cells using Lipofectamine 2000 Transfection Reagent (ThermoFisherScientific, 11668030) as per manufacturer's instructions. $1x10^5$ 2838c3 tumour cells were re-suspended in virus-containing media supplemented with polybrene (Merck, TR-1003-G) to a final concentration of 8 µg/ml and left to incubate at 37°C for 48 hours. These cells were then passaged and sorted via fluorescence-activated cell sorting (FACS) into 96-well plates ($5x10^3$ tdTomato$^+$ cells per well), and expanded for future use.

2.4. *In vivo* experiments

Mice

All mouse experiments were performed in the CRUK Cambridge Institute Biological Resources Unit (BRU) in accordance to the UK Animals (Scientific Procedures) Act 1986 and with approval from the CRUK CI Animal Welfare and Ethical Review Body (AWERB). All C57BL/6 mice were purchased from Charles River (UK) and allowed to acclimatize to the CRUK CI BRU for 7 days prior to enrolment into experiments. KPC (*Kras$^{LSL\text{-}G12D/+}$Trp53$^{LSL\text{-}R172H/+}$Pdx1$^{Cre/+}$*) mice were maintained by the CRUK CI Preclinical Genome Editing (PGE) core facility. *Nr4a1$^{Katushka\text{-}Cre\text{-}ERT2}$Rosa26$^{LSL\text{-}EYFP}$* (AgRSR, provided by James Thaventhiran), *Kras$^{LSL\text{-}G12D/+}$Ptf1a$^{Cre/+}$* (KC), *Il7ra$^{Cre/+}$* (provided by Hans-Reimer Rodewald), *Il7ra$^{Cre/+}$Rora$^{loxP/loxP}$* (ILC2KO, provided by Andrew McKenzie), *129(Cg)-Foxp3$^{tm3(DTR/GFP)Ayr}$/J* (Foxp3^{DTR}), *Il7ra$^{Cre/+}$Rora$^{loxP/loxP}$Rag2^{tm1Fwa}* (ILC2;Rag2KO), *Il33$^{cit/cit}$* (IL33KO, provided by Andrew McKenzie), *129S1(C)-^{Gata1tm6Sho}/LvtzJ* (ΔdblGATA), *Il13$^{tom/tom}$* (IL13KO), *Il7ra$^{Cre/+}$OX40L$^{loxP/loxP}$* (ILC2-OX40L KO, provided by Timothy Vyse and Marina Botto), *Foxp3$^{YFP\text{-}iCre}$OX40$^{loxP/loxP}$* (Foxp3-OX40 KO), *Rag2^{tm1Fwa}* (Rag2KO) and

Rag2^{tm1Fwa}Tg(TcraTcrb)1100Mjb (OT-I Rag2KO) mice were bred and maintained in-house. All mice were at least 8 weeks of age before enrolment and experimental cohorts were age- and sex-matched. For adoptive transfer of OT-I CD8$^+$ T cells, spleens from OT-I Rag2KO mice were dissociated to generate a single-cell suspension and 1x10^5 splenocytes were injected intravenously (IV) into the host.

PDAC allograft tumour models

For subcutaneous allografts, 1x10^6 tumour cells in a 100 µl mixture of 1:1 PBS and Matrigel (Corning, 354234) were injected subcutaneously into the right flank. Tumours were left to grow for 14 days before randomization into experimental groups. In survival studies, tumours were measured twice weekly using callipers and tumour volume was calculated using the formula (π/6)*(width)2*length. Mice were killed at specified endpoints, or in the case of survival studies when the tumour reaches 2000 mm^3 (or the appearance of clinical signs, whichever is first). For orthotopic allografts, mice were anaesthetized with isoflurane and an incision was made in the left abdominal area to expose the pancreas. 10 µl of 1:1 PBS and Matrigel cell suspension (containing 1x10^4 cells for the T69a organoid model or 2.5x10^4 cells for all other cell lines) was injected into the tail of the pancreas. The peritoneal membrane was sutured with absorbable Vicryl Rapide suture (Ethicon, W9913) and the skin was closed with tissue glue (GLUture, Zoetis) and wound clips (FST, 12022-09). Mice were given pre- and post-surgical analgesia (a combination of meloxicam and buprenorphine) and wound clips were removed one week post-surgery. All orthotopic tumour injections were performed by Dr Tim Halim, whereas I was responsible for all pre- and post-surgical care. For survival studies, the humane endpoint was determined using a combination of clinical signs (e.g. inactivity, piloerection and a hunched posture). All survival studies were terminated at day 90 post-implantation, at which point all mice are culled.

Drugs and antibodies

Gemcitabine hydrochloride (LKT labs, G1745) was dissolved in saline to a concentration of 20 mg/ml and dosed via intraperitoneal (IP) administration at 100 mg/kg. AZD6738 (AstraZeneca) was dissolved in 10% DMSO, 40% propylene glycol and 50% deionised water to a concentration of 2.5 mg/ml and dosed via oral gavage (OG) at 25 mg/kg. Tamoxifen (Sigma, T5648) was dissolved in a solution of 5% ethanol (Sigma, 51976) in sunflower oil (Sigma, S5007)

and dosed IP at 2 mg per mouse. DQ-OVA (ThermoFisherScientific, D-12053) was dissolved in endotoxin-free PBS (Merck, TMS-012-A) and directly injected into the tumour (50 µg). Diphtheria toxin (Sigma, D0564) was dissolved in endotoxin-free PBS and dosed IP at 25 µg/kg. InVivoPlus anti-CD40 (100 µg, clone FGK4.5/FGK45; BioXCell, BP0016-2), InVivoPlus rat IgG2a isotype control, anti-trinitrophenol (100 µg, clone 2A3; BioXCell, BP0089), recombinant mouse IL-33 (200 ng; BioLegend, 580506), InVivoMab rat IgG2b isotype control (250 µg, clone LTF-2; BioXCell, BE0090), InVivoMab rat anti-mouse CD8a (250 µg, clone 2.43; BioXCell, BE0061) and InVivoMab anti-mouse NK1.1 (50 µg, clone PK136; BioXCell, BE0036) were prepared in endotoxin-free PBS and dosed via IP injection.

2.5. Tissue collection and processing for flow cytometry

Immediately after necropsy, murine spleen and lungs were collected in PBS, lymph nodes (LNs) were collected in Hanks' Balanced Salt Solution (HBSS; ThermoFisherScientific, 24020117), and pancreas and tumour were collected in PBS containing 10% FBS, 1% glucose, 0.1 mg/ml soybean trypsin inhibitor (Sigma, T6522) and 1X cOmplete™ Mini Protease Inhibitor Cocktail (Merck, 11836153001). To generate single-cell suspensions, spleens were mashed on a 70 µm cell strainer, washed and incubated in red blood cell (RBC) lysis buffer (0.15 M ammonium chloride, 10 mM potassium hydrogen carbonate and 0.1 mM EDTA) for 5 minutes at room temperature (RT). Lungs were mechanically chopped into smaller pieces and digested in HBSS containing 750 U/ml type I collagenase (Gibco, 17100017) and 0.3 mg/ml DNAse I (Sigma, DN25-1G) for 45 minutes. Digested lung tissue were mashed through a 70 µm cell strainer and incubated in RBC lysis buffer for 3 minutes at RT. LNs were digested in HBSS with 375 U/ml type I collagenase and 0.15 mg/ml DNAse I for 45 minutes, followed by mechanical dissociation using a 21G needle. Pancreata were mechanically chopped into smaller pieces and digested in HBSS with 375 U/ml type I collagenase and 0.15 mg/ml DNAse I for 30 minutes. They were then mechanically dissociated using a 21G needle, filtered through a 70 µm cell strainer and incubated in RBC lysis buffer for 3 minutes at RT. Tumours were mechanically chopped into smaller pieces and digested in HBSS with 750 U/ml type I collagenase and 0.3 mg/ml DNAse I for 45 minutes. Digested tissues were then mechanically dissociated using a 16G needle, followed by an 18G needle and filtered through a 70 µm cell strainer. All digestion steps were performed at 37°C in a shaking incubator.

2.6. Antibody staining and flow cytometry

Single-cell suspensions were transferred into a round-bottomed 96-well plate for staining. When staining for cytokines, cells were first incubated in 1X cell stimulation cocktail with protein transport inhibitor (eBioscience, 00-4975-03) or 1X protein transport inhibitor cocktail (eBioscience, 00-4980-93) at 37°C for 2 hours in complete RPMI prior to antibody staining. To detect OVA-specific $CD8^+$ T cells, cells were incubated in PBS with anti-mouse CD16/32 antibody (BioLegend, 101320) for 15 minutes at 4°C, followed by incubation with APC-conjugated tetramers specific for H-2K(b)/SIINFEKL (NIH Tetramer Facility, Emory University) and anti-mouse CD16/32 antibody for 30 minutes at 4°C. Cell surface staining was performed in PBS with fluorophore-conjugated antibodies and Live/Dead fixable stain (**Table 2.1**) along with anti-mouse CD16/32 antibody for 30 minutes at 4°C. For intra-nuclear staining of transcription factors, the Foxp3/Transcription Factor Staining Buffer Set (eBioscience, 00-5523-00) was used as per manufacturer's instructions. Intracellular staining for cytokines was performed using the Cytofix/Cytoperm™ fixation/permeabilization kit (BD, 554714) as per manufacturer's instructions. Counting beads (ThermoFisherScientific, 01-1234-42) were added immediately before flow cytometry analysis. Samples were acquired on the FACSymphony™ (BD) or Amnis® ImageStream®XMk II (Luminex) flow cytometers and analysed using FlowJo software. Images acquired with the ImageStream were analysed using the Amnis® IDEAS® Image Analysis Software. All gating strategies are shown in **Figure 2.1 – Figure 2.4**.

2.7. Histology and image analysis

Tissues were fixed in 10% neutral buffered formalin for 24 hours and stored in 70% ethanol solution prior to paraffin embedding. 4 µm tissue sections were subjected to haematoxylin & eosin (H&E) staining or immunohistochemical staining using anti-mouse CD8α (CST, 98941), anti-mouse CD4 (Abcam, ab183685) or anti-mouse Foxp3 (ThermoFisherScientific, 14-5773-82) antibodies. Stained slides were imaged using the Aperio AT2 scanner (Leica Biosystems) and analysed using the HALO® image analysis platform (Indica Labs). Tissue embedding, sectioning, staining and scanning were performed by the CRUK CI histopathology core facility.

Table 2.1. List of antibodies used for flow cytometry.

Fluorophore	Protein	Clone	Manufacturer	Catalogue #	Dilution
AF488	FoxP3	FJK-16S	ThermoFisher	53-5773-80	1:250
AF700	CD4	RM4-5	Biolegend	300526	1:500
AF700	CD11c	N418	Biolegend	337219	1:500
APC	CD103	2E7	Biolegend	121414	1:500
APC-eF780	B220	A3-6B2	ThermoFisher	47-0452-82	1:500
APC-eF780	F4/80	BM8	ThermoFisher	47-4801-82	1:500
APC-Fire750	CD86	GL-1	Biolegend	105045	1:200
BB700	CD197 (CCR7)	4B12	BD	566464	1:250
BB700	CD172a (SIRPα)	P84	BD	742205	1:500
BUV395	NK1.1	PK136	BD	564144	1:500
BUV395	MHCII (I-A/I-E)	CI2G9	BD	743876	1:2000
BUV395	Ki67	B56	BD	564071	1:100
BV510	CD45	30-F11	Biolegend	103138	1:500
BV605	CD279 (PD-1)	29F.1A12	Biolegend	135219	1:250
BV650	RORyt	Q31 378	BD	563424	1:250
BV650	CD8α	53-6.7	Biolegend	100741	1:100
BV650	XCR1	ZET	Biolegend	148220	1:500
BV650	CD80	16-10A1	Biolegend	104732	1:200
BV711	CD64/FcγRI	X54-5/7.1	Biolegend	139311	1:250
BV785	CD44	IM7	Biolegend	103059	1:250
BV785	CD11b	M1/70	Biolegend	101243	1:500
eF450	CD5	53-7.3	ThermoFisher	48-0051-82	1:2000
eF450	CD11b	M1/70	ThermoFisher	48-0112-82	1:2000
eF450	CD11c	N418	ThermoFisher	48-0114-82	1:2000
eF450	Gr-1	RB6-8C5	ThermoFisher	48-5391-82	1:2000
eF450	Ter119	TER-119	ThermoFisher	48-5921-82	1:2000
eF450	CD19	eBio1D3	ThermoFisher	48-0199-42	1:2000
eF450	F4/80	BM8	ThermoFisher	48-4801-82	1:2000
eF450	FcεR1α	MAR-1	ThermoFisher	13-5898-82	1:2000
eF450	NK1.1	PK136	ThermoFisher	48-5941-82	1:2000
eF450	CD3ε	145-2C11	ThermoFisher	48-0031-82	1:2000
eF450	B220	RA3-6B2	ThermoFisher	48-0452-82	1:2000
eF660	Gata3	TWAJ	ThermoFisher	50-9966-42	1:250
PE	TCF-7/TCF-1	S33-966	BD	564217	1:200
PE-CF594	CD127	SB/199	BD	562419	1:250
PE-Cy7	CD3ε	145-2C11	ThermoFisher	25-0031-82	1:250
PE-Cy7	Ly-6C	HK1.4	ThermoFisher	25-5932-82	1:2000
PE-Dazzle594	PD-L1	10F.9G2	Biolegend	124324	1:250
PE-eF610	Gr-1 (Ly-6G)	1A8-Ly6g	ThermoFisher	61-9668-82	1:1000
PE-eF610	CD45	30-F11	ThermoFisher	61-0451-80	1:100
PerCP-eF710	CD8α	53-6.7	ThermoFisher	46-0081-82	1:250
PerCP-eF710	CD39	24DMS1	ThermoFisher	46-0391-80	1:250
SB600	Siglec F/CD170	1RNM44N	ThermoFisher	63-1702-82	1:250

Fluorophore	Protein	Clone	Manufacturer	Catalogue #	Dilution
-	CD16/32	-	Biolegend	101320	1:500
Fixable Viability Dye eF455 UV	Live/Dead	-	ThermoFisher	65-0868-14	1:500
Fixable Viability Dye eF780	Live/Dead	-	ThermoFisher	65-0865-14	1:2000

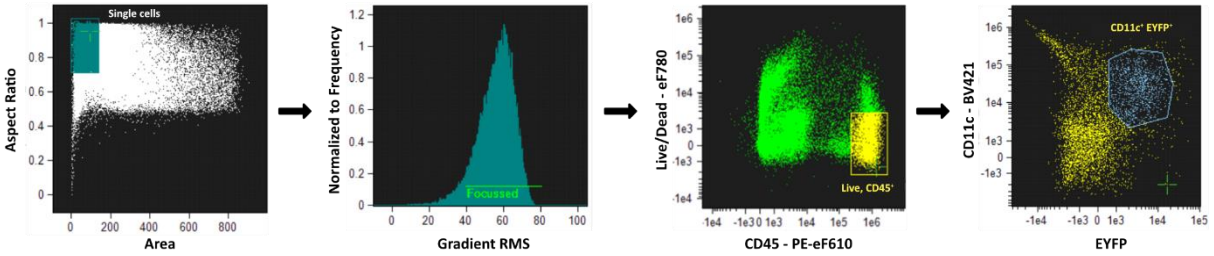

Figure 2.1. Imagestream gating strategy. Events were gated for single cells, then for cells in focus (Gradient RMS > 40). Live, CD45$^+$ cells were then gated, followed by CD11c$^+$ EYFP$^+$ double-positive cells.

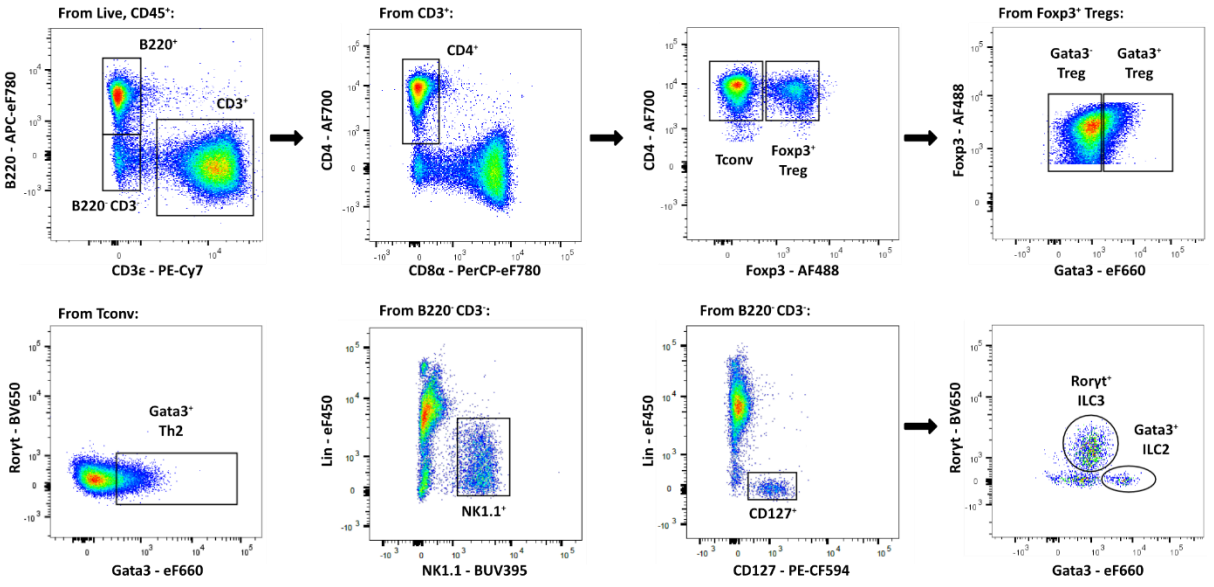

Figure 2.2. Lymphoid CD4$^+$ T cell panel gating strategy. A pancreatic lymph node sample is used as an example. From live, CD45$^+$ cells, B cells (B220$^+$), T cells (CD3$^+$) and double-negative cells (B220$^-$ CD3$^-$) were identified. From CD3$^+$ cells, CD4$^+$ T cells were isolated and separated into conventional CD4$^+$ T cells (Tconv - Foxp3$^-$) and Tregs (Foxp3$^+$). Foxp3$^+$ Tregs were further sub-divided into Gata3$^+$ and Gata3$^-$ Tregs. Gata3$^+$ Th2 cells were gated from the Tconv population. From the B220$^-$ CD3$^-$ double-negative population, NK1.1$^+$ cells were gated. ILCs (CD127$^+$) were also gated from the B220$^-$ CD3$^-$ double-negative population and further separated into ILC2 (Gata3$^+$) and ILC3 (Rorγt$^+$).

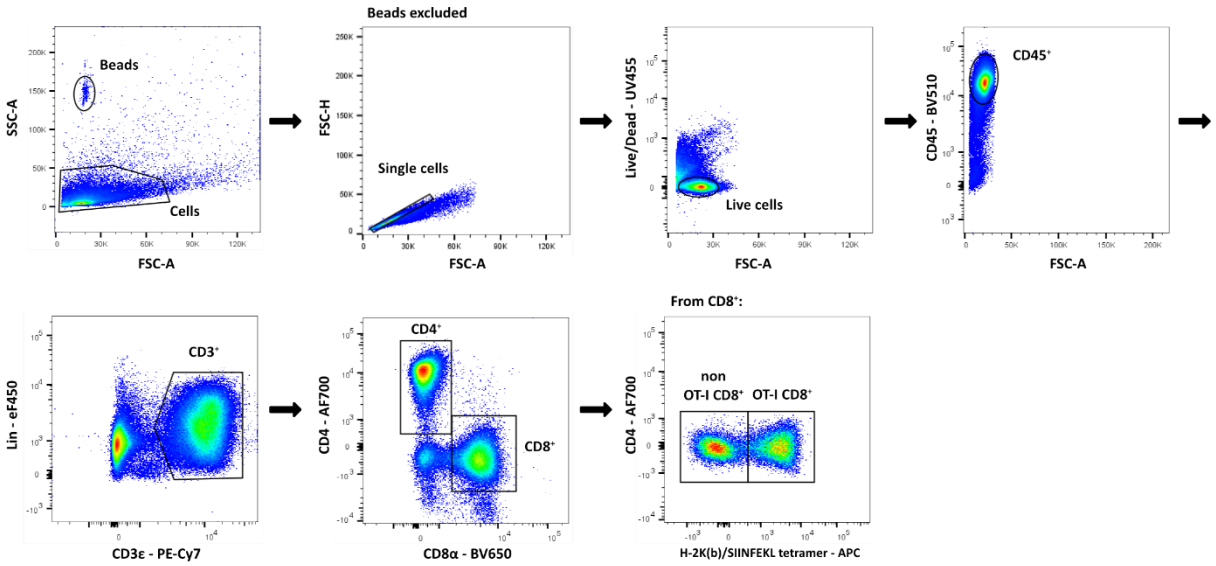

Figure 2.3. Lymphoid CD8⁺ T cell panel gating strategy. A pancreatic lymph node sample is used as an example. From live, CD45⁺ cells, CD3⁺ cells were gated and separated into CD4⁺ and CD8⁺ T cells. Tetramer-positive, OVA-specific CD8⁺ T cells were then gated from total CD8⁺ T cells.

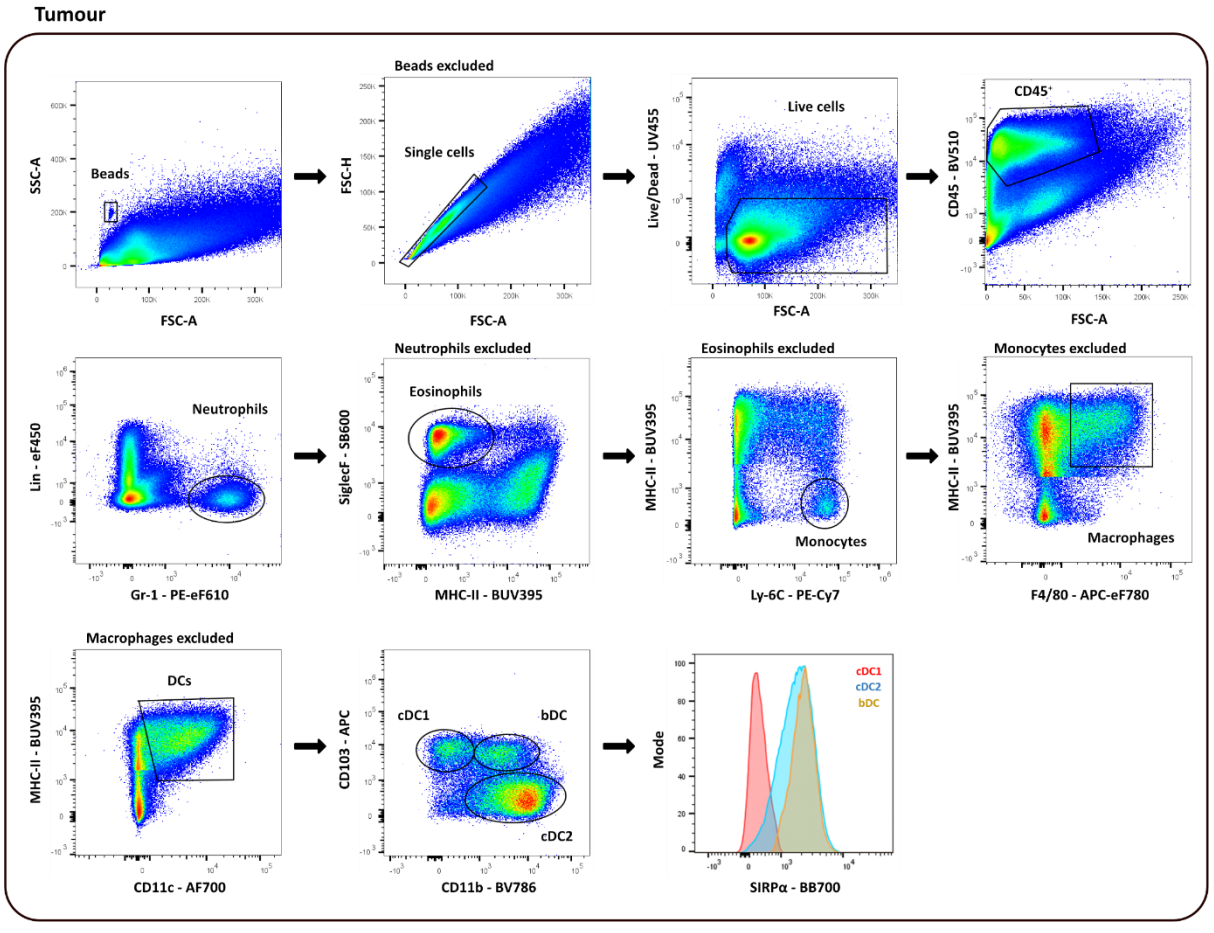

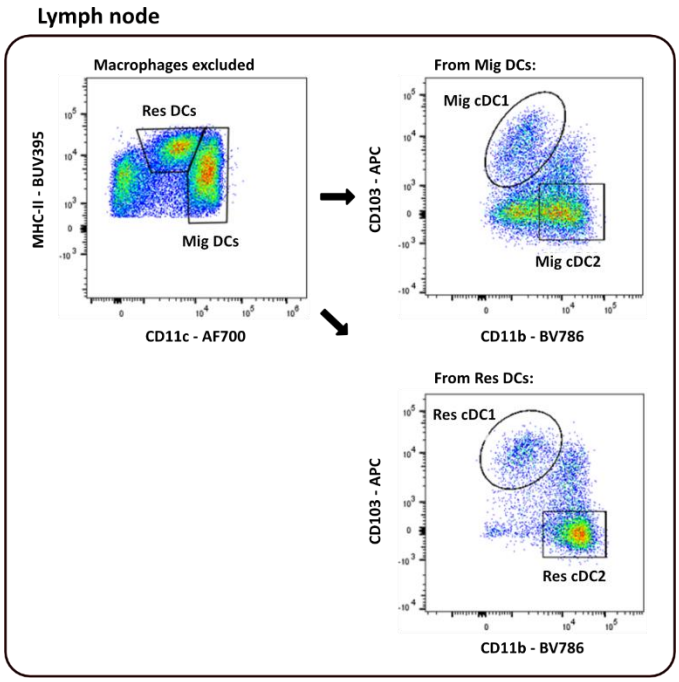

Figure 2.4. Myeloid panel gating strategy. A tumour and lymph node sample is used as an example. After gating for single cells and live, CD45$^+$ cells, neutrophils (Lin$^-$ Gr-1$^+$) were first identified. Neutrophils were then excluded and eosinophils gated as MHC-II$^-$ SiglecF$^+$ cells. Once eosinophils were excluded, monocytes were identified as MHC-II$^-$ Ly-6C$^+$. Monocytes were then excluded and macrophages gated as MHC-II$^+$ F4/80$^+$. After excluding macrophages, DCs were gated as MHC-II$^+$ CD11c$^+$. DCs were then separated into three subsets based on CD103 and CD11b expression – cDC1 (CD103$^+$ CD11b$^-$), cDC2 (CD103$^-$ CD11b$^+$) and bDC (CD103$^+$ CD11b$^+$). cDC2 and bDC shows high expression of CD172a (SIRPα) compared to cDC1. For lymph nodes, the same strategy was used for gating myeloid cells up until the gate for macrophages. After excluding macrophages, DCs in the lymph node were separated into two populations by CD11c and MHC-II expression - LN-resident DCs (Res DCs) were CD11c^{hi} MHC-II^{lo} whereas migratory DCs (Mig DCs) were CD11c^{lo} MHC-II^{hi}. From there they were further sub-divided into cDC1 and cDC2 based on CD11b and CD103 expression.

2.8. IFN-β ELISA

IFN-β concentration in cell culture supernatant was determined using the Mouse IFN-beta DuoSet ELISA kit (R&D Systems, DY8234-05) as per manufacturer's instructions. Optical density was read using the CLARIOstar® Plus plate reader (BMG LABTECH) and concentrations were interpolated from a standard curve generated by GraphPad Prism (Dotmatics).

2.9. Western blotting

Cells cultured on 60 mm dishes were washed once with PBS and lysed using RIPA buffer (ThermoFisherScientific, 89901) supplemented with cOmplete™ Protease Inhibitors (Roche, 4693159001) and PhosSTOP™ phosphatase inhibitors (Roche, 4906845001). Cell lysate was then scraped into a microcentrifuge tube and kept on ice for downstream processing. Frozen tumour fragments (~30 mg) were homogenized in RIPA buffer supplemented with protease and phosphatase inhibitors using the gentleMACS™ Dissociator (Miltenyi Biotec). Lysates were then sonicated 3 times at 10 second intervals, followed by agitation at 4°C for an hour, then centrifuged at 20,000 x g and the supernatant taken for downstream analysis. Protein concentration was measured using the Direct Detect Spectrometer (Merck). Proteins were resolved on NuPAGE™ 4-12% Bis-Tris Protein Gels (ThermoFisherScientific, NP0336PK2), transferred onto a nitrocellulose membrane using the iBlot 2 Dry Blotting System (ThermoFisherScientific) and probed with the following primary antibodies from Cell Signaling Technology (CST) or Abcam (ab): STING (CST 13647S), phospho-STING, Ser365 (CST 72971S), TBK1/NAK (CST 3504S) phospho-TBK1/NAK, Ser172 (CST 5483S), IRF3 (CST 4302S), phospho-IRF3, Ser396 (CST 29047S), PD-L1 (ab213480), vinculin (CST 13901S). Primary antibodies were detected using IRDye secondary antibodies (LI-COR) and imaged on the Odyssey CLx imaging system (LI-COR). Scanned images were visualized and analysed using Image Studio (version 5.2) (LI-COR).

2.10. Quantitative RT-PCR

Upon resection, small tumour fragments (< 30mg) were kept in RNAlater™ Stabilization Solution (Invitrogen, AM7024) overnight at 4°C followed by storage at -80°C. Tumours were homogenized using the TissueLyser II (QIAGEN) followed by RNA extraction using the RNeasy Plus Mini Kit (QIAGEN, 74134) as per manufacturer's instructions. RNA concentration was determined using the Qubit™ RNA BR Assay Kit (ThermoFisher, Q10211). Quantitative RT-PCR

was performed using the Luna® Universal Probe One-Step RT-qPCR Kit (NEB, E3006) with 100 ng RNA template. All targets were amplified (40 cycles) using pre-designed PrimeTime qPCR primers and probes (Integrated DNA Technologies) on a QuantStudio™ 3 Real-Time PCR Instrument (Applied Biosystems). Relative gene expression was quantified using the ddCt method and gene expression levels were normalized to the housekeeping gene Hprt.

2.11. Bulk RNA-seq of KPC tumours

KPC tumours were immediately flash-frozen in liquid nitrogen upon resection, followed by embedding in OCT. Ten 8 µm-thick sections were collected in RLT buffer at 4°C and total RNA was isolated using the Qiagen AllPrep DNA/RNA/Protein Micro Kit per the manufacturer's instructions. RNA integrity and purity was measured using an Agilent TapeStation before poly(A) selection and library construction, followed by single-end 50-bp sequencing on an Illumina HiSeq4000 sequencer at a depth of 20 million reads per sample by the CRUK CI Genomics core facility. Reads were aligned against the mouse genome assembly GRCm38 using the STAR alignment tool[128] (version 2.7.2) and counted against genes using featureCounts from the Subread package[129] (version 1.5.2). For differential expression analysis, the DEseq2 package[130] (version 1.26.0) was used. GSEA preranked analysis was performed using GSEA software[131] (version 3). All bioinformatics analyses were performed by the CRUK CI Bioinformatics core facility.

2.12. Statistical analysis

Statistical analysis between two experimental groups was performed using an unpaired t test. Analysis between multiple groups was performed using a one-way ANOVA with Tukey's multiple comparison test whilst comparisons between multiple groups of grouped data were performed using a two-way ANOVA with Šídák's multiple comparison test. All statistical analyses were performed with Graphpad Prism (Dotmatics). Error bars show standard error of the mean (SEM). $p < 0.05$ was considered statistically significant. * indicates $p < 0.05$, ** $p < 0.01$, *** $p < 0.001$.

CHAPTER THREE: The immunomodulatory effects of Gem/ATRi in PDAC

3.1. Background

As part of the innate immune system, dendritic cells act as sentinels by sampling their immediate environment for antigens and presenting these antigens to naïve $CD8^+$ and $CD4^+$ T cells via MHC class I and II respectively. While all nucleated cells express MHC-I for presentation of endogenous antigens, DCs are also capable of presenting exogenous antigens on MHC-I through a process known as cross-presentation[132]. In addition to providing antigenic stimulation for T cell receptor (TCR) activation, DCs also express co-stimulatory molecules (B7-1 and B7-2, or CD80 and CD86, respectively) that provide the secondary signal required for full T cell activation[133]. As such, they have a critical role in the initiation of antigen-specific adaptive immune responses and sit at the interface between innate and adaptive immunity. Our understanding of DCs have progressed significantly since they were first discovered in the 1970s[134], and it is now known that there are multiple subsets of DCs with different ontogeny, localization and immunological function (**Figure 3.1**).

Monocyte-derived DCs (moDCs), also known as inflammatory DCs (iDCs) are absent during steady state and are only found under inflammatory conditions[135]. They are derived from circulating blood monocytes and differentiate *in situ* at the site of inflammation[136]. Found in both lymphoid and non-lymphoid organs, they can present antigens to both $CD4^+$ and $CD8^+$ T cells and have been identified in many models of microbial infection and autoimmune disease. MoDCs can contribute to Th1, Th2 or Th17 immune responses depending on the experimental conditions, therefore they are highly plastic and adapt their phenotype to the signals present in their immediate environment[135]. However, given that there are no *in vivo* models that allow selective ablation of moDCs, it is still unknown if they have any non-redundant functions.

Plasmacytoid DCs (pDCs) originate from common dendritic cell progenitors (CDPs) and their differentiation is driven by the transcription factor E2-2[137]. Although pDCs express MHC class II and have demonstrated antigen presenting capacity under certain inflammatory conditions, their most prominent role is thought to be the production of type I interferons (T1IFN) during viral infection. This is mediated by their expression of toll-like receptor 7 (TLR7) and TLR9 (which detect endosomal RNA and DNA, respectively) and high expression of IRF7 that drive

T1IFN production[138]. In breast and ovarian cancer, the presence of pDCs has been associated with poorer prognosis as intratumoural pDCs were shown to support Treg proliferation via indoleamine 2,3-dioxygenase (IDO) production and ICOS stimulation[139–141]. The ability of pDCs to produce T1IFN is suppressed by tumour-derived TGF-β and tumour necrosis factor-α (TNF-α)[142], but treatment with TLR7 ligands can reverse this immunosuppressive phenotype to restore T1IFN production and promote anti-tumour immunity[143].

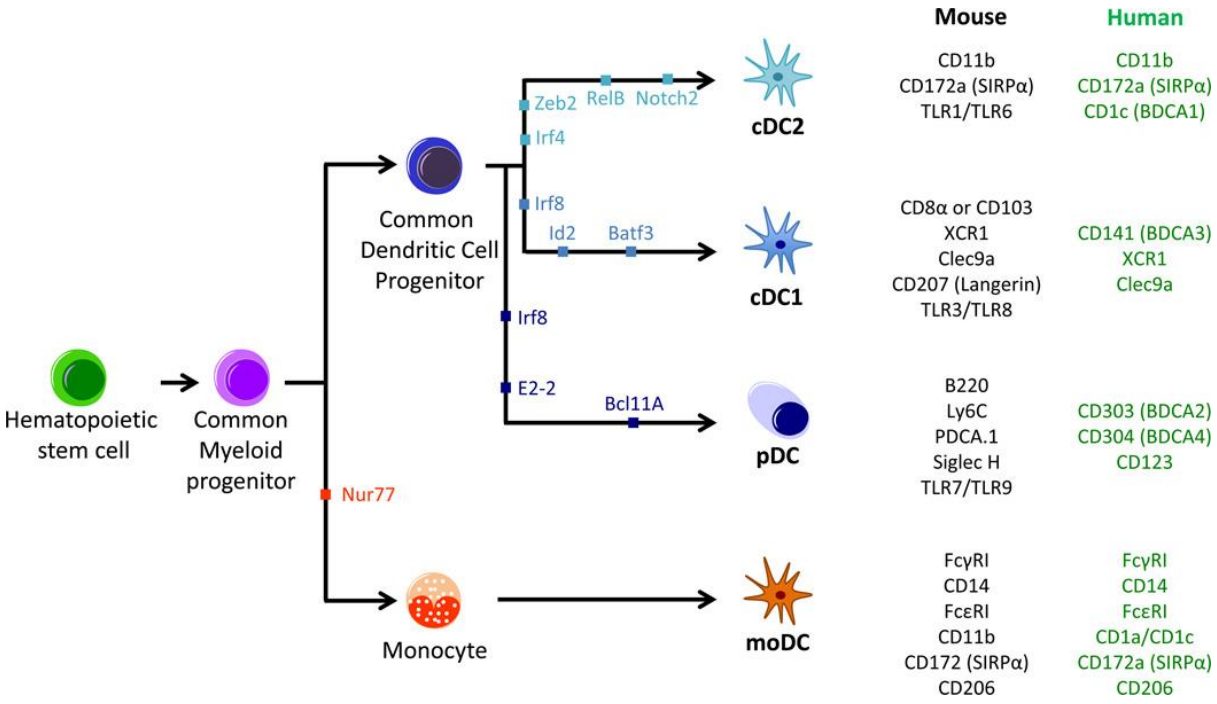

Figure 3.1. Ontogeny of dendritic cell subsets. Dendritic cells (DCs) originate from haematopoietic stem cells (HSC) in the bone marrow. The transcription factor Nur77 drives the differentiation of common myeloid progenitors (CMPs) into monocytes, which further differentiate into monocyte-derived DCs (moDCs) under inflammatory conditions. In the absence of Nur77, CMPs will differentiate into common dendritic cell progenitors (CDPs). The type 1 conventional DC (cDC1), type 2 conventional DC (cDC2) and plasmacytoid DC (pDC) subsets arise from the CDP, each driven by critical transcription factors shown for each lineage. These DC subsets can be identified using a combination of cell surface markers in both mice and humans. Figure from Gardner and Ruffell (2016)[144].

Conventional dendritic cells (cDCs) also differentiate from CDPs and they can be divided into two main groups: cDC1 is characterized by the expression of the transcription factors IRF8, ID2 and BATF3 and they are particularly efficient at priming $CD8^+$ T cells via MHC-I-mediated cross-presentation[145]. They can be identified via surface expression of CLEC9A and the chemokine receptor XCR1. CLEC9A (also known as DNGR-1) is a receptor for F-actin, a component of the cytoskeleton that is only present in the extracellular environment on dead cell debris[146]. This allows CLEC9A to detect the presence of dead cells in its vicinity, and CLEC9A receptor activation promotes intracellular phagosome rupture that enables phagocytosed antigens to access the cytosolic MHC-I antigen processing pathway[147]. As CLEC9A is specifically expressed by cDC1s, this may contribute to the superior cross-presenting capacity of cDC1s compared to other DC subsets. cDC1s can be further sub-divided into two populations: the CD8α-expressing, lymphoid-resident cDC1 and the CD103-expressing, peripheral tissue-resident cDC1. In comparison, cDC2s are characterized by IRF4 and ZEB2 transcription factor expression and preferentially activate $CD4^+$ T cells via MHC-II antigen presentation. cDC2s express high levels of SIRPα (CD172) and CD11b, and recent transcriptomic analyses have identified two main subsets of cDC2s, characterized by expression of T-bet (cDC2A) or RORγt (cDC2B)[148]. These two subpopulations have distinct ontogeny, transcriptional identity and immunological function, as shown by how they respond differently to inflammatory challenge and have different $CD4^+$ T cell priming capacity[148]. Tissue-resident cDC1 and cDC2 have the potential to migrate to their tissue-draining lymph node to engage naïve T cells, and this migration is dependent on the CCR7-CCL19/CCL21 chemokine axis[149].

Dendritic cells play an important role in the cancer-immunity cycle, where they endocytose tumour-specific antigens and prime naïve T cells against these antigens[150]. Although DCs typically only represent a small proportion of tumour-infiltrating immune cells, they are a highly heterogenous population that can exert opposing effects on anti-tumour immunity[151,152]. $CD103^+$ cDC1 are the most well-studied DC subset in the context of cancer and their presence has been associated with extended survival across many different cancers, including PDAC[63,66,145]. They are critical for the transport of tumour antigens to the draining lymph node, where they engage and prime $CD8^+$ T cells[153,154]. Intratumoural cDC1s also support $CD8^+$ T cell recruitment and effector function within the tumour as they are a major

source of CXCL9/10[155–157]. The presence of DCs correlates with $CD8^+$ T cell abundance within PDAC tumours[98], and the $CD103^+$ cDC1 population is required for response to ICPI in a variety of tumour-bearing models[154,158,159] and correlate with responsiveness to anti-PD-1 immunotherapy in melanoma patients[160]. It is therefore clear that cDC1 play a key role in the initiation and maintenance of $CD8^+$ T cell-dependent anti-tumour immunity. However, $CD103^+$ cDC1 is often the least prevalent DC population within the tumour microenvironment[145], and many immunosuppressive mechanisms exist in the TME to suppress their function (previously discussed in Chapter 1)[161]. Therefore, restoring cDC1 function via therapeutic interventions that activate dendritic cells or promote intratumoural dendritic cell recruitment might promote $CD8^+$ T cell-dependent anti-tumour immunity.

There are a number of novel approaches targeted at activating dendritic cells for cancer therapy[162], but there is accumulating evidence to show that cytotoxic chemotherapeutics (which are already used as standard of care therapy for most cancers) are capable of potentiating intratumoural DC function[163]. DCs may be directly activated by a subset of chemotherapeutic agents (through mechanisms that are yet unknown)[164–166], or they may be indirectly activated by the effects of chemotherapy on other cells in the TME, such as the immunogenic cell death (ICD) of cancer cells[167,168] and/or depletion of various immunosuppressive immune cell populations[169]. ICD is an immunogenic form of apoptosis and the hallmarks of ICD include cell-surface exposure of calreticulin, active exocytosis of ATP and the release of damage-associated molecular patterns (DAMPs) such as heat shock protein 70 (HSP70) and high-mobility group box 1 (HMGB1)[170]. These factors have been shown in different settings to drive the immunogenicity and preclinical efficacy of chemotherapy - for example, anthracycline chemotherapy induces the recruitment and differentiation of inflammatory DCs in the TME, and this was dependent on the release of ATP from dying cancer cells[171]. Some chemotherapeutic agents can also promote MHC-I cross-presentation by tumour-infiltrating DCs[172] or promote immune recognition of cancer cells via upregulation of MHC-I molecules on cancer cells[173,174]. Gemcitabine is commonly used in PDAC treatment and there is substantial evidence to show that gemcitabine has strong immunomodulatory properties in both PDAC mouse models and patients. Gemcitabine has been shown to deplete MDSCs and Tregs in both PDAC mouse models and patients, and in preclinical models this depletion effect was associated with increased $CD8^+$ T cell-dependent anti-tumour response

and extended survival[175–179]. Despite the antiproliferative effect of gemcitabine on cancer cells, T cells isolated from peripheral blood mononuclear cells (PBMCs) of gemcitabine-treated patients did not show any *ex vivo* proliferative defect when compared to healthy controls[175,176].

Many cytotoxic chemotherapies induce cancer cell death by causing DNA damage during DNA synthesis in S phase, and there are multiple mechanisms by which DNA damage can activate pro-inflammatory signalling pathways[180–184]. Unrepaired DNA damage can lead to the release of nucleic acids into the cytosol, resulting in the activation of cytosolic nucleic acid sensing pathways. Retinoic acid-inducible gene-I (RIG-I)-like receptors (RLRs) and cyclic GMP-AMP (cGAMP) synthase (cGAS) act as receptors for cytosolic RNA and DNA respectively, and their activation leads to the production of T1IFNs and other pro-inflammatory cytokines[185]. Upon binding to double-stranded DNA (dsDNA), cGAS catalyses the conversion of ATP and GTP into cGAMP. The second messenger cGAMP then binds to and activates stimulator of interferon genes (STING), leading to the recruitment and activation of TANK-binding kinase 1 (TBK1). TBK1 is responsible for activating the transcription factors interferon regulatory factor 3 (IRF3) and NF-κB subunits to activate transcription of downstream pro-inflammatory genes[186]. Alternatively, STING may also be activated downstream of Ataxia Telangiectasia Mutated (ATM) signalling in response to DNA double-strand breaks (DSBs) in a manner that is independent of cytosolic DNA and cGAS[187]. The STING pathway evolved as a mechanism of antiviral defence, but it is clear that this pathway also plays an important role in the process of tumourigenesis where it can have pro- or anti-tumourigenic effects[188]. Mice deficient in key components of the cGAS-STING-IRF3 pathway show decreased tumour control (due to a defect in tumour-specific $CD8^+$ T cell priming)[189], whereas STING activation (via intratumoural administration of cyclic dinucleotides (CDNs)) has been shown to induce a strong anti-tumour immune response in many different preclinical models of cancer, including PDAC[190–195]. STING-mediated anti-tumour immunity is strongly driven by T1IFN production in the TME, and its effects include depletion and/or repolarization of the myeloid compartment, intratumoural $CD8^+$ T cell and natural killer (NK) cell recruitment and activation, and production of a wide range of pro-inflammatory chemokines and cytokines. In particular, type I IFNs potently activate dendritic cells, leading to upregulation of co-stimulatory molecules (such as CD86, CD80 and CD40), secretion of IFN-γ and increased T-cell priming activity[196].

Indeed, targeted delivery of T1IFN to CLEC9A-expressing cDC1 *in vivo* slows tumour growth and enhances preclinical response to chemotherapy and ICPI[197].

The idea of combining conventional chemotherapeutics and immunotherapy to achieve greater therapeutic efficacy has steadily garnered interest as more immunostimulatory effects of chemotherapy were discovered[198]. In 2016, the KEYNOTE-021 trial was the first clinical trial to show the superiority of ICPI (anti-PD-1) in combination with chemotherapy (pemetrexed and carboplatin) over chemotherapy alone in advanced NSCLC patients[199], and now there is significant interest in combining different chemotherapeutic and immunotherapeutic agents across different malignancies[200]. In this chapter, I report on my efforts to characterize the immunomodulatory effects of gemcitabine in combination with the ATR inhibitor, AZD6738, in pancreatic cancer. This drug combination was chosen as the focus of this chapter as previous work in the Jodrell group had shown that gemcitabine synergises with AZD6738 to cause tumour regression and confer improved survival in mouse models of PDAC[201,202]. These work also led to an ongoing phase I clinical trial (ATRiUM, NCT03669601) to investigate the safety and anti-tumour effect of gemcitabine in combination with AZD6738 in advanced solid tumours. As the combination of gemcitabine and ATRi (Gem/ATRi) causes significant DNA damage in pancreatic cancer cells, I hypothesized that it may also promote intratumoural DC activation and potentiate anti-tumour $CD8^+$ T cell responses. If true, this could form the basis of a mechanistic rationale to combine Gem/ATRi with ICPI for greater therapeutic efficacy.

Results

3.2. Gem/ATRi induces DC activation *in vivo*

This project started from previous work in the lab to characterize the effect of Gem/ATRi on the transcriptome of KPC PDAC tumours[201]. KPC mice were dosed with Gem/ATRi and tumours taken for bulk RNA-seq to characterize the impact of Gem/ATRi on the tumour microenvironment. Among the cohort dosed with Gem/ATRi, there were 4 responders and 6 non-responders (as determined by changes in tumour diameter from start of treatment, **Figure 3.2a**). Differential gene expression analysis revealed upregulation of T1IFN and DC-related genes in responding tumours, and gene set enrichment analysis (GSEA) showed an upregulation of T1IFN signalling and dendritic cell differentiation (**Figure 3.2b & 3.2c**). This suggested that Gem/ATRi has an immunostimulatory effect in tumours responding to this treatment, and this may include activation of intratumoural DCs. To validate these findings, I first determined if Gem/ATRi will induce DC activation in non-tumour-bearing mice, and if so, what the kinetics of activation were. WT C57BL/6 mice were dosed with a 4-day cycle of Gem/ATRi and the spleen and lungs were taken for flow cytometry analysis at 24 hours, 1 week and 2 weeks after the final dose. cDC1 and cDC2 in both organs were only activated at the 24-hour timepoint, as assessed by CD86 upregulation (**Figure 3.3a**). In a follow-up experiment to narrow down the timeframe of DC activation, maximal CD86 and CD80 upregulation on both cDC1 and cDC2 was observed 24 and 48 hours after the final dose, respectively (**Figure 3.3b**). Although maximal CD80 upregulation was delayed compared to CD86, CD80 expression on both DC subsets at 24 hours after the final dose is still significantly higher compared to vehicle-treated mice. Therefore, all subsequent experiments used the 24-hour timepoint to assess Gem/ATRi-mediated DC activation.

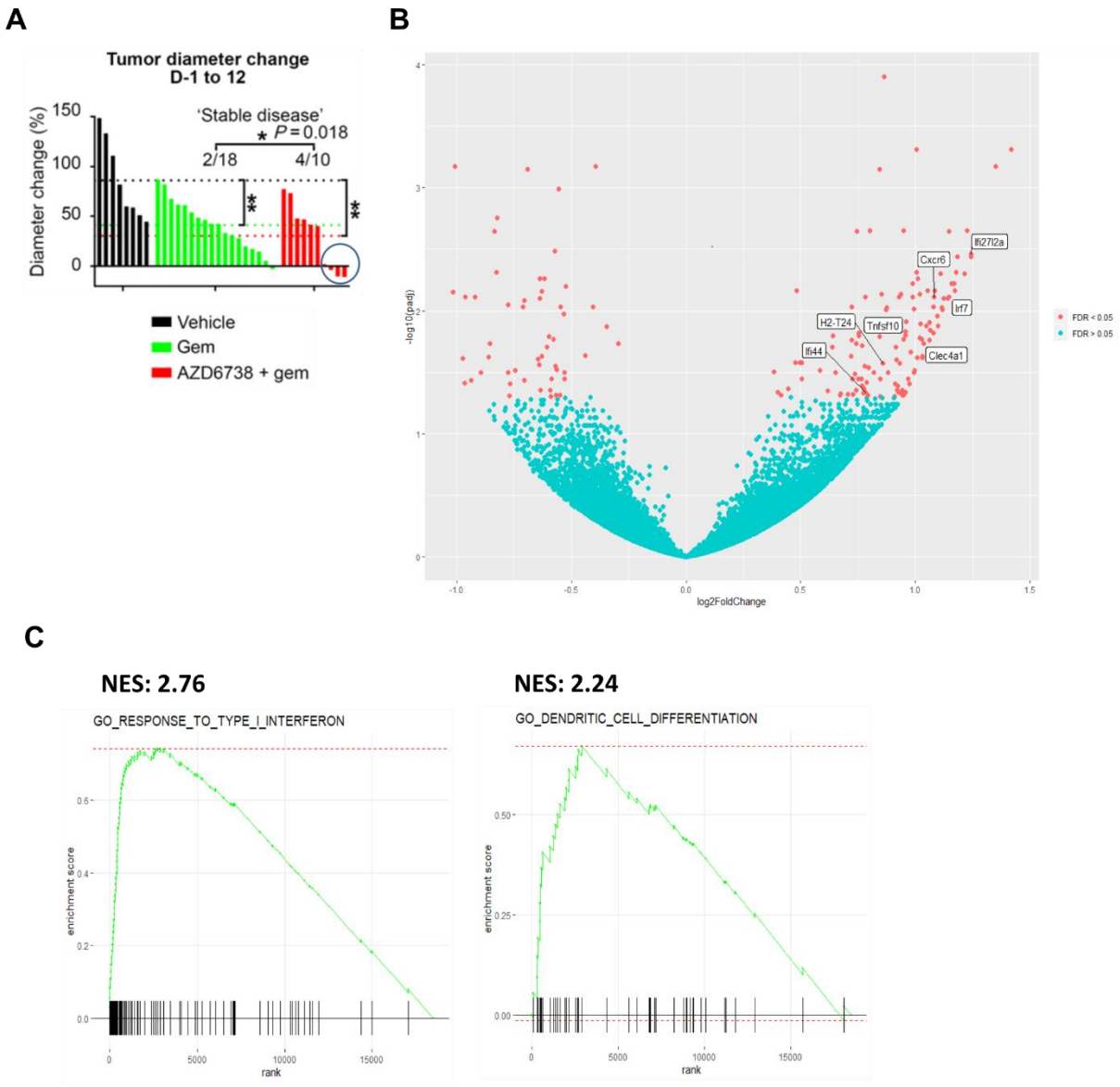

Figure 3.2. Upregulation of genes associated with a pro-inflammatory immune response in KPC PDAC tumours responding to Gem/ATRi. (A) Gem/ATRi administration causes tumour regression in a subset of KPC mouse PDAC tumours. In the combination group, tumour regression was observed in 4 out of 10 mice. Bulk RNA-seq was performed on all tumours. Figure taken from Wallez et al (2018)[201]. (B) Volcano plot comparing the gene expression profile of responding (n=4) vs non-responding (n=6) tumours, with select differentially expressed genes highlighted. (C) GSEA enrichment score plot for two pathways of interest – type I interferon signalling and dendritic cell differentiation. NES, normalized enrichment score.

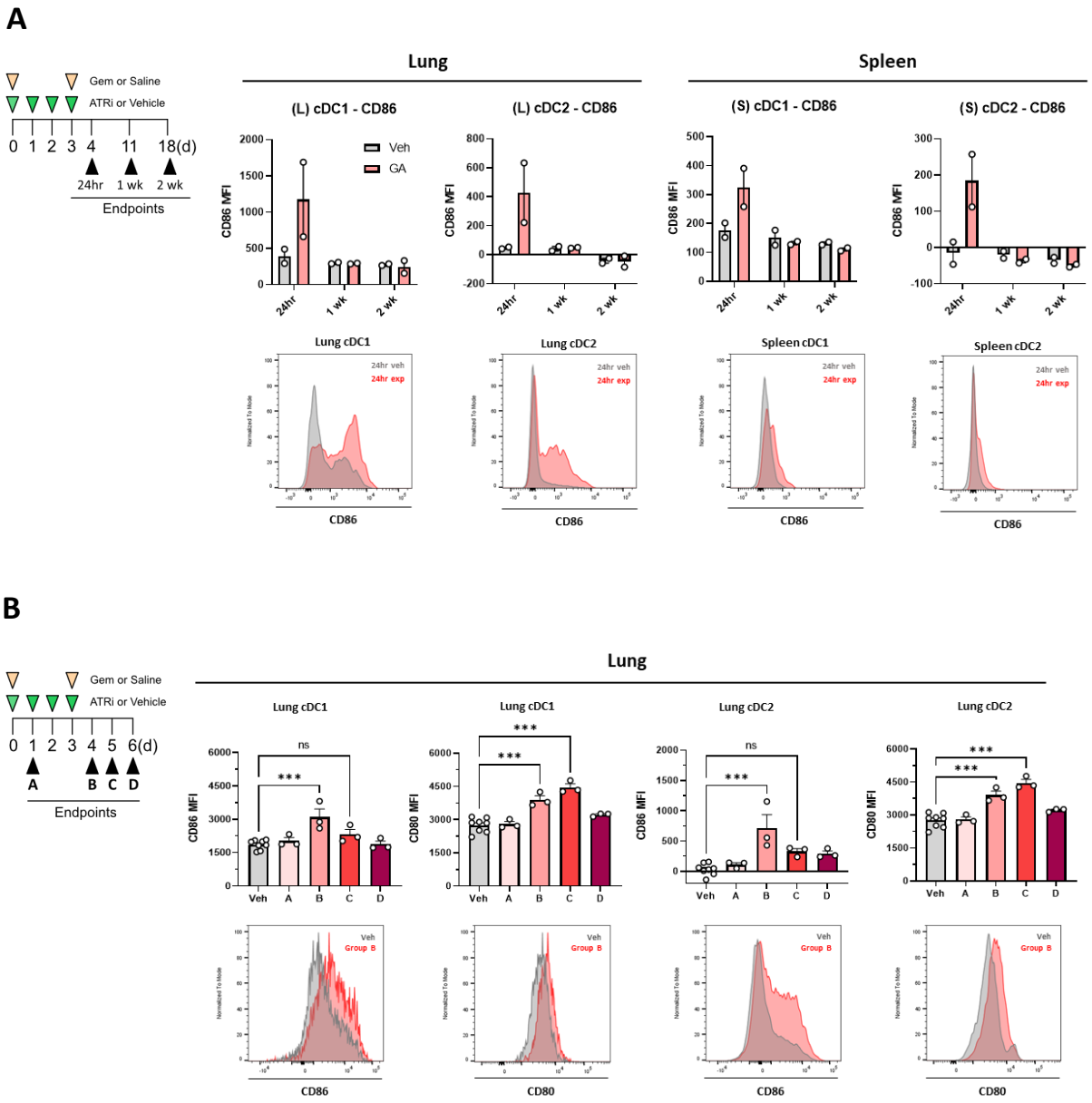

Figure 3.3. Kinetics of DC activation with a 4-day cycle of Gem/ATRi. (A, left) Schematic showing schedule of Gem/ATRi dosing and sampling timepoints. (A, right) Upregulation of CD86 on cDC1 and cDC2 in the spleen and lungs of non-tumour-bearing C57BL/6 mice dosed with Gem/ATRi at indicated timepoints. (B, left) Schematic showing schedule of Gem/ATRi dosing and sampling timepoints. (B, right) Upregulation of CD80 and CD86 on cDC1 and cDC2 in the lungs of non-tumour-bearing C57BL/6 mice dosed with Gem/ATRi at indicated timepoints. MFI, median fluorescence intensity. One-way ANOVA with Tukey's multiple comparisons test was performed in B. Error bars indicate mean ± SEM. ***, $P < 0.001$.

3.3. Gem/ATRi slows 2838c3 tumour growth and induces intratumoural DC activation

Previous studies have demonstrated the preclinical efficacy of Gem/ATRi in the KPC and K8484 subcutaneous allograft model[201], but its effects on the 2838c3 tumour model is not known. WT tumour-bearing mice were given weekly cycles of Gem/ATRi, and three repeated cycles of Gem/ATRi significantly slowed tumour growth compared to vehicle (**Figure 3.4a**). However, the anti-tumour effect was primarily attributed to Gem as the addition of ATRi provided a modest, non-significant decrease in tumour volume compared to Gem alone. In a follow-up study, mice were also given three weekly cycles of Gem/ATRi but all tumours were taken one week after the final dose of Gem/ATRi for time-matched immunohistochemistry (IHC) analysis. IHC analysis showed a trend towards decreased intratumoural $CD8^+$ cells in Gem-treated or Gem/ATRi-treated samples compared to controls, whereas there were no changes in $CD4^+$ cell numbers (**Figure 3.4b**). These results suggest that intratumoural $CD8^+$ T cells are depleted one week after repeated cycles of Gem/ATRi but the same was not true for $CD4^+$ T cells.

To determine whether Gem/ATRi induces intratumoural DC activation, flow cytometry analysis was performed to characterize DC populations within the tumour and tumour-draining lymph node (dLN, inguinal lymph node on the right flank) after Gem/ATRi administration. Intratumoural DCs were defined as $CD11c^+$ MHC-II^+ and split into subsets based on their expression of CD103 and CD11b. Unexpectedly, in addition to the $CD103^+$ cDC1 and $CD11b^+$ cDC2 populations, a third $CD103^+$ $CD11b^+$ population was observed in the tumour. To my knowledge, $CD103^+$ $CD11b^+$ DCs were first characterized in pancreatic tumours by Barilla and colleagues[68] and so for the remainder of this thesis they are referred to as bDC. A previous report of $CD103^+$ $CD11b^+$ DCs in the gut suggests that these DCs differentiate locally from cDC2-like $CD103^-$ $CD11b^+$ DCs[203], and in support of this hypothesis, bDC (similar to cDC2) express high levels of SIRPα (data shown in gating strategy).

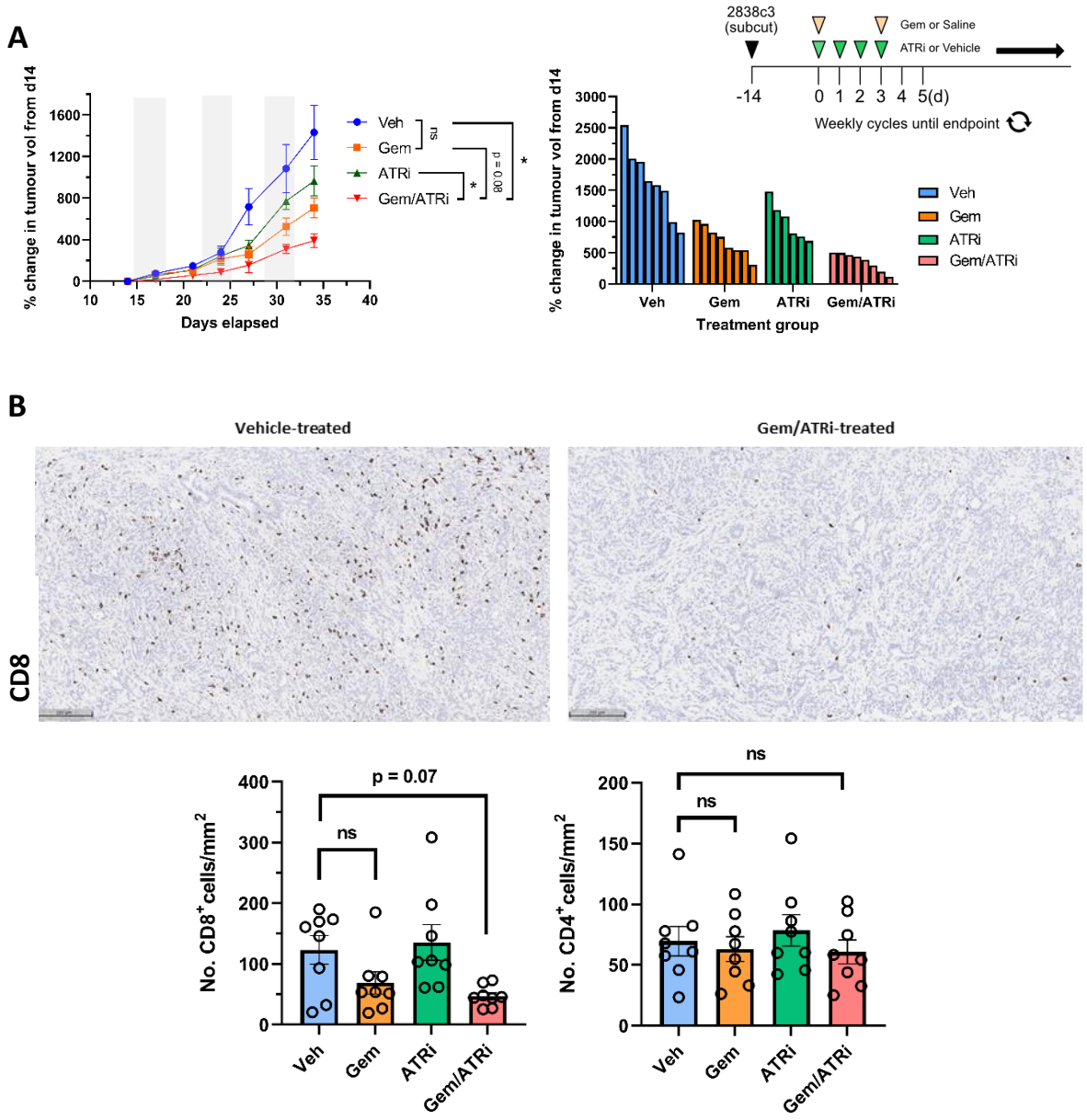

Figure 3.4. The combination of gemcitabine and ATRi slows 2838c3 subcutaneous tumour growth. 2838c3 KPCY tumour cells were implanted subcutaneously into the right flank of C57BL/6 mice and dosed with Gem/ATRi as indicated in the schematic. Drugs were given on the first 4 days of the week, with three 'rest' days between cycles. (A) Percentage change in tumour volume across 3 consecutive weekly cycles of Gem/ATRi. Grey bars indicate days during which mice are dosed. Waterfall plot shows changes in individual tumour volume between day 14 and day 34. (B) 2838c3 tumours implanted and dosed as in (A) but all tumours were taken one week after the final dose of Gem/ATRi for time-matched analysis. CD8 and CD4 IHC were performed on formalin-fixed, paraffin-embedded (FFPE) tumour sections to quantify the number of intratumoural $CD8^+$ and $CD4^+$ cells, respectively. Representative CD8 IHC images of tumours treated with vehicle or Gem/ATRi are also shown (Scale bar, 200µm). Mixed-effects model (REML) followed by Tukey's multiple comparisons test was performed in A; One-way ANOVA with Tukey's multiple comparisons test was performed in B. Error bars indicate mean ± SEM. *, $P < 0.05$.

Gem/ATRi induced partial activation of intratumoural cDC1 (with only slight CD80 and CD86 upregulation and no effect on PD-L1 expression) but had a greater effect on cDC2 and bDC as significant upregulation of CD80, CD86 and PD-L1 was observed in these two populations (**Figure 3.5a**). CCR7, a marker for cells with migratory potential, was not significantly upregulated in any population. DC activation was accompanied by a reduction in all intratumoural $CD45^+$ immune cells and total DCs (**Figure 3.5b**). As for DCs in the dLN, Mig DCs were preferentially activated by Gem/ATRi (there were no changes in CD80 or CD86 expression in Res DCs, data not shown) (**Figure 3.5c**). Res DCs and Mig DCs also showed several distinct characteristics - in line with their migratory origin, Mig DCs showed higher expression of CCR7 compared to Res DCs. They also expressed higher levels of PD-L1, possibly a reflection of their higher activation state (**Figure 3.5d**). Finally, Gem/ATRi induced a striking depletion of Res DCs in the dLN whereas Mig DC numbers were unaffected (**Figure 3.5e**).

3.4. Gem/ATRi promotes tumour antigen uptake by intratumoural cDC1

In addition to the upregulation of co-stimulatory molecules, antigen processing and presentation is essential for DCs to engage and prime naïve T cells. As a form of cytotoxic chemotherapy, Gem/ATRi-induced tumour cell death should increase the level of tumour antigens available for uptake in the tumour microenvironment. This might then result in an increase in tumour antigen uptake in intratumoural DCs. As 2838c3 tumour cells express EYFP, EYFP fluorescence can be used to track antigen uptake in DCs. At 24 hours post-Gem/ATRi administration, the proportion of $EYFP^+$ intratumoural cDC1 doubled compared to vehicle-treated tumours (**Figure 3.6a**). This effect was not observed in cDC2 or bDC. Migratory DCs are known to take up antigens in the tumour and migrate to the dLN to present these antigens to naive T cells, but there was no increase in the number of $EYFP^+$ Mig DCs in the dLN in response to Gem/ATRi (**Figure 3.6b**). To confirm that this fluorescent signal is indeed coming from EYFP, these intratumoural and dLN DCs were also analysed using the Imagestream to localize EYFP fluorescence within these cells. In both intratumoural and dLN DCs, EYFP signal was localized in a punctate pattern, suggesting that these antigens have been taken up into vacuoles (**Figure 3.6c**). In summary, one cycle of Gem/ATRi induces DC activation within the tumour and dLN and increases tumour antigen uptake in intratumoural cDC1. This is however associated with substantial depletion of all intratumoural DC subsets and specific depletion of LN-resident DCs.

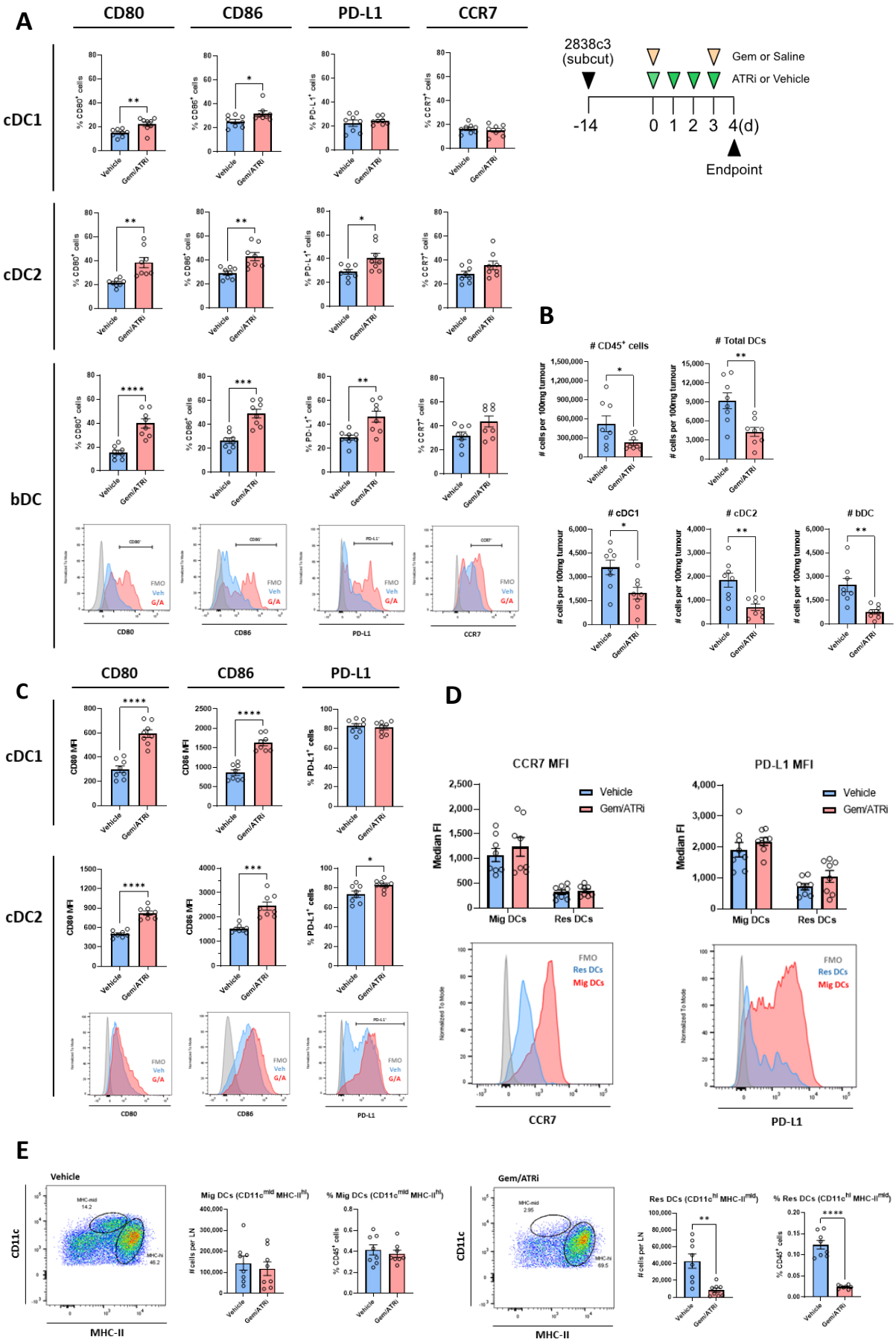
A
CD80
CD86
PD-L1
CCR7
cDC1
cDC2
bDC
2838c3 (subcut)
Gem or Saline
ATRi or Vehicle
-14
0 1 2 3 4(d)
Endpoint
Vehicle
Gem/ATRi
B
CD45+ cells
Total DCs
cDC1
cDC2
bDC
cells per 100mg tumour
C
CD80 MFI
CD86 MFI
% PD-L1+ cells
FMO
Veh
G/A
D
CCR7 MFI
PD-L1 MFI
Median FI
Mig DCs
Res DCs
FMO
Res DCs
Mig DCs
CCR7
PD-L1
E
Vehicle
Gem/ATRi
CD11c
MHC-II
Mig DCs (CD11c^mid MHC-II^hi)
% Mig DCs (CD11c^mid MHC-II^hi)
Res DCs (CD11c^hi MHC-II^mid)
% Res DCs (CD11c^hi MHC-II^mid)
# cells per LN
% CD45+ cells

Figure 3.5. Gem/ATRi induces DC activation in 2838c3 tumour and tumour-draining lymph node (dLN). 2838c3 KPCY tumour cells were implanted subcutaneously into the right flank of C57BL/6 mice and dosed with Gem/ATRi as indicated in the schematic. Tumours and their draining inguinal lymph node were taken 24 hours after the final dose for flow cytometry analysis. (A) Expression of activation markers CD80, CD86, PD-L1 and CCR7 on cDC1, cDC2 and bDC in the tumour. (B) Quantification of $CD45^+$ cells, total DCs and DC subsets (cDC1, cDC2 and bDC) in the tumour. (C) Expression of activation markers CD80, CD86 and PD-L1 on Mig DCs in the dLN. (D) Comparison of CCR7 and PD-L1 expression between Mig DCs and Res DCs in the dLN. (E) Changes in the number of Mig DCs and Res DCs in the dLN in response to Gem/ATRi. Two-tailed unpaired t-test was used to determine statistical significance. Error bars indicate mean ± SEM. *, $P < 0.05$, **, $P < 0.01$, ***, $P < 0.001$, ****, $P < 0.0001$.

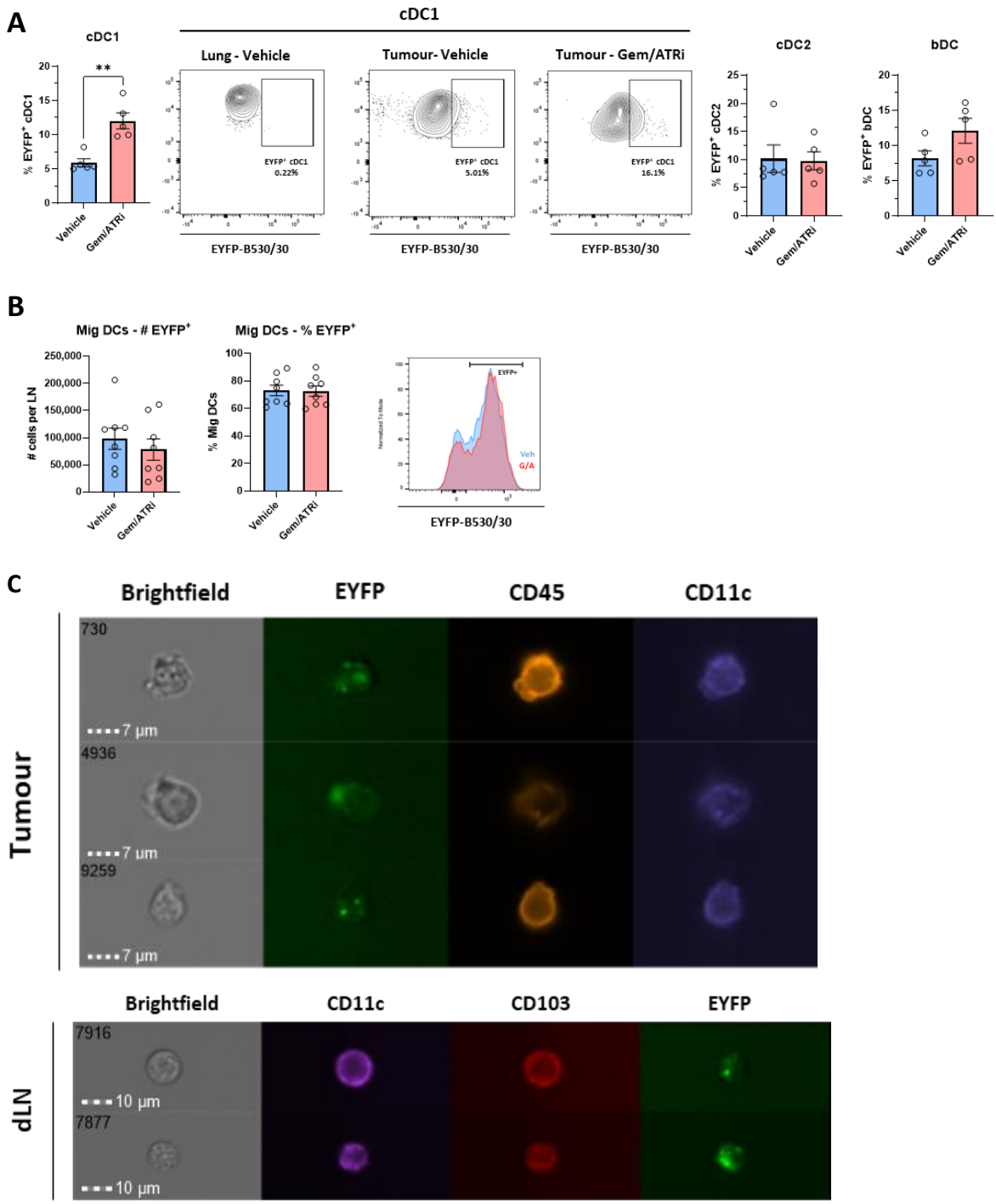

Figure 3.6. Gem/ATRi promotes the uptake of tumour antigens in intratumoural cDC1. 2838c3 tumours were implanted and dosed as in Fig 3.5. Tumours and their draining inguinal lymph node were taken 24 hours after the final dose for flow cytometry analysis. (A) Quantification of EYFP$^+$ DCs in the tumour. Lung cDC1 and cDC2 were used as negative controls to set the gate for EYFP positivity. (B) Quantification of EYFP$^+$ Mig DCs in the draining lymph node. (C) Imagestream analysis of intratumoural and dLN DCs to visualize intracellular EYFP localization. Two-tailed unpaired t-test was used to calculate significance. Error bars indicate mean ± SEM. **, $P < 0.01$.

To further investigate the effect of Gem/ATRi on DC antigen uptake and processing, a pilot experiment was performed using DQ ovalbumin (DQ-OVA). DQ-OVA is a conjugate of ovalbumin and BODIPY FL dye which fluoresces strongly upon proteolytic degradation. Antigen processing in DCs can therefore be quantified via detection of BODIPY FL fluorescence. However, the excitation/emission spectra of BODIPY FL (505/515 nm) is highly similar to EYFP (513/527 nm), therefore it was not possible to differentiate between EYFP and BODIPY FL fluorescence using conventional flow cytometers. DQ-OVA was directly injected into the tumour, followed by flow cytometry analysis of the tumour, dLN and non-draining lymph node (ndLN, inguinal lymph node on contralateral flank) 24 hours post-injection. As a positive control, lung DCs pulsed *in vitro* with DQ-OVA were also included in the analysis. While strong EYFP/DQ-OVA fluorescence was observed in lung DCs pulsed with DQ-OVA, there was only a slight increase in signal in DCs taken from tumours injected with DQ-OVA compared to PBS-injected tumours (**Figure 3.7a**). The same was observed in the dLN, where there was no difference in MFI between DCs from DQ-OVA or PBS-injected mice (**Figure 3.7b**). There was a small subset (~1%) of Mig DCs which showed higher fluorescence signal in DQ-OVA injected mice which was absent in PBS-injected mice, but there were doubts whether this was a real population of cells as the events recorded were very scattered. Due to the low signal and potential interference with EYFP fluorescence, work with DQ-OVA was no longer pursued.

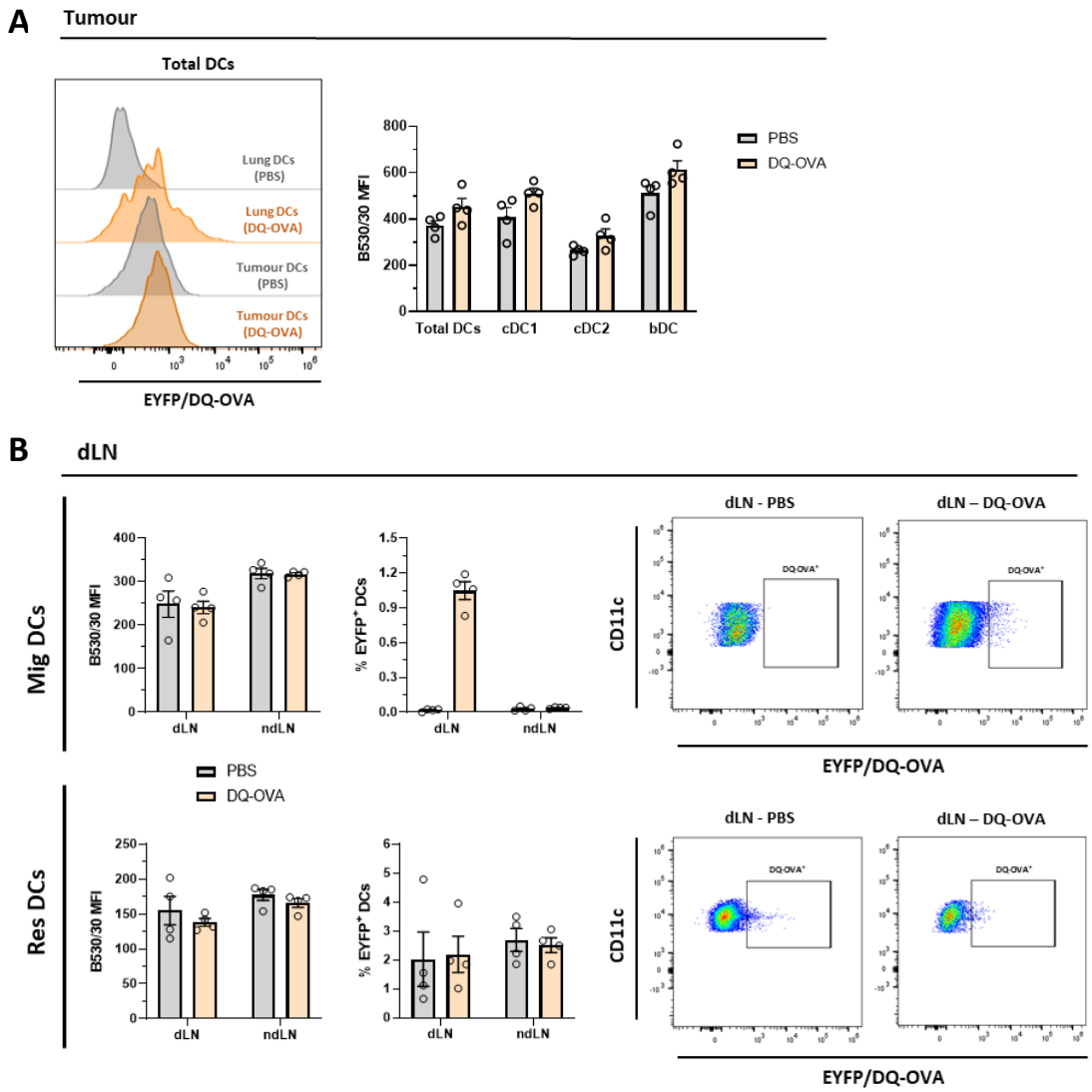

Figure 3.7. Difficulty in distinguishing between DQ-OVA and tumour-derived EYFP fluorescence. 2838c3 KPCY tumour cells were implanted subcutaneously into the right flank of WT mice and left to grow for 14 days. 50 µg of DQ-OVA or PBS was directly injected into the tumours, and tissues (tumour, dLN and non-draining lymph node (ndLN)) were taken for flow cytometry analysis 24 hours post-injection. Single-cell suspensions of lung tissue were pulsed with either 20 µg/ml DQ-OVA or PBS at 37°C for 45 minutes as a positive control. (A) Comparison of fluorescence intensity in the B530/30 channel between intratumoural DCs isolated from DQ-OVA or PBS-treated tumours, with lung DCs as a control. (B) Comparison of fluorescence intensity in the B530/30 channel between DCs in the dLN and ndLN.

3.5. Differential effect of Gem/ATRi on intratumoural CD8$^+$ and CD4$^+$ T cells

When DCs take up antigens and become activated, they then present these antigens to naïve T cells to initiate antigen-specific adaptive immunity. Given that intratumoural and dLN Mig DCs are activated by Gem/ATRi, I proceeded to investigate the downstream effect of DC activation by characterizing the intratumoural T cell population one week post-dosing in genetically engineered AgRSR mice (kindly provided by Dr James Thaventhiran). In this mouse model, TCR activation in the presence of tamoxifen leads to permanent expression of EYFP in the activated T cell clone and its progeny. It is thus possible to quantify the number of T cells that have been newly primed in the timeframe during which tamoxifen is present. Tumour-bearing AgRSR mice were randomized into 5 groups and dosed with Gem/ATRi and tamoxifen as indicated in the schematics, followed by flow cytometry analysis of tumours at endpoint (**Figure 3.8a**). Gem/ATRi administration increased intratumoural CD8$^+$ and CD4$^+$ T cell infiltration one week post-dosing (**Figure 3.8b & 3.8c**). The second cycle of Gem/ATRi depleted CD8$^+$ T cells to baseline levels, and their numbers do not increase even after 1 week of recovery. The similar number of EYFP$^+$ CD8$^+$ T cells between groups D and E suggests that the second cycle of Gem/ATRi permanently impairs proliferation of T cells primed during the first cycle. This is in contrast to CD4$^+$ T cells which were depleted after the second cycle but were able to re-populate after 1 week. EYFP$^+$ CD4$^+$ T cells primed during the first cycle were also able to continue proliferating after the second cycle of Gem/ATRi. As this pilot experiment included a small number of mice, a follow-up experiment was initiated to confirm these findings. Tumour-bearing C57BL/6 mice were dosed with one cycle of Gem/ATRi or vehicle, followed by flow cytometry analysis of tumours and dLN one week post-dosing (using the schematics of groups A & B from the previous experiment). Unexpectedly, Gem/ATRi led to the depletion of intratumoural CD8$^+$ T cells and had no effect on CD4$^+$ T cell numbers (**Figure 3.8d**). In the dLN, CD4$^+$ and CD8$^+$ T cell numbers were unaffected by Gem/ATRi (**Figure 3.8e**). Assessment of various activation/exhaustion markers on intratumoural CD8$^+$ T cells revealed a decrease in the percentage of PD-1- and CD39-expressing cells coupled with an increased proportion of proliferating (Ki-67$^+$) cells in response to Gem/ATRi (**Figure 3.8f**). There were no significant changes in these markers for CD8$^+$ T cells in the dLN (data not shown). Taken together with the CD8 and CD4 IHC results obtained from the survival study (**Figure 3.4b**), it seems that Gem/ATRi has a depleting effect on intratumoural CD8$^+$ T cells but not CD4$^+$ T cells. Additionally, a decrease in the proportion of CD39- and PD-1-expressing CD8$^+$

T cells in Gem/ATRi-treated tumours suggests that Gem/ATRi may selectively deplete exhausted CD8⁺ T cells within the tumour.

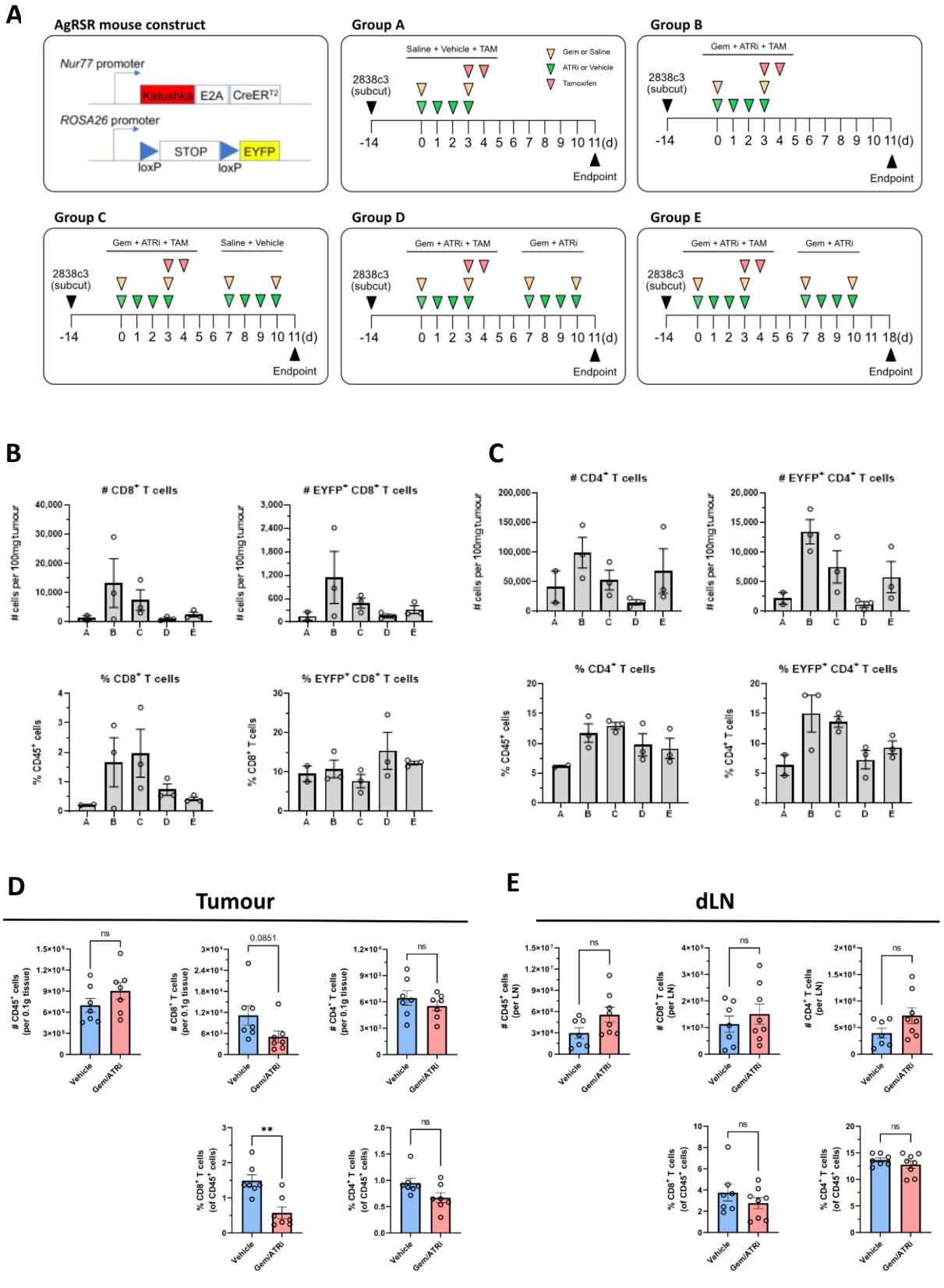

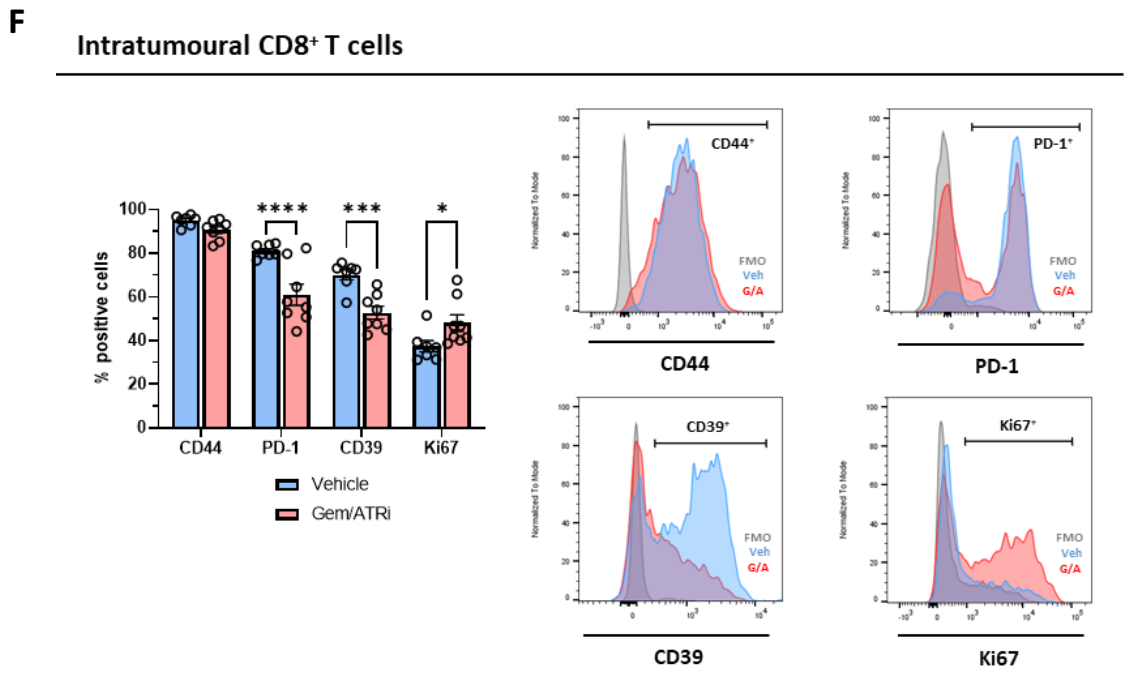

Figure 3.8. Gem/ATRi depletes intratumoural CD8⁺ T cells but has no effect on CD4⁺ T cells. (A) 2838c3 tumours were implanted in AgRSR mice and dosed with Gem/ATRi or vehicle followed by flow cytometry analysis at endpoint as indicated in the schematics. The AgRSR mouse transgenic construct is also shown. (B) Quantification of intratumoural CD8⁺ and (C) CD4⁺ T cells. (D) 2838c3 tumours were implanted in C57BL/6 mice and dosed with Gem/ATRi or vehicle as in group A and B of schematic in (A), followed by flow cytometry analysis of tumours and dLN one week after the final dose. Graphs show quantification of CD8⁺ and CD4⁺ T cells in the tumour and (E) dLN. (F) Expression of CD44, PD-1, CD39 and Ki-67 in intratumoural CD8⁺ T cells. Two-tailed unpaired t tests were used to determine statistical significance. Error bars indicate mean ± SEM. *, P < 0.05, **, P < 0.01, ***, P < 0.001, ****, P < 0.0001.

3.6. Intratumoural cDC1 dysregulation in 6419c5 ‘T cell low' pancreatic tumours

As mentioned previously, the 2838c3 cell line is part of a library of clones generated by the Stanger lab, and it is a ‘T cell high’ clone which gives rise to tumours that have a relatively high T cell infiltrate and is responsive to chemo-immunotherapy. As part of this library they've also generated T cell 'intermediate' and 'low' cell lines which give rise to tumours with lower T cell infiltrates and are less responsive to the same chemo-immunotherapy regimen[123]. As they've also shown the importance of cDC1 in determining response to this therapy in the 2838c3 tumour model, intratumoural cDC1 dysregulation may be one of the reasons why their chemo-immunotherapy regimen failed in the T cell low model. Given this difference in response between the 2838c3 ‘T cell high' clone and 6419c5 ‘T cell low' clone, I then

compared if Gem/ATRi administration had a different effect on DC activation in these two models.

To investigate the effect of Gem/ATRi on intratumoural DCs in 6419c5 tumours, flow cytometry analysis was performed 24 hours after one cycle of Gem/ATRi. Intriguingly, intratumoural cDC1 in 6419c5 tumours did not show upregulation of CD80 or CD86 in response to Gem/ATRi (**Figure 3.9**). In contrast, cDC2 and bDC showed upregulation of both markers. As was observed in 2838c3 tumours, all DC populations were depleted by Gem/ATRi. As Gem/ATRi was able to induce CD80 and CD86 upregulation in 2838c3 cDC1, there seems to be a difference between the phenotype of cDC1 in 2838c3 and 6419c5 tumours. To validate this finding, tumour-bearing mice were dosed with agonistic aCD40 antibody as CD40 activation is well known to strongly activate intratumoural DCs[67]. Intratumoural DC populations were characterized 14hr and 24hr post-dosing, and at both timepoints, aCD40 antibody induced a greater upregulation of CD80 and CD86 in 2838c3 cDC1 compared to 6419c5 cDC1 (**Figure 3.10**). The CD86 histogram shows that the entire bulk of cDC1 in 2838c3 tumours was able to upregulate CD86 at the 24hr timepoint, whereas in 6419c5 tumours a significant proportion of cDC1 remain unresponsive to CD40 stimulation. The same trend was observed in CD80 expression. 2838c3 cDC1 also showed greater upregulation of CCR7 compared to 6419c5 cDC1 at the 24hr timepoint. It is interesting to note that at baseline (in isotype-treated mice), cDC1 in both 2838c3 and 6419c5 tumours express similar levels of co-stimulatory molecules and the dysfunction is only apparent upon stimulation. Given that Gem/ATRi and aCD40 are likely activating DCs via different mechanisms, I then combined Gem/ATRi and aCD40 to determine if both agents used together can overcome the dysfunctional phenotype observed in 6419c5 cDC1s. In this experiment, aCD40 was given 24hr after the final dose of Gem/ATRi and tumours were analysed 24hr after aCD40 dosing. cDC1 in 2838c3 tumours strongly responded to this combination and upregulated both CD86 and CD80 at much higher levels compared to cDC1 in 6419c5 tumours (**Figure 3.11**). DCs in groups B and E (mice dosed with only Gem/ATRi) show no activation compared to controls, which suggests that the activation signal provided by one cycle of Gem/ATRi is no longer detectable 48 hours after the final dose.

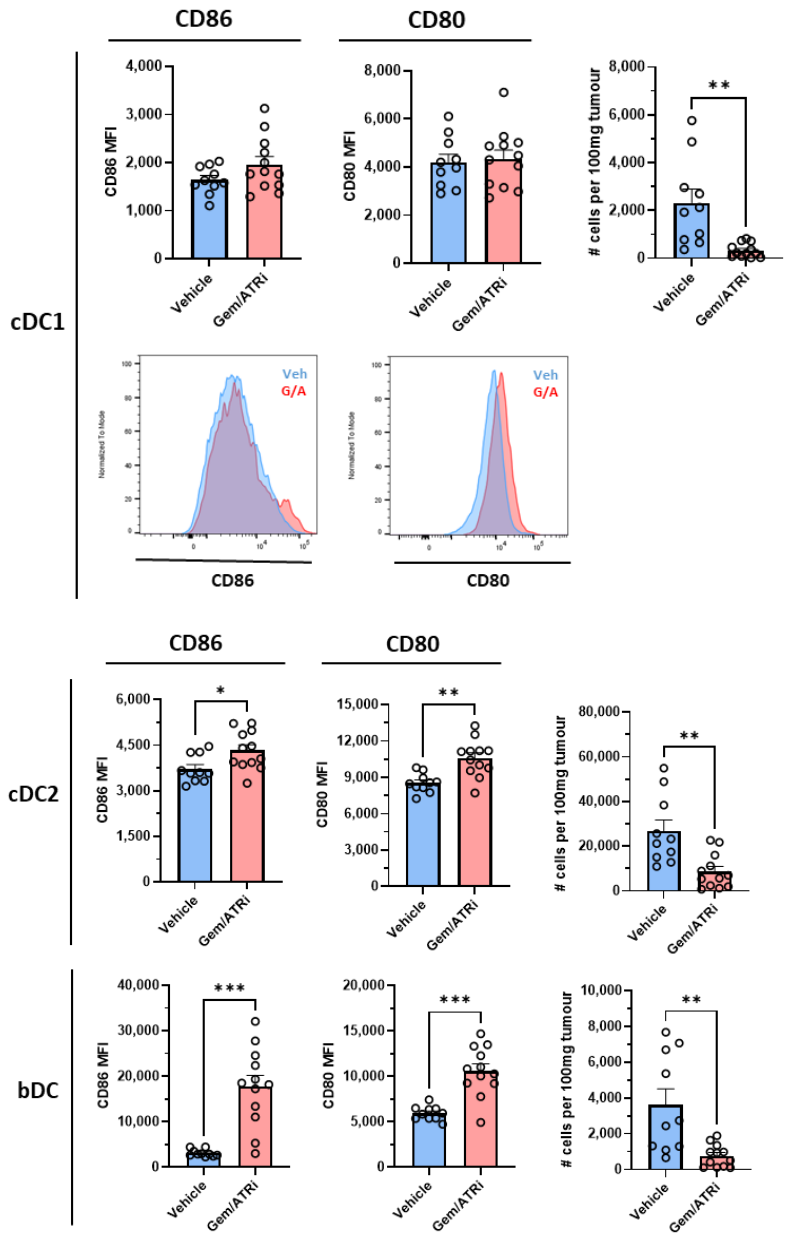

Figure 3.9. Gem/ATRi induces activation of cDC2 and bDC but not cDC1 in 6419c5 tumours. 6419c5 KPCY tumour cells were implanted subcutaneously into the right flank of C57BL/6 mice and dosed with Gem/ATRi as in Fig 3.5. Expression of CD86 and CD80 on intratumoural cDC1, cDC2 and bDC are shown. Two-tailed unpaired t test was used to determine statistical significance. Error bars indicate mean ± SEM. *, $P < 0.05$; **, $P < 0.01$; ***, $P < 0.001$.

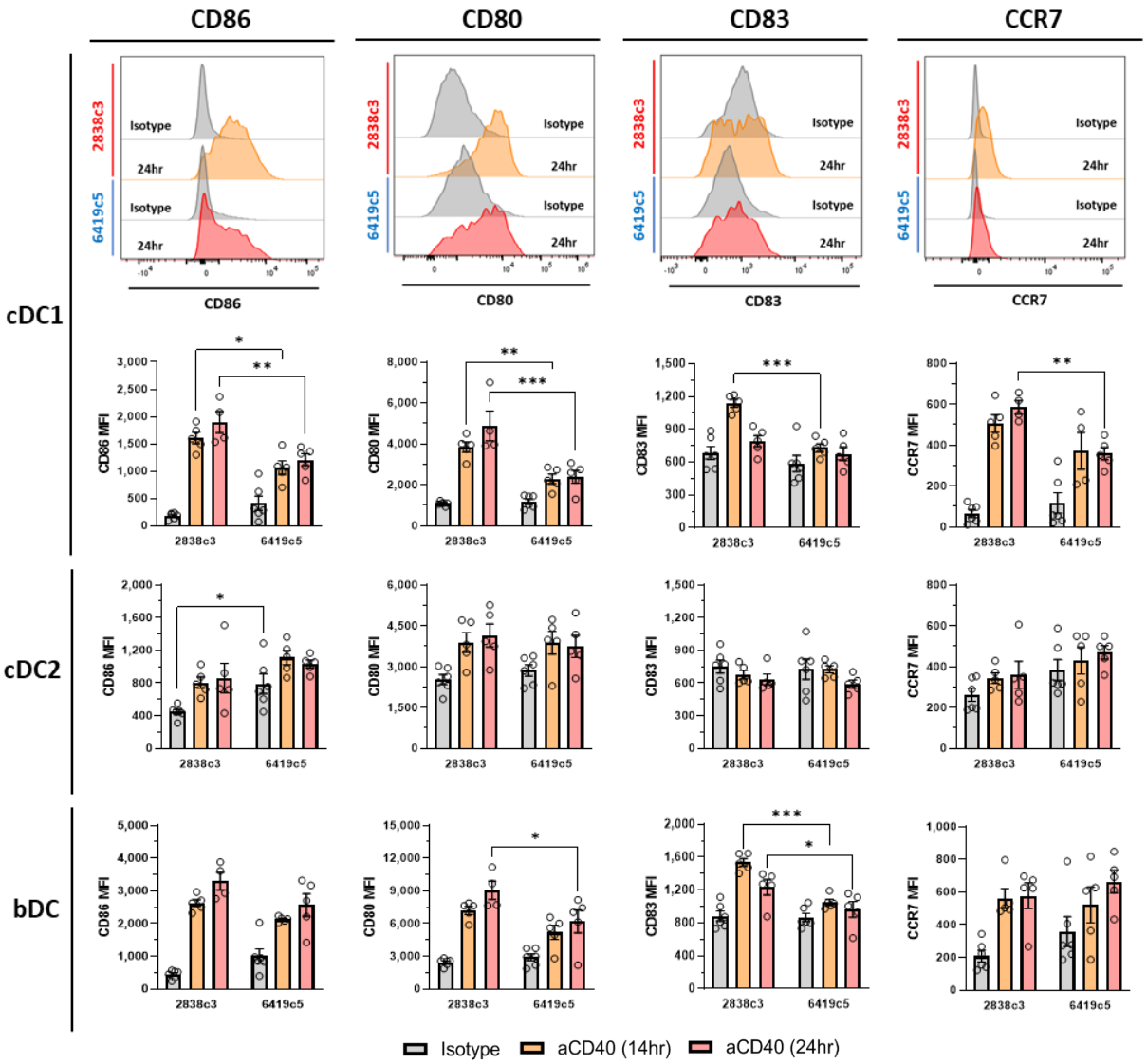

Figure 3.10. A significant proportion of cDC1 in 6419c5 tumours are unresponsive to aCD40 stimulation. 6419c5 or 2838c3 KPCY tumours were implanted subcutaneously into the right flank of C57BL/6 mice and left to grow for 14 days before receiving 100µg isotype or anti-CD40 agonistic antibody. Mice were culled 14 hours or 24 hours post-injection and tumours were taken for flow cytometry analysis. Comparison of CD86, CD80, CD83 and CCR7 expression between cDC1, cDC2 and bDC in 2838c3 and 6419c5 tumours. Two-way ANOVA with Šídák's multiple comparison test was used to determine statistical significance. Error bars indicate mean ± SEM. *, $P < 0.05$; **, $P < 0.01$; ***, $P < 0.001$.

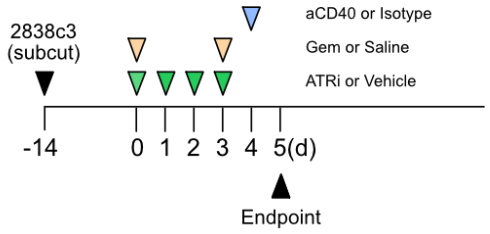

Group	Tumour	Vehicle/Gem/ATRi	Isotype/aCD40
A	2838c3	Vehicle	Isotype
B	2838c3	Gem/ATRi	Isotype
C	2838c3	Gem/ATRi	aCD40
D	6419c5	Vehicle	Isotype
E	6419c5	Gem/ATRi	Isotype
F	6419c5	Gem/ATRi	aCD40

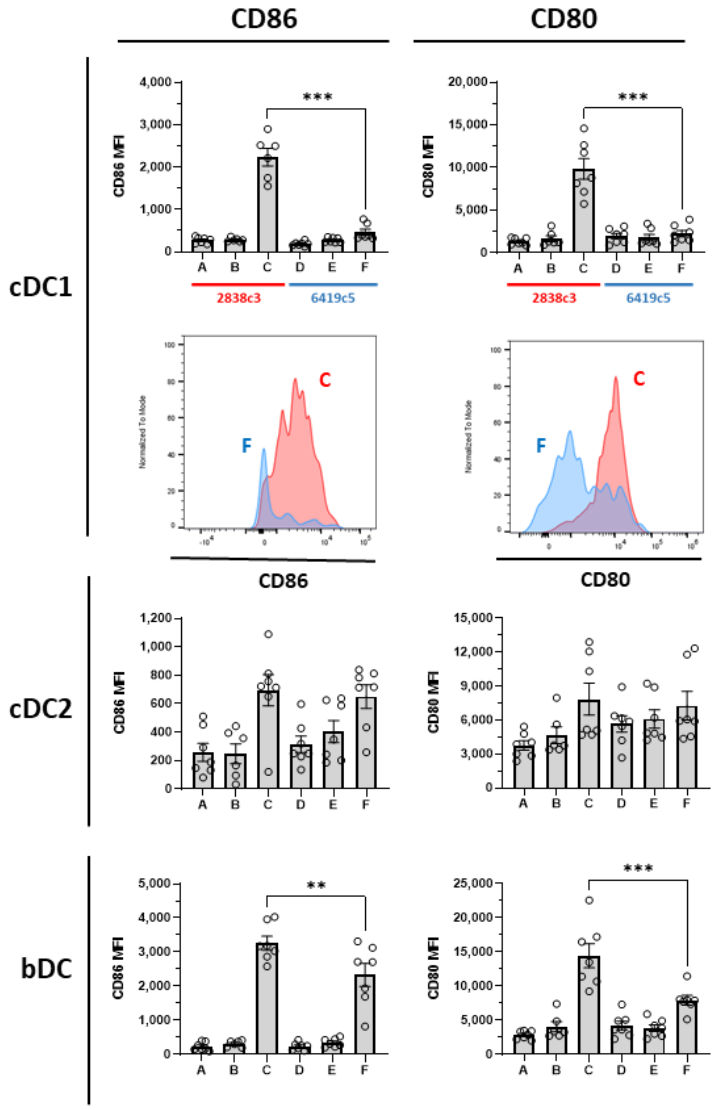

Figure 3.11. A significant proportion of cDC1 in 6419c5 tumours are unresponsive to Gem/ATRi in combination with aCD40. 6419c5 or 2838c3 KPCY tumours were implanted subcutaneously into the right flank of C57BL/6 mice and left to grow for 14 days before randomization into 6 experimental groups as indicated in the schematic. Flow cytometry analysis was performed to compare CD86 and CD80 expression between intratumoural cDC1, cDC2 and bDC in 2838c3 and 6419c5 tumours. Two-way ANOVA with Šídák's multiple comparison test was used to determine statistical significance. Error bars indicate mean ± SEM. **, $P < 0.01$; ***, $P < 0.001$.

3.7. DC activation in response to Gem/ATRi is not mediated by STING pathway activation

Bulk RNA-seq analysis of KPC tumours dosed with Gem/ATRi showed an upregulation of T1IFN signalling in responders compared to non-responders (**Figure 3.2**), and of the many mechanisms by which chemotherapy may induce T1IFN signalling, a growing number of reports have shown that the STING-TBK1-IRF3 pathway is activated by chemotherapeutic agents[204]. Gem/ATRi induces DNA damage in pancreatic cancer cells, and this may lead to the accumulation of cytosolic DNA that activates the STING pathway. To investigate the expression of STING pathway proteins in pancreatic cancer cells, a panel of 5 pancreatic cancer cell lines (with 4T1 breast cancer cells as a positive control)[181] were dosed with the murine STING agonist 5,6-dimethylxanthenone-4-acetic acid (DMXAA) *in vitro* and processed for Western blotting. Surprisingly, STING protein was detected in 6620c1 (one of the 'T cell high' cell clones of the Stanger library) and MiaPaCa-2 (human PDAC cell line) cells, but not in 2838c3, 6419c5 or K8484 (KPC PDAC cell line) cells (**Figure 3.12a**). However, TBK1 (a downstream target of STING) was expressed in all cell lines. Exposure to DMXAA led to STING activation in 6620c1 cells as shown by pSTING and pTBK1 positivity in these cells. STING activation in MiaPaCa-2 cells was not expected as DMXAA only binds to murine STING[205]. Given that the loss of STING expression in pancreatic cancer cells has not been previously reported in the literature, qPCR analysis was used to determine expression of the STING mRNA (*Tmem173*) in STING-deficient 2838c3 and 6419c5 cells. Results showed that 4T1 cells express *Tmem173* at much higher levels compared to 2838c3 and 6419c5, which supports findings at the proteomic level (**Figure 3.12b**).

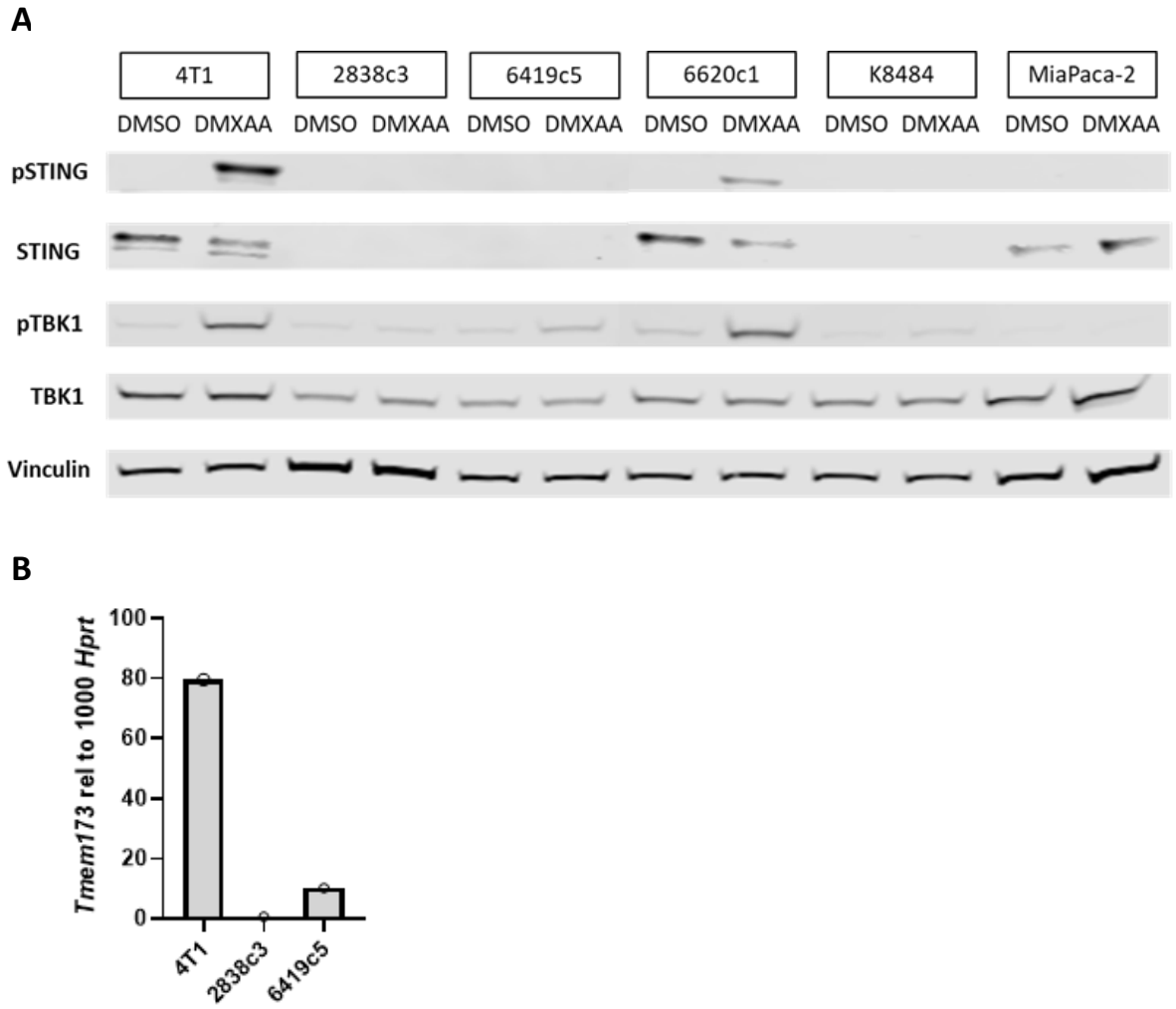

Figure 3.12. STING protein expression varies between KPC and human PDAC-derived cell lines. (A) A panel of murine KPC-derived (2838c3, 6419c5, 6620c1, K8484) and human PDAC-derived (MiaPaCa-2) cell lines were dosed with DMSO or 50ug/ml DMXAA *in vitro* for 30 minutes followed by protein extraction for western blot to determine expression of STING pathway proteins (STING, TBK1) and their phosphorylated/activated forms (pSTING, pTBK1). 4T1 cells were included as a positive control. (B) qPCR analysis was performed on RNA extracted from 4T1, 2838c3 and 6419c5 cells to determine mRNA expression of STING (*Tmem173*). *Hprt* was used as a reference gene. Each data point is a biological replicate (derived from the mean of three technical replicates).

Even though 2838c3 and 6419c5 tumour cells did not express detectable levels of STING protein, the STING pathway might still have a role in Gem/ATRi-mediated intratumoural DC activation *in vivo* as there are many other cell types within the tumour microenvironment which express STING[206]. 2838c3 and 6419c5 tumour-bearing mice were therefore dosed with one cycle of Gem/ATRi and the tumours taken for protein extraction 24 hours after the final dose to determine the presence of activated STING protein. In all samples, STING, TBK1 and IRF3 were detected but no Gem/ATRi-mediated STING pathway activation was observed (**Figure 3.13a**). All samples showed constitutive activation of TBK1 and in 6419c5 tumours there was a low level of constitutive IRF3 activation. RNA was also extracted from these 2838c3 tumours to compare the expression of IFN-related genes (*Ifna4, Ifnb1* and *Irf7*) between vehicle- and Gem/ATRi-treated tumours but no significant differences were found (**Figure 3.13b**).

Many pathways of chemotherapy-mediated DC activation have been described in the literature, but the majority of these pathways ultimately converge on the expression of T1IFNs. 2838c3 and 6620c1 cells were therefore dosed *in vitro* with gemcitabine, ATRi, Gem/ATRi or DMXAA for 72 hours and the cell culture supernatant taken for IFN-β ELISA. However, both cell lines did not produce detectable levels of IFN-β under any condition (**Figure 3.14**). Surprisingly, 6620c1 cultures dosed with DMXAA were also negative for IFN-β even though it had detectable levels of STING protein. The 24-hour timepoint was also tested for all conditions but similarly no IFN-β was detected (data not shown).

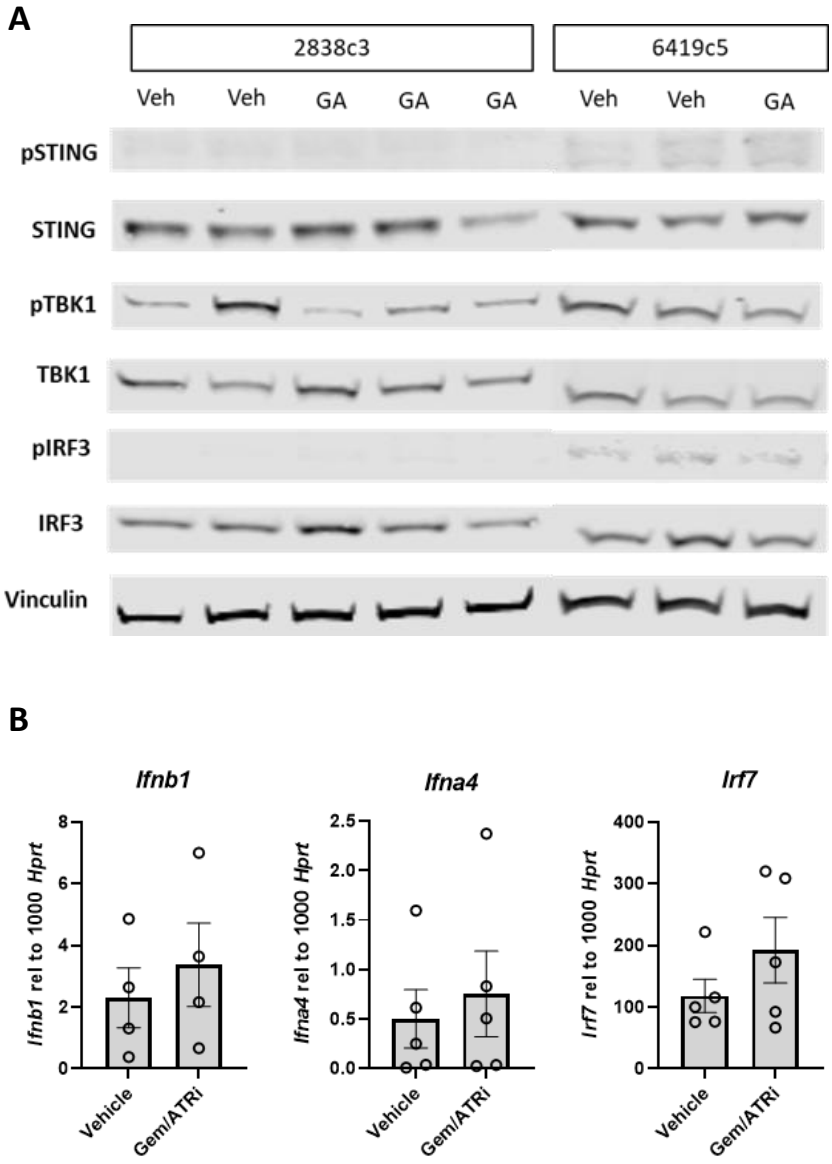

Figure 3.13. Gem/ATRi does not induce STING pathway activation in 2838c3 and 6419c5 tumours. 2838c3 and 6419c5 KPCY tumours were implanted subcutaneously into the right flank of C57BL/6 mice and dosed with one cycle of Gem/ATRi at day 14. Tumours were taken 24 hours after the final dose for protein and RNA extraction. (A) Western blot analysis of 2838c3 and 6419c5 tumour protein extracts to determine STING pathway protein expression and activation. (B) qPCR analysis of RNA extracted from 2838c3 tumours to quantify expression of *Ifna4, Ifnb1* and *Irf7* in these tumours. *Hprt* was used as a reference gene. Two-tailed unpaired t test was used to determine statistical significance. Error bars indicate mean ± SEM. GA, Gem/ATRi.

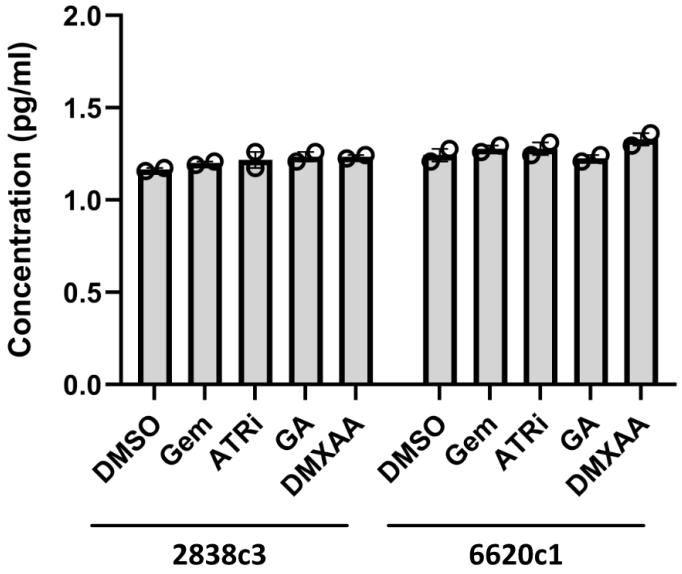

Figure 3.14. Gem/ATRi does not induce IFN-β production in 2838c3 and 6620c1 tumour cells. 2838c3 and 6620c1 tumour cells were dosed *in vitro* with DMSO, Gem, ATRi, Gem/ATRi or DMXAA and cell culture supernatant was taken for IFN-β ELISA after 72 hours. Each data point is a biological replicate (derived from the mean of two technical replicates).

To determine whether Gem/ATRi can directly activate DCs, I cultured cDC1 from mouse bone marrow cells using the protocol described in Mayer et al (2014)[126]. Bone marrow cells were cultured *ex vivo* for 14 days and subsequently characterized by flow cytometry (**Figure 3.15a**). As described in the publication, this protocol generates cultures which are 90% $CD103^+$ cDC1 (expressing moderate levels of MHC-II, 'MHC-II mid'), with a ~7% MHC-II high population resembling a mixed population of activated DCs. The yield of cDC1 was 3-4 million cells per culture and these bone marrow-derived DCs (BMDCs) were used in downstream *in vitro* assays to investigate Gem/ATRi-mediated DC activation. BMDCs were cultured with or without the presence of 2838c3 tumour cells and dosed with DMSO, Gem/ATRi or poly-I:C (pIC) as a positive control for 5 hours. While pIC-dosed DCs showed robust upregulation of CD86, CD80 and PD-L1, there was no difference between vehicle- and Gem/ATRi-dosed cells (**Figure 3.15b**). Two subsequent experiments were performed to try longer timepoints (8hr and 16hr dosing), but in these longer timepoints the majority of DCs were found to be dead at the end of the experiment (data not shown). The poor viability of these *in vitro* cultured bone marrow-derived DCs precluded any further extended drug dosing experiments.

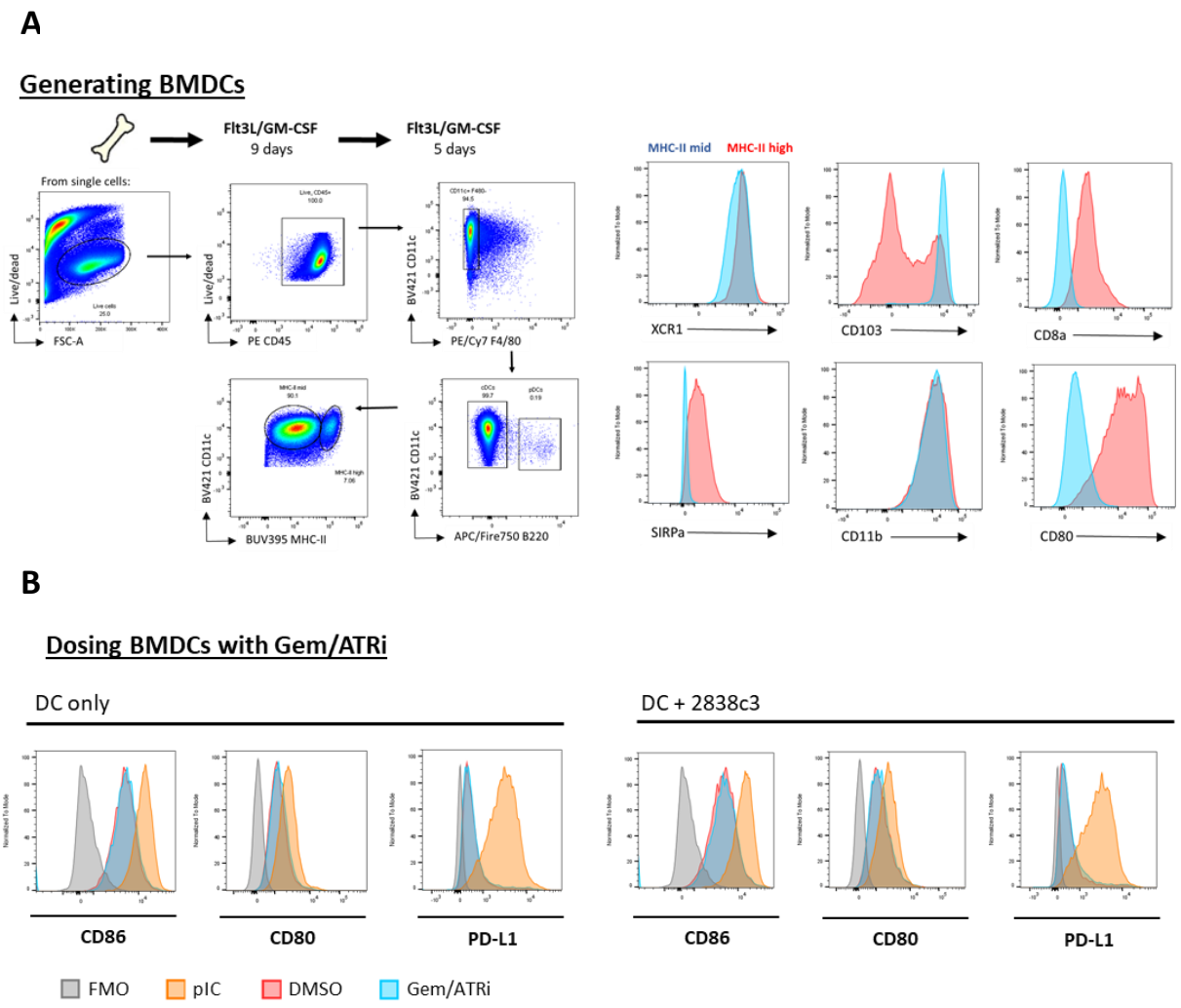

Figure 3.15. Poor viability of *in vitro* cultured bone marrow-derived DCs precludes extended drug dosing experiments. Bone marrow-derived DCs (BMDCs) were generated by culturing bone marrow cells in media containing Flt3L and GM-CSF for 9 days, followed by re-plating of non-adherent cells in Flt3L and GM-CSF media for an additional 5 days. (A) Flow cytometry characterization of BMDCs after 14-day culture. (B) BMDCs with or without 2838c3 tumour cells were cultured in vitro with either DMSO, Gem + ATRi or poly-I:C (pIC) for 5 hours and harvested for flow cytometry analysis.

Discussion

The priming of tumour-specific T cells by DCs is one of the first events in the cancer-immunity cycle and is a key step in the initiation of $CD8^+$ T cell-dependent anti-tumour immunity[150]. Although chemotherapy has long been considered immunosuppressive and counterproductive to anti-tumour immunity, much preclinical work has now demonstrated the potential synergy between chemotherapy and immunotherapy[207]. Results in this chapter show that Gem/ATRi can induce DC activation and antigen uptake within the tumour, although the extent of DC activation differs between tumour models. Notably, repeated cycles of Gem/ATRi depletes intratumoural $CD8^+$ T cells but spares $CD4^+$ T cells.

3.8. Effect of Gem/ATRi on intratumoural DCs

Some commonly used chemotherapeutic agents (such as oxaliplatin[208], fluorouracil[208], anthracyclines[171] and vinblastine[165]) have been shown to induce intratumoural DC maturation in various mouse models, and results from this chapter shows that the combination of Gem/ATRi has a similar immunostimulatory effect. Although co-stimulatory molecule upregulation on intratumoural DCs is generally considered to have a positive effect on anti-tumour immunity, it is difficult to accurately infer the downstream effect of Gem/ATRi-mediated DC activation by solely assessing co-stimulatory molecule expression. The process of DC maturation involves many distinct but interconnected pathways, including changes in the antigen uptake and processing machinery, antigen presentation via MHC class I/II, upregulation of co-stimulatory molecules and cytokine production. Additionally, DC activation is not a binary state but rather a spectrum, such that some DCs exist in an intermediate state of DC maturation (known as semi-mature DCs) – these DCs may have undergone phenotypic maturation (i.e. upregulation of co-stimulatory molecules) but not functional maturation (i.e. production of pro-inflammatory cytokines) or vice versa, and these DCs have been shown to play ambivalent roles in shaping the anti-tumour immune response[209]. Given that DCs are able to secrete inflammatory (e.g. IL-12, IL-1β etc.) or immunosuppressive (e.g. IL-10, TGF-β etc.) cytokines under different conditions and that co-stimulatory molecule expression does not always correlate with pro-inflammatory cytokine production, it would have been very informative to assess DC cytokine production to obtain a better picture of how DCs functionally respond to Gem/ATRi.

Although intratumoural DCs in PDAC are highly heterogeneous, the bulk DC population has been shown to be pro-tumourigenic as systemic DC depletion using the CD11c-DTR mouse model reduces PDAC growth[68]. This is unsurprising given that only the $CD103^+$ $CD11b^-$ cDC1 subset is known to promote anti-tumour immunity but they make up less than 10% of the intratumoural DC population. $CD103^-$ $CD11b^+$ cDC2 and $CD103^+$ $CD11b^+$ bDC make up ~80% of the intratumoural DC population, and these DCs are thought to primarily produce cytokines such as IL-6, TGF-β and IL-17A[68]. These cytokines have been associated with cDC1 dysfunction[67] and Treg/Th17 skewing of $CD4^+$ T cells (which is associated with PDAC progression[70,72,88]). If cDC2 and bDC activated by Gem/ATRi are primed to produce these cytokines, this might act to instead promote tumour progression. To clarify this, *ex vivo* DC-T cell co-culture experiments using DCs isolated from tumours treated with Gem/ATRi could have been done to further investigate how these activated DCs influence naïve $CD4^+$ T cell polarization *in vitro*. A more in-depth characterization of intratumoural $CD4^+$ T helper cell populations in response to Gem/ATRi would also be useful in determining how Gem/ATRi influences $CD4^+$ T cell polarization *in vivo*. As for cDC1, DC-T cell co-culture experiments would be useful to determine if Gem/ATRi promotes $CD8^+$ T cell priming, proliferation and effector function.

$CD103^+$ $CD11b^+$ DCs in PDAC tumours were first characterized by Barilla and colleagues[68] and to my knowledge they have not been discussed in other PDAC-related publications. $CD103^+$ $CD11b^+$ DCs were previously thought to be a subset unique to the intestinal mucosa and its draining lymphoid tissues, and they have been shown to be ontogenically distinct from the $CD103^+$ $CD11b^-$ cDC1 population. They were implicated in the priming of $Foxp3^+$ Tregs and Th17 cells in the intestinal mucosa, and they differentiate locally from $CD103^-$ $CD11b^+$ cells in response to TGF-β signalling[203]. My results support these findings as I have not been able to detect a similar population of $CD103^+$ $CD11b^+$ DCs in the lung, spleen, blood or pancreas of tumour-bearing mice via flow cytometry. Intriguingly, I was able to identify these DCs in both subcutaneous and orthotopic (pancreatic) tumours, indicating that they are not exclusive to the skin or pancreas. It is therefore likely that they are recruited from the circulation in an 'immature' state and differentiate locally into $CD103^+$ $CD11b^+$ DCs in the TGF-β rich TME.

In addition to activating DCs, Gem/ATRi also caused a substantial depletion of all DC subsets within the tumour. This is in contrast to findings with other forms of chemotherapy, where an enrichment of intratumoural DCs after anthracycline[171] or cyclophosphamide[210] therapy was reported. A decrease in tissue-resident DCs after a stimulus can usually be explained by their migration to the draining lymph node, but I did not find an increase in migratory DCs (CD11c^{mid} MHC-II^{hi} DCs) within the tumour dLN post-Gem/ATRi. Alternative explanations include a direct cytotoxic effect of Gem/ATRi on intratumoural DCs, or that intratumoural DCs undergo activation-induced apoptosis[211,212]. These hypotheses could have been studied *in vitro* using bone marrow-derived DCs, but poor viability of these DCs in culture precluded any such experiments.

3.9. Effect of Gem/ATRi on the anti-tumour T cell response

As cDC1s have been shown to promote intratumoural CD8$^+$ T cell infiltration via production of CXCL9/10[155], it was hypothesized that Gem/ATRi-mediated cDC1 activation in 2838c3 tumours will lead to an increase in intratumoural CD8$^+$ T cells. However, flow cytometry analysis of tumours after one cycle of Gem/ATRi showed a slight decrease in intratumoural CD8$^+$ T cells, and this was consistent with immunohistochemistry data from tumours that have received 3 consecutive cycles of Gem/ATRi. Although this was unexpected, considering that 2838c3 tumours are already highly infiltrated by CD8$^+$ T cells at baseline, a further increase in CD8$^+$ T cell infiltration (in response to Gem/ATRi) might not necessarily be a reliable measure of DC-T cell engagement. A more detailed phenotypic characterisation of intratumoural CD8$^+$ T cells could have been done to reveal whether increased DC activation was associated with an increase in CD8$^+$ T cell effector function (in terms of cytokine production and degranulation). Indeed, changes in the expression of some CD8$^+$ T cell surface markers post-therapy points towards phenotypic differences induced by Gem/ATRi. Namely, there was a decrease in the proportion of PD-1$^+$ and CD39$^+$ cells and an increase in the proportion of proliferating Ki-67$^+$ cells. As PD-1 and CD39 is used in combination to identify terminally exhausted CD8$^+$ T cells[213,214], Gem/ATRi may be eliminating these exhausted T cells and promoting the repopulation of intratumoural CD8$^+$ T cells from a pool of Ki-67$^+$ cells that retain the capacity for self-renewal. Indeed, chemotherapy-resistant memory CD8$^+$ T cells have been identified in patients undergoing repeated cycles of chemotherapy, and these memory T cells were specifically induced to proliferate in lymphocytopenic patients[215,216]. Perhaps if tumour

immune profiling was performed at a later timepoint, $CD8^+$ T cells would have had more time to repopulate the tumour microenvironment. Although intratumoural $CD8^+$ T cells were depleted one week post-Gem/ATRi dosing, $CD4^+$ T cell numbers were unaffected – this suggests that $CD4^+$ T cells are more resistant to Gem/ATRi-mediated depletion. This might be due to increased local proliferation of intratumoural $CD4^+$ T cells or an increased recruitment of these cells into the tumour. To determine the relative contribution of intratumoural proliferation versus extratumoural recruitment, T cells from congenic CD45.1 mice can be intravenously transfused into tumour-bearing CD45.2 mice immediately after one cycle of Gem/ATRi, and the ratio of intratumoural CD45.1 to CD45.2 T cells determined at endpoint.

Regardless of the changes in intratumoural $CD8^+$ T cell number or function, the administration of repeated cycles of Gem/ATRi was found to delay 2838c3 tumour growth. This anti-tumour efficacy is likely not $CD8^+$ T cell-dependent given the drug-induced depletion of these cells, but a survival study involving mice dosed with $CD8^+$ T cell-depleting antibodies prior to Gem/ATRi is required to confirm this hypothesis. A key question that remains unanswered is whether the presence of DCs (and their activation) is necessary for tumour regression in response to Gem/ATRi or if they are just bystanders responding to Gem/ATRi-induced tumour cell death. The dose of Gem/ATRi used in these studies likely has a direct cytotoxic effect on tumour cells (given that a similar dose of Gem/ATRi has been previously shown to delay the growth of MIA PaCa-2 PDAC xenografts in immunodeficient NSG mice[202]) but it is unclear how intratumoural DCs contribute to drug-induced tumour growth delay in 2838c3-bearing immunocompetent mice. This question can be answered using Batf3KO mice[217] which lack cDC1 or CD11c-DTR mice[218] which allows conditional ablation of DCs using diphtheria toxin. Even though 6419c5 tumours harbour dysfunctional cDC1s, it does not have a significant impact on preclinical response to Gem/ATRi as 6419c5 tumours also show significant growth delay when dosed with repeated cycles of Gem/ATRi[219].

3.10. cDC1 dysfunction in pancreatic cancer

cDC1 function in the context of cancer has been increasingly studied in the past decade and it is now widely accepted that cDC1 plays an indispensable role in the development of $CD8^+$ T cell-dependent anti-tumour immunity. Many studies cite cDC1 dysfunction as a major cause of unchecked tumour progression, and various strategies to augment cDC1 number or

function (e.g. Flt3L, anti-CD40 agonists, STING agonists etc.) have shown promising results in preclinical models[67,154,158,192,220,221]. Consequently, many of these strategies to boost cDC1 number or function are now undergoing clinical trials and are frequently used in combination with other forms of immunotherapy such as immune checkpoint inhibitors[222]. My experiments comparing the 2838c3 and 6419c5 tumour models have shown that cDC1 are present in both tumours at similar abundance and express comparable levels of co-stimulatory molecules at baseline, but intratumoural cDC1 in 6419c5 tumours are unresponsive to stimulation - it is tempting to speculate that cDC1 dysregulation contributes to the failure of chemo-immunotherapy in this model. These PDAC cell lines were first generated and characterized in the Stanger lab, and they have since performed further studies to show multiple key immunosuppressive mechanisms that dominate in the T cell 'low' models (including 6419c5), such as tumour-cell intrinsic overexpression of CXCL1[123], EPHA2[223], USP22[224] and EGFR[225]. It is interesting to note that cDC2 and bDC are still amenable to stimulation from Gem/ATRi and aCD40, which suggests that there are different requirements that trigger the maturation process between cDC1 and cDC2/bDC.

3.11. Mechanism of Gem/ATRi-mediated DC activation

RNA-seq data previously generated in the lab (by Charles Dunlop, a previous PhD student) showed that T1IFN signalling was upregulated in KPC tumours responding to Gem/ATRi. As the STING-TBK1-IRF3 pathway is often implicated in T1IFN production in response to DNA damage, my investigation into the mechanism of Gem/ATRi-mediated DC activation focussed on this pathway. It was surprising to find that 2838c3 and 6419c5 tumour cells did not express detectable levels of STING protein, as no prior literature had described the loss of STING in pancreatic cancer cells. The 6620c1 cell line (also a clone from the Stanger library) expressed STING that was activated by DMXAA, suggesting that differential STING expression may contribute to clonal heterogeneity in pancreatic tumours and perhaps specific clones of cancer cells lose STING expression as part of evolution. I was unable to detect activated STING protein in 2838c3 or 6419c5 tumours dosed with Gem/ATRi, nor was there any upregulation of genes associated with a T1IFN response. Curiously, pTBK1 was consistently detected in both cell lines *in vitro* and *in vivo* even though there was no sign of STING activation. This suggests that in this context, TBK1 is not activated by STING in response to innate immune stimuli. Indeed, TBK1 is known to be activated downstream of Axl signalling in pancreatic

cancer cells, leading to TBK1-mediated activation of NF-κB and AKT/mTORC1 pathways that are crucial in sustaining the survival of KRAS-mutant cancer cells[226–228]. Unfortunately I did not have time to investigate other potential mechanisms by which Gem/ATRi may activate intratumoural DCs, but there are many potential candidates (e.g. cytosolic RNA sensing by TLR3[229], TLR4[230] and RIG-I[184], B cell mediated DC activation[231], IL-12 mediated activation[166] etc.). Although most of these pathways ultimately lead to IFN-β expression, I was unable to detect IFN-β in the cell culture supernatant of 2838c3 and 6620c1 cells dosed with Gem/ATRi. A possible explanation for this finding is that cancer cells may have downregulated or impaired innate immune sensing mechanisms and IFN-β is instead produced in neighbouring antigen-presenting cells (APCs)[19,189,206]. *In vitro* co-culture of bone marrow-derived DCs and tumour cells would have been appropriate to further investigate this hypothesis but this was not possible due to poor DC viability in extended cultures. To circumvent this issue, cancer cells could have been pre-treated with Gem/ATRi before a short co-culture with DCs, or the DCs treated with conditioned media from cancer cells dosed with Gem/ATRi.

In conclusion, the combination of gemcitabine and ATRi slows 2838c3 tumour growth and induces DC activation in both the tumour and draining LN. There was however a greater upregulation of activation markers in intratumoural cDC2 and bDC compared to cDC1, while tumour antigen uptake was specifically enhanced in cDC1. Mechanistically, this was not mediated by the activation of STING within the tumour. Gem/ATRi administration was also associated with a substantial depletion of all intratumoural DC subsets in the tumour and a selective depletion of LN-resident DCs in the dLN. Gem/ATRi similarly caused a depletion of intratumoural $CD8^+$ T cells, but of the remaining population there was a decrease in the percentage of PD-1- and CD39-expressing cells along with an increased proportion of proliferating ($Ki\text{-}67^+$) cells. Gem/ATRi did not have the same stimulatory effect on intratumoural cDC1 in 'T cell low' 6419c5 tumours compared to 2838c3 tumours, and further experiments using agonistic anti-CD40 antibody showed that intratumoural cDC1 in 6419c5 tumours had a dysfunctional phenotype and were unresponsive to stimulation.

CHAPTER FOUR: The pro-tumourigenic role of ILC2s in PDAC

4.1 Introduction to innate lymphoid cells (ILCs)

ILCs are a group of relatively novel immune cells that sit at the interface between innate and adaptive immunity. The ILC family is comprised of NK cells and more recently discovered helper ILC lineages with discrete developmental and functional characteristics. Since their discovery, they have been shown to have critical, non-redundant roles in regulating tissue homeostasis, infection and inflammation across different tissues[93]. Similar to other cells of the innate immune system, they do not express recombination activating gene (RAG)-dependent antigen receptors and therefore do not mount antigen-specific immune responses. However, they do not share the same developmental origin with myeloid cells, nor do they express prototypical myeloid cell markers. ILCs are conventionally thought to arise from the common lymphoid progenitor (CLP) in the bone marrow, but recent evidence suggests that ILC progenitors can also develop from thymocytes in a process that is dependent on several factors, including the status of TCR rearrangement and strength of Notch signalling[232]. NK cells were the first in the ILC family to be discovered – in 1975, these non-B and non-T lymphocytes were shown to possess cytolytic activity against leukaemia cells *in vitro*[233]. This was followed by the discovery of lymphoid tissue-inducer cells (LTi) in 1997 by Mebius and colleagues[234]. Between the years 2000 – 2010, there was an explosion of interest in ILCs and many novel ILC subsets were characterized in this period of time[235]. Notably, multiple ILC subsets appeared to have cytokine expression profiles that mirror those of Th cell subsets and were involved in the same inflammatory conditions as their respective Th subsets. These newly identified ILC subsets were given many different names, and it was not until 2013 that they were given a uniform nomenclature and categorized into three groups based on cytokine and transcription factor expression (**Figure 4.1**)[236]. It is now clear that the non-cytotoxic 'helper' ILC subsets (ILC1, ILC2 and ILC3) directly mirror $CD4^+$ T helper subsets (Th1, Th2 and Th17) in terms of cytokine and transcription factor expression, but an ILC subset analogous to Foxp3-expressing Tregs have not been identified to date. In 2017, a population of 'ILCregs' was described in both mouse and human intestines – similar to Tregs, these cells produce high levels of IL-10 and TGF-β to suppress inflammation[237]. They do not express Foxp3, instead relying on the transcription factor inhibitor of DNA-binding 3 (ID3) for development. However, the existence

of ILCregs as a distinct ILC subset is controversial as a subsequent study was unable to replicate these findings, instead suggesting that ILCregs are in fact IL-10 producing ILC2s[238]. It is now known that ILC2s can be alternatively activated in response to IL-33 or retinoic acid to generate a transcriptionally distinct IL-10-producing regulatory ILC2 subset[239,240].

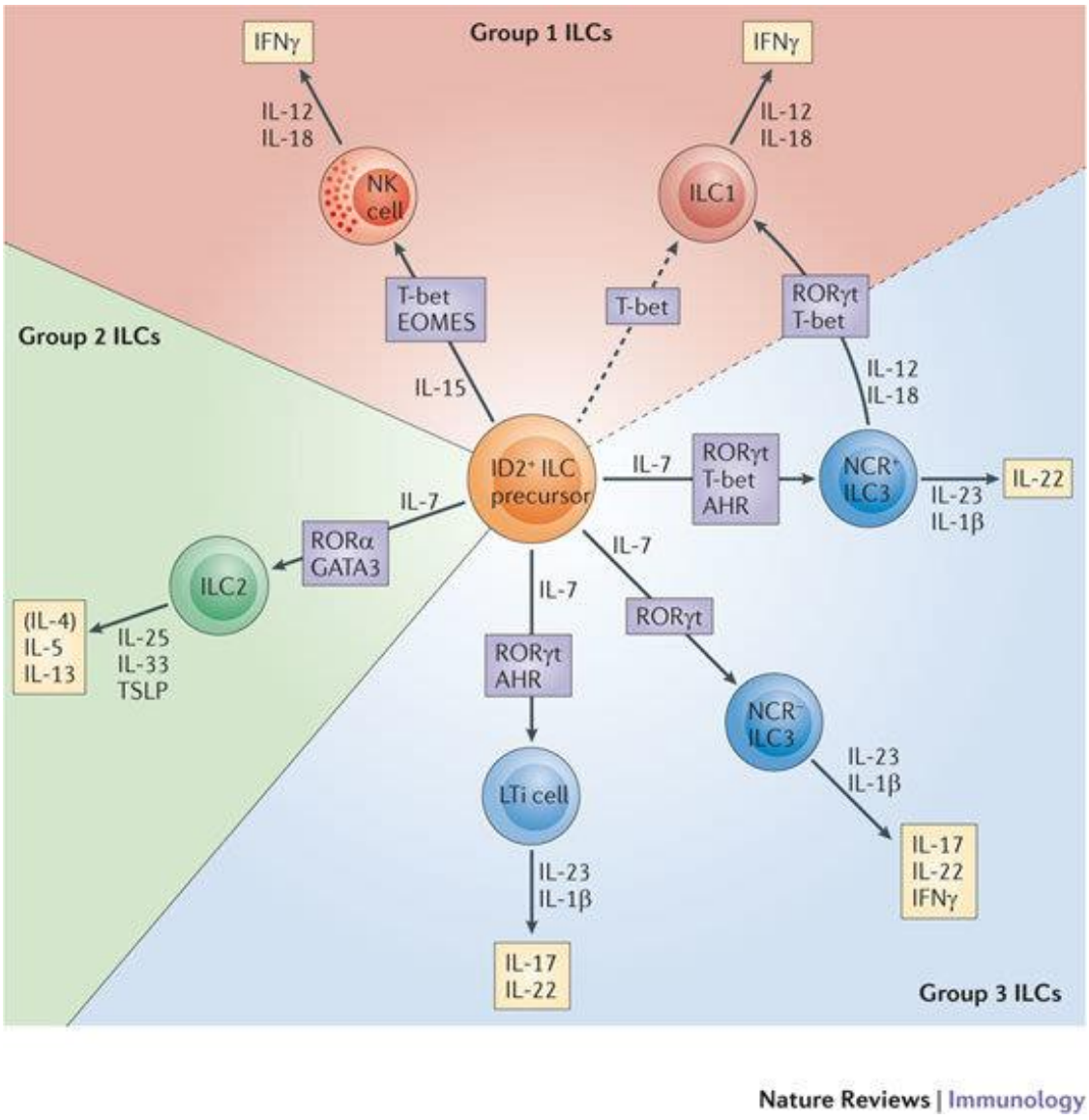

Figure 4.1. Classification of ILCs into three groups based on cytokine and transcription factor expression. All ILCs arise from common innate lymphoid progenitors (CILPs) that express the transcription factor inhibitor of DNA binding 2 (ID2). Group 1 ILCs include NK cells and ILC1, and similar to Th1 cells they are defined by their expression of the transcription factor T-bet and their capacity to produce IFNγ when activated. Group 2 ILCs require the transcription factors GATA-binding protein 3 (GATA3) and retinoic acid receptor-related orphan receptor-α (RORα) for development, and they produce Th2-related cytokines IL-4, IL-5 and IL-13. Reminiscent of Th17 cells, group 3 ILCs express the transcription factor RORγt and produce IL-17 and IL-22 when activated. These include lymphoid tissue-inducer (LTi) cells and two subsets of ILC3s which differentially express the natural cytotoxicity receptor (NCR) NKp46. (Figure from Spits et al., (2013)[236])

ILCs have been characterized in many lymphoid and non-lymphoid tissues but they are highly enriched in barrier tissues (e.g. lung, gut and skin mucosa) where they play key roles in both health and disease[241]. Circulating ILC precursors can be found in the blood, and it is thought that these precursors 'seed' into peripheral tissues which then differentiate into various subsets in response to local signals[242]. Mature ILC populations are therefore largely tissue-resident, and they proliferate locally under steady state to maintain their numbers[243]. Notably, ILCs from different tissues are imprinted with distinct transcriptional profiles that allow them to respond to tissue-specific signalling cues in both mice[244,245] and humans[246,247]. ILC populations are known to proliferate locally upon inflammatory challenge or infection, but they also have the capacity to migrate into peripheral lymph nodes and traffic between different organs under certain inflammatory conditions[243,248]. For example, a subset of ILC2s resident in the intestinal lamina propria was found to acquire an inflammatory phenotype in response to IL-25 or helminth infection and migrate to the lung in a sphingosine 1-phosphate (S1P)-dependent manner[249,250]. This phenomenon is not restricted to ILC2s resident in the intestine, as a subsequent study showed that lung-resident ILC2s also become activated and enter into the circulation in response to helminth infection[251]. Notably, these circulating ILC2s still maintain their tissue-specific identity and can be tracked to their tissue of origin based on their surface expression of ST2 (IL33R) and IL17RB[251]. It is hypothesized that this circulating pool of mature, activated ILC2s represent a mechanism by which local immune responses transition to systemic type 2 immunity as a form of host defence.

ILCs are highly plastic and can transdifferentiate to acquire characteristics of other subsets depending on local cues in the tissue microenvironment. This is particularly evident under inflammatory conditions, where they are exposed to elevated levels of pro-inflammatory cytokines that skew differentiation into other subsets[252]. In the context of cancer, tumours have been shown to hijack this plastic nature of ILCs to avoid immunosurveillance. For example, TGF-β signalling promotes the development of ILC1s by suppressing Eomes expression, a critical transcription factor involved in NK cell specification[253]. Within the TGF-β-rich TME, anti-tumourigenic NK cells can be converted into pro-tumourigenic ILC1-like cells in a TGF-β-dependent manner, resulting in loss of tumour control[254]. In pulmonary squamous cell carcinoma (SqCC), tumour cell-derived IL-23 induced the conversion of intratumoural ILC1s into IL-17-producing ILC3s that promote tumour cell proliferation[255]. The function and

relative abundance of intratumoural ILC populations can also change throughout the course of tumour development - in a mouse model of colorectal cancer, six clusters of intratumoural ILCs were identified via scRNA-seq (ILC1, ILC2A-C, ILC3 and ILCreg) and these ILCs displayed functional changes as the tumour progressed[256]. In late stage tumours, the relative proportion of ILC2 subsets shifted to favour a pro-tumourigenic PD-1^{high} ILC2 subset, and ILC3s were shown to undergo TGF-β-mediated transdifferentiation into immunosuppressive ILCregs. Altogether, these findings suggest that ILCs are a group of plastic cells that can quickly adapt to cues in their microenvironment to substantially alter local immune responses.

4.2 ILC2s in health and disease

An innate source of type 2 cytokines was first described in 2002, when the Coffman lab reported the existence of an IL-5-producing cell population in the lung that is induced by intranasal administration of IL-25 or *Aspergillus* infection[257]. These cells were present in *Rag2*$^{-/-}$ mice, and they were defined as c-kit$^-$, Ly6G$^-$, Ly49$^-$, CD3$^-$, CD4$^-$ and γδ TCR$^-$, with low to negative expression of Thy-1 and CD45R/B220. In 2006, two consecutive reports described the key role of IL-25 in the initiation of type 2 immunity, particularly in the immune response to intestinal helminths[258,259]. The report from the McKenzie lab also showed that IL-25 administration or helminth infection induced an expansion of a novel population of non-B, non-T, c-kit$^+$, FcεR1$^-$ cells in the mesenteric lymph node that produces canonical type 2 cytokines[258]. Subsequent studies then built on these early discoveries to show that these type 2 cytokine-producing innate cells are widely distributed across the body (lymph nodes, spleen, liver, fat etc.) and are activated in response to IL-25, IL-33 or helminth infection[260–262]. These cells were given multiple names by different labs (i.e nuocytes, Ih2 cells and natural helper cells) and it was not until 2013 that they were uniformly called ILC2s[236]. Depending on their tissue of residence, ILC2s can activated by a wide range of alarmins including IL-18[245], IL-25[257], IL-33[261,263] and TSLP[263]. In addition to these canonical ILC2-activating cytokines, ILC2 function is also modulated by other cytokines, lipid mediators, neuropeptides and hormones, with many of these mediators shown to have important roles in ILC2-related homeostatic functions and pathologies[264–266]. Upon activation, ILC2s can express a wide range of soluble effector molecules - these include prototypical type 2 cytokines[265] (e.g. IL-4, IL-5, IL-9 and IL-13) and other mediators associated with specific functions, for example amphiregulin[267] (tissue repair and remodelling) and methionine-enkephalin peptides[268] (adipose tissue

homeostasis). ILC2s can also be alternatively activated to express the immunosuppressive cytokine IL-10, and these IL-10-producing ILC2s have been implicated in a wide range of pathologies including allergic airway inflammation, intestinal inflammation and tumourigenesis[238,240,269]. Additionally, ILC2s also express various membrane-bound effector molecules such as MHC-II[270] and T cell co-stimulatory molecules ICOSL[271] and OX40L[272] that facilitate both homeostatic and inflammatory functions.

ILC2s were first discovered and characterized in the context of parasitic infections, but it is now clear that ILC2s have highly diverse roles in regulating local immune responses and tissue homeostasis. Allergic asthma is strongly driven by the overproduction of type 2 cytokines in the lung, where IL-5 induces lung eosinophilia and IL-13 mediates airway remodelling and mucus hyperproduction[273]. Although Th2 cells were first identified to be a source of type 2 cytokines in asthma, it is now known that ILC2s are also an important source of these cytokines, especially in the early/sensitisation phase. The allergens papain and *A. alternata* were able to induce airway eosinophilia in *Rag1*$^{-/-}$ mice that are deficient in adaptive immunity, but this response was abolished in *Rag2*$^{-/-}$*IL2rγ*$^{-/-}$ mice that lacked ILC2[263,274]. Mechanistically, papain treatment induces IL-33 and TSLP release from stromal cells, and these alarmins then activate ILC2s to produce IL-5 and IL-13[263]. In addition to their role during the early phase, ILC2s also play a key role in the development of allergen-specific Th2 cells from naïve CD4$^+$ T cells. IL-33 release in response to papain exposure leads to ILC2 activation, and ILC2-derived IL-13 is critical for promoting the migration of IL13R-expressing CD40$^+$ lung DCs into the draining lymph node, where they promote the differentiation of naïve CD4$^+$ T cells into Th2 cells[275]. Notably, ILC2-derived IL-13 is also critical for inducing CCL17 expression by IRF4$^+$CD11b$^+$CD103$^-$ cDC2s, a chemokine which recruits Th2 cells during allergen re-challenge[276]. ILC2s can also directly interact with CD4$^+$ T cells to promote Th2 responses – a subset of MHC-II-expressing ILC2s can act as antigen presenting cells to induce Th2 differentiation, and in response these activated T cells produce IL-2 which promote type 2 cytokine expression by ILC2s[270,277]. This ILC2-T cell crosstalk therefore mutually promotes their function and expansion and is important in the induction of an efficient anti-helminthic immunity[270]. ILC2-T cell crosstalk is also mediated by co-stimulatory molecules such as OX40L. In response to IL-33 administration or inflammatory challenge with papain or *N. brasiliensis* infection, lung-resident ILC2s upregulate OX40L to support tissue-specific expansion of Th2

and Treg[272]. ILC2s were found to be the main source of OX40L in response to these stimuli, and targeted deletion of OX40L on ILC2s led to impaired Th2 and Treg responses that corresponds to poorer anti-helminthic immunity[272].

While ILC2s are best known for potentiating type 2 inflammation in mucosal tissues, they also have crucial roles in regulating tissue homeostasis and repair. ILC2s can be found in white adipose tissue (WAT) where they act as the primary source of IL-5 and IL-13 for the recruitment and maintenance of eosinophils and alternatively activated M2 macrophages, respectively[278]. Eosinophil-derived IL-4 acts on adipocyte precursors to promote beige fat biogenesis, leading to increased insulin sensitivity and decreased adiposity[279,280]. Alternatively, ILC2s were also shown to produce methionine-enkephalin peptides that act directly on adipocytes to induce beiging by upregulating *Ucp1* expression[268]. These processes are dependent on IL-33 mediated activation of ILC2s, and a recent study has identified the source of IL-33 as WAT-resident stromal cells[281]. The maintenance of a type 2 immune environment consisting of ILC2s, eosinophils and M2 macrophages in WAT is therefore important for healthy metabolic homeostasis. ILC2s can also contribute to tissue repair and remodelling via production of the epidermal growth factor (EGF)-like molecule amphiregulin[282]. ILC2s upregulate amphiregulin expression in response to IL-33-mediated activation, and ILC2-derived amphiregulin is crucial for lung tissue repair in response to acute damage caused by influenza virus or helminth infection[267,283]. This effect is not restricted to the lung as ILC2-derived amphiregulin is also implicated in limiting intestinal[284] and renal[285] damage in response to dextran sodium sulfate (DSS)-induced inflammation and renal ischemia-reperfusion injury, respectively.

4.3 ILC2s in cancer

Among all ILC populations, the role of NK cells in cancer immunosurveillance was the first to be recognized[233]. Cytotoxic NK cells have the capacity to directly engage and kill malignant cells, and they are a major source of IFNγ that promote type 1 anti-tumour immunity[286]. Helper ILC subsets were discovered much later, and for many years research into their function was focussed on microbial infection and autoimmunity. Only recently have they been studied in the context of cancer, and scientific interest in the role of ILCs in cancer has grown exponentially in the past few years. It is now clear that intratumoural ILC abundance and/or

transcriptional signatures can have significant prognostic value in various human malignancies, and much progress has been made in elucidating the mechanisms by which they influence tumour immunosurveillance[287].

ILC2s are known to accumulate in many different cancers but their role in the tumour microenvironment remains ambiguous, due in part to their tissue-specific features and relatively low abundance in solid tumours[288]. ILC2s are activated and expand in response to intratumoural IL-33[289–291], IL-25[292] and/or PGD_2[293,294] signalling, and they act as a major source of type 2 cytokines (IL-4, IL-5 and IL-13) which can have anti- or pro-tumourigenic roles in different contexts[295]. IL-13 promotes the recruitment of monocytic-MDSCs (M-MDSCs) into the tumour, and this immunosuppressive ILC2-IL-13-M-MDSC axis has been shown to correlate with decreased survival and increased disease recurrence in colorectal cancer (CRC)[292], hepatocellular carcinoma[296], acute myeloid leukaemia[297], acute promyelocytic leukaemia[293] and bladder cancer[298]. IL-13 and IL-4 also promotes the polarization of macrophages into an 'M2' phenotype, and M2 macrophages have been shown to have a pro-tumourigenic role in a wide range of solid tumours including PDAC[299]. In acute myeloid leukaemia, ILC2-derived IL-5 was shown to expand a population of $IL5R\alpha^+$ Tregs, which in turn promotes malignant hematopoietic stem progenitor cell (HSPC) proliferation[294]. ILC2s are also known to promote tumour growth by suppressing NK cell function – this can occur via a direct ILC2-NK interaction (upregulation of the immunosuppressive ectoenzyme CD73 on activated ILC2s)[300] or indirectly (by restraining NK cell glucose metabolism in an eosinophil-dependent manner)[290]. The pro-tumourigenic role of IL-13 is not restricted to its effects on immune cells, as some tumour cells have been shown to express IL-13 receptors and can directly respond to IL-13. In a mouse model of CRC, IL-13 signalling in tumour cells promotes EMT, leading to increased tumour cell migration and invasion[301,302]. In PDAC tumour cells, oncogenic KRAS signalling drives the expression of IL-4 and IL-13 receptors, and these receptors signal through the JAK1–STAT6 pathway to upregulate MYC expression. This leads to metabolic reprogramming of these cells to favour glycolysis and is associated with increased tumour cell proliferation[303]. As tumours progress, the changing tumour microenvironment will also influence ILC2 function. In a mouse model of CRC, a larger proportion of intratumoural ILC2s acquired PD-1 expression as the tumour progressed, and these PD-1^{high} ILC2s were shown to

promote tumour growth when co-engrafted with tumour cells (whereas co-engraftment with PD-1^{low} ILC2s did not have any effect)[256].

Conversely, some studies provide evidence that ILC2s and their associated type 2 cytokines can promote tumour rejection. In melanoma patients, high intratumoural ILC2 and eosinophil infiltration correlates with a better prognosis[304]. Upon IL-33-mediated activation, intratumoural ILC2s produce IL-5 or GM-CSF to recruit eosinophils that suppress melanoma growth[304,305]. The anti-tumourigenic function of ILC2s is restrained by PD-1 signalling and accumulation of lactic acid in the TME, and removal of these immunosuppressive mechanisms (via PD-1 blockade or lactate dehydrogenase A (*Ldha*) knockdown in tumour cells) synergized with IL-33 to improve anti-tumour immunity[304,305]. In a mouse model of metastatic melanoma, ILC2s were found to directly suppress tumour growth via production of TNF-α, and PD-1 blockade further enhanced TNF-α-mediated killing of tumour cells[306]. Many studies also highlight the anti-tumourigenic function of IL-33 – in mouse models of lymphoma, lung cancer, colon carcinoma and metastatic melanoma, tumour cells genetically engineered to express IL-33 had reduced capacity to form tumours *in vivo*[307,308]. Mechanistically, IL-33 promotes intratumoural ILC2 activation and expansion, and they produce CXCR2 ligands which directly induce apoptosis on CXCR2-expressing tumour cells[307]. There is also *in vitro* evidence showing that ILC2s can promote CD8$^+$ T cell mediated cytotoxicity by upregulating MHC-I on tumour cells[308]. *In vivo*, CD8$^+$ T cells have been shown to express ST2 in the context of viral infection and IL-33 signalling in these cells augments their effector function[309]. In CRC patients, an elevated ILC2 gene signature is associated with improved overall survival, and mice deficient in ILC2s were more susceptible to azoxymethane/dextran sodium sulfate (AOM/DSS)-induced CRC[310].

In PDAC, the role of ILC2s and type 2 cytokines in the process of tumourigenesis is equally controversial. Pancreatitis is known to accelerate PanIN progression in the presence of activating *Kras* mutations, and levels of the alarmin IL-33 is significantly upregulated in damaged pancreatic tissue[311,312]. A recent study has now shown that pancreatitis cooperates with mutant *Kras* to induce an epigenetic state in pancreatic epithelial cells that is associated with neoplastic transformation, and IL-33 signalling is responsible for this epigenetic remodelling[313]. The source of IL-33 in advanced PDAC is disputed, with studies claiming

tumour cells[291], CAFs[314] or MDSCs[73] to be the primary source of IL-33 in the tumour microenvironment. IL-33 has been shown to directly inhibit pancreatic cancer cell proliferation and induce cancer cell apoptosis *in vitro*[315], and suppressing soluble ST2 (sST2) expression by tumour cells led to decreased tumour growth *in vivo*[316]. In PDAC patients, higher expression levels of *Il33* and ILC2-related gene transcripts independently correlates with extended survival[73]. ILC2s were shown to promote $CD8^+$ T cell-mediated anti-tumour immunity via CCL5-dependent recruitment of $CD103^+$ DCs, and preclinical response to recombinant IL-33 (rIL-33) was further enhanced in combination with PD-1 blockade[73]. However, ILC2s have also been shown to have a pro-tumourigenic role in PDAC. The hypoxic PDAC TME reprograms ILC2s to acquire an immunoregulatory phenotype, and these IL-10-producing ILC2s were found to be enriched in a subset of human PDAC tumour[317]. Mice with fibroblast-specific deletion of *Il33* exhibit reduced PDAC growth, and this was attributed to a decrease in the infiltration of immunosuppressive macrophages[314]. The tumour microbiome is known to significantly influence tumour progression and anti-tumour immunity[291,318], and intrapancreatic fungi are 3000 times more abundant in human PDAC tumours compared to healthy pancreas[319]. IL-33 production by tumour cells is dependent on the intratumoural mycobiome, and ablation of the mycobiome or IL-33 decreased Th2 and ILC2 infiltration, leading to extended survival[291]. The presence of intratumoural fungi also activates the complement cascade, and the binding of C3a to its receptors on tumour cells promotes tumour cell proliferation[319].

While the role of ILC2s in type 2 inflammatory conditions is well established, their role in cancer is ill defined and highly controversial. Given that ILC2s have highly tissue-specific features, it is likely that the role of ILC2s in different cancer types cannot be generalized. Combined with the plastic nature of ILCs in an evolving tumour microenvironment, it is unsurprising that ILC2s and its associated cytokines have been attributed both pro- and anti-tumour functions. In this chapter, I report on my efforts to characterize the role of ILC2s in PDAC, specifically to investigate the mechanisms by which they influence anti-tumour immunity.

Results

4.4 Genetic ablation of ILC2 reduces pancreatic tumour burden and alters the profile of intratumoural immune infiltrate

To assess the role of ILC2s in PDAC, 2838c3 tumour cells were orthotopically implanted into *Il7ra*$^{Cre/+}$*Rora*$^{loxP/loxP}$ ILC2-deficient (ILC2KO) and *Il7ra*$^{Cre/+}$ control mice. ILC2-deficient mice were found to have a significant survival advantage compared to control mice, with approximately 50% of ILC2-deficient mice having no signs of macroscopic tumours in the pancreas at the end of the 90-day study (**Figure 4.2a**). In contrast, greater than 90% of control mice eventually succumbed to disease. To determine whether ILC2s influence the intratumoural immune infiltrate, tumours and adjacent pancreas from ILC2-deficient and control mice were taken 21 days post-implantation for immune profiling. At this relatively early timepoint, ILC2-deficient mice had smaller tumours compared to control mice (**Figure 4.2b**). Immune profiling showed a decrease in intratumoural CD45$^+$ immune cells in ILC2-deficient mice that was primarily driven by a decrease in myeloid cells, but also of Tregs and CD8$^+$ T cells (**Figure 4.2c and 4.2d**). The transcription factor GATA3 is expressed in a subset of Foxp3$^+$ Tregs, and GATA3$^+$ Tregs are known to have enhanced suppressive function and be preferentially expanded in type 2 immune responses[272,320]. ILC2 deficiency led to an increase in intratumoural GATA3$^+$ Tregs with a decrease in GATA3$^-$ Tregs, resulting in a shift in the proportion of intratumoural Tregs to favour the GATA3$^+$ subset. This was the opposite of what was observed in the pancreas, where there was a decrease in the proportion of GATA3$^+$ Tregs. This inversion of GATA3$^+$ Treg numbers between the pancreas and tumour was also true for Th2 cells, suggesting that type 2 immune responses are diminished in the pancreas but amplified within the tumour in ILC2-deficient mice. ILC3s were scarcely found in the pancreas and tumour, and their numbers were unchanged in ILC2-deficient mice. I was unable to identify any RORγt$^+$ Th17 cells in the pancreas or tumour, despite their known existence from other studies[72]. This is unlikely to be a problem with the antibody or staining conditions as I was able to identify RORγt$^+$ ILC3s from the same samples.

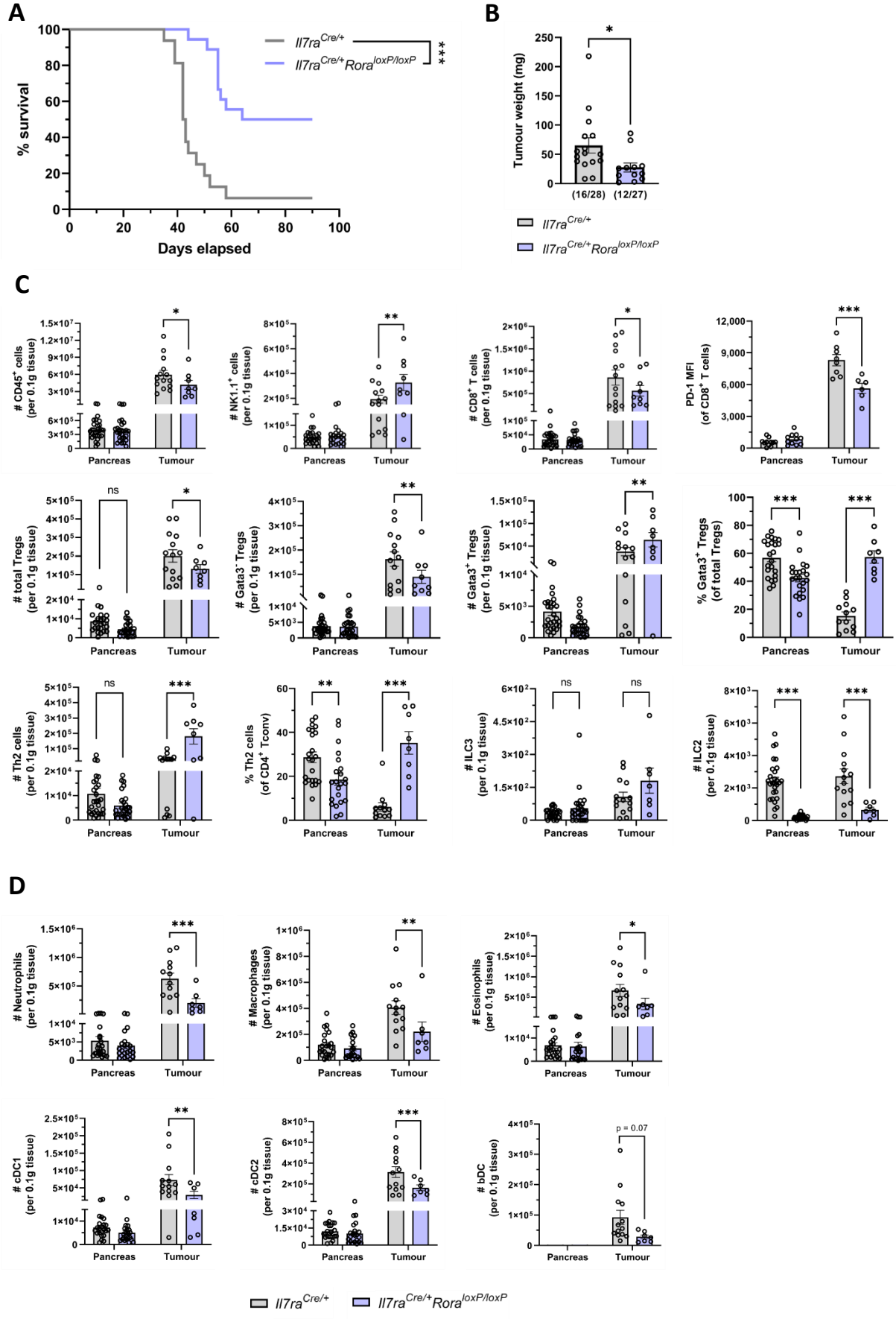
A
% survival
Days elapsed
Il7ra^Cre/+
Il7ra^Cre/+Rora^loxP/loxP
***
B
Tumour weight (mg)
(16/28)
(12/27)
C
CD45+ cells (per 0.1g tissue)
NK1.1+ cells (per 0.1g tissue)
CD8+ T cells (per 0.1g tissue)
PD-1 MFI (of CD8+ T cells)
total Tregs (per 0.1g tissue)
Gata3- Tregs (per 0.1g tissue)
Gata3+ Tregs (per 0.1g tissue)
% Gata3+ Tregs (of total Tregs)
# Th2 cells (per 0.1g tissue)
% Th2 cells (of CD4+ Tconv)
# ILC3 (per 0.1g tissue)
# ILC2 (per 0.1g tissue)
Pancreas
Tumour
ns
D
# Neutrophils (per 0.1g tissue)
# Macrophages (per 0.1g tissue)
# Eosinophils (per 0.1g tissue)
# cDC1 (per 0.1g tissue)
# cDC2 (per 0.1g tissue)
# bDC (per 0.1g tissue)
p = 0.07
Il7ra^Cre/+
Il7ra^Cre/+Rora^loxP/loxP

Figure 4.2. Genetic ablation of ILC2 reduces pancreatic tumour burden and induces changes in tumour immune infiltrate. 2838c3 tumour cells were orthotopically implanted into the mouse pancreas. (A) Survival of tumour-bearing ILC2-deficient (*Il7ra*$^{Cre/+}$*Rora*$^{loxP/loxP}$, n = 18) and control (*Il7ra*$^{Cre/+}$, n = 16) mice. (B) Weight of tumours in ILC2-deficient and control mice 21 days post-implantation. Numbers in brackets indicate the number of mice with macroscopically visible tumours at endpoint/total number of mice in the group. Flow cytometry analysis of (C) lymphoid and (D) myeloid cells in 2838c3 tumour and adjacent pancreas in ILC2-deficient (n = 28) and control (n = 28) mice 21 days post-implantation. Data are pooled from two or more independent experiments, and error bars indicate mean ± SEM. The following tests were used to determine statistical significance: (A) log-rank test; (B) unpaired two-tailed t test; (C) two-way ANOVA with Šídák's multiple comparison test. * $P < 0.05$, ** $P < 0.01$, *** $P < 0.001$.

Histological analysis of early-stage 2838c3 tumours in control mice shows that CD8$^+$ T cells are able to infiltrate into the tumour and co-localize with tumour cells, whereas the majority of Foxp3$^+$ Tregs are located in the tumour margin (**Figure 4.3a**). Histological quantification of CD8$^+$ T cells and Foxp3$^+$ Tregs revealed a decrease in intratumoural Treg infiltration in ILC2-deficient mice with no changes in CD8$^+$ T cell abundance (**Figure 4.3b**).

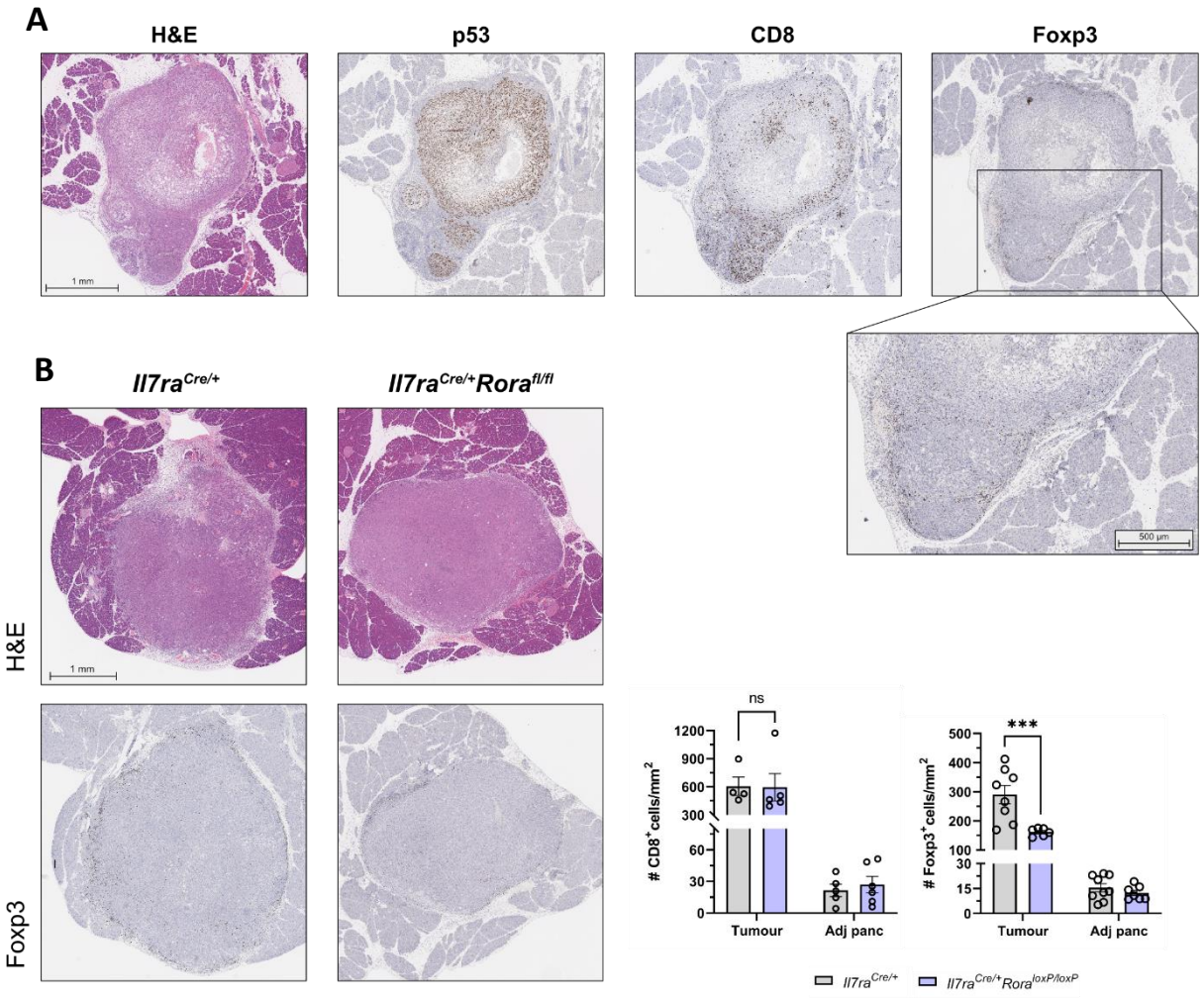

Figure 4.3. Genetic ablation of ILC2 reduces Foxp3⁺ Treg infiltration into pancreatic tumours. Histological analysis of 2838c3 tumours 21 days post-implantation into the mouse pancreas. (A) Representative images showing H&E staining and localization of tumour cells (p53⁺), CD8⁺ cells and Foxp3⁺ cells in the tumour and adjacent pancreas of *Il7ra*$^{Cre/+}$ mice. (B, left) Representative images showing localization of intratumoural Foxp3⁺ cells and (right) quantification of CD8⁺ cells and Foxp3⁺ cells in the tumour and adjacent pancreas of ILC2-deficient (*Il7ra*$^{Cre/+}$*Rora*$^{loxP/loxP}$, n = 7) and control (*Il7ra*$^{Cre/+}$, n = 9) mice. Error bars indicate mean ± SEM. A two-way ANOVA with Šídák's multiple comparison test was used to determine statistical significance. *** $P < 0.001$.

4.5 IL-33, IL-13, eosinophils and NK cells do not significantly influence 2838c3 pancreatic tumour growth.

Pancreatic ILC2s are strongly activated by IL-33[73,291], and previous work in the lab has shown that IL-33-mediated ILC2 activation leads to NK cell immunosuppression in an eosinophil-dependent manner (**Figure 4.4a**)[290]. Given the increase in intratumoural NK1.1^{+} cells in ILC2-deficient mice, I hypothesized that the same mechanism might be true in PDAC. To dissect the role of IL-33 in PDAC growth, 2838c3 tumour cells were orthotopically implanted in IL-33-deficient mice and WT mice dosed with IL-33 or PBS. All three experimental groups showed similar survival, suggesting that IL-33 does not significantly modulate orthotopic PDAC growth (**Figure 4.4b**). In a separate experiment, pancreas, tumour and pancreatic LN (pLN) from IL-33 or PBS-treated WT mice were taken for flow cytometry analysis at day 21 post-tumour implantation to characterize IL-33 induced changes in immune infiltrate. At this early timepoint, there was no difference in tumour weight between both treatment groups (**Figure 4.4c**). Immune profiling revealed ILC2 expansion and activation in response to IL-33 in all tissues assessed, suggesting that increasing ILC2 function and abundance prior to tumour implantation had no significant effect on tumour growth (**Figure 4.4d and 4.4e**). Moreover, eosinophil loss did not have an impact on tumour growth as there was no difference in survival between tumour-bearing eosinophil-deficient ΔdblGATA and WT mice (**Figure 4.4f**). Antibody-mediated depletion of NK cells in tumour-bearing WT mice similarly did not have a significant impact on survival (**Figure 4.4g**). As IL-13 is a major effector cytokine of ILC2s, I also assessed the effect of IL-13 loss on PDAC growth but there was no difference between the survival of tumour-bearing IL13-deficient and WT mice (**Figure 4.4h**).

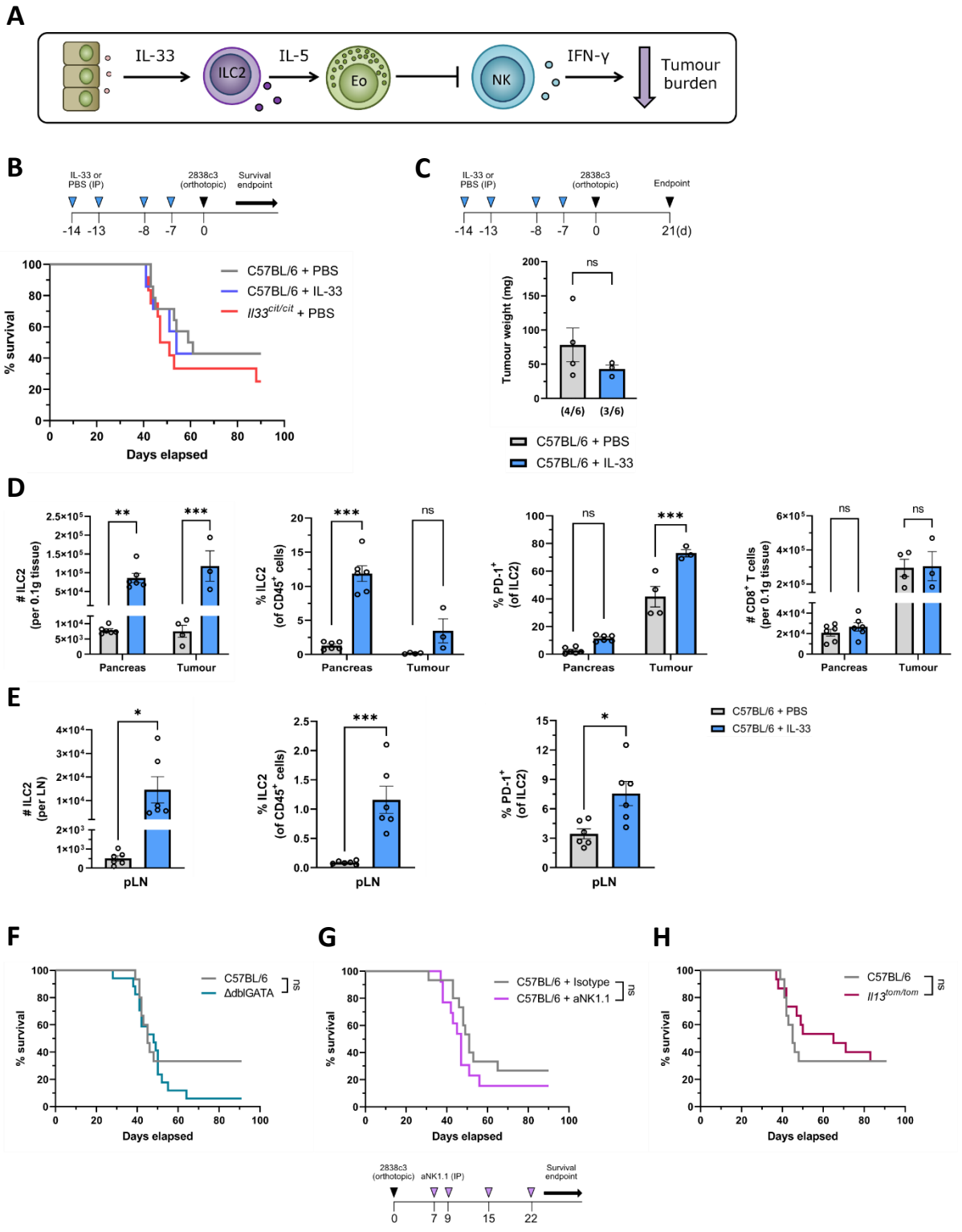

Figure 4.4. IL-33, IL-13, eosinophils and NK cells do not significantly influence PDAC tumour growth. (A) Schematic depiction of the pro-tumourigenic role of ILC2 described in Schuijs et al (2020)[290]. Lung epithelial cells are an important source of IL-33, and activated ILC2s were shown to suppress NK cell function via eosinophil-dependent modulation of NK cell metabolism (B, top) Schematic of IL-33 dosing schedule and (bottom) survival of tumour-bearing C57BL/6 and IL33-deficient (*Il33*$^{cit/cit}$, n = 12) mice pre-treated with IL-

33 (n = 7) or PBS (n = 14). (C, top) Schematic of IL-33 dosing schedule and (bottom) weight of tumours at day 21 post-implantation in C57BL/6 mice pre-treated with IL-33 or PBS. Numbers in brackets indicate the number of mice with macroscopically visible tumours at endpoint/total number of mice in the group. (D and E) ILC2 frequency and PD-1 expression in the tumour, adjacent pancreas and pancreatic lymph node of mice in C. (F) Survival of 2838c3-bearing eosinophil-deficient (ΔdblGATA, n = 17) and C57BL/6 (n = 16) mice. (G) Schematic of NK cell-depleting antibody dosing schedule and survival of 2838c3-bearing C57BL/6 mice dosed with NK cell-depleting antibody (n = 15) or isotype antibody (n = 15). (H) Survival of tumour-bearing C57BL/6 (n = 15) and IL-13-deficient (*Il13*$^{tom/tom}$, n = 15) mice. Data are pooled from two or more independent experiments, and error bars indicate mean ± SEM. The following tests were used to determine statistical significance: log-rank test in B, F, G and H; unpaired two-tailed t test in C and E; two-way ANOVA with Šídák's multiple comparison test in D. * P < 0.05, ** P < 0.01, *** P < 0.001.

4.6 ILC2s do not promote PDAC tumour growth via OX40L-mediated Treg expansion

Given the changes in intratumoural Treg profile in ILC2-deficient mice, I then investigated possible mechanisms of ILC2-Treg interaction that may contribute to PDAC growth. Notably, previous work has shown that ILC2s can contribute directly to the expansion of Tregs and Th2 cells via expression of OX40L[272]. As Tregs and Th2 cells are known to promote PDAC growth, this might represent one of the mechanisms underlying the pro-tumourigenic role of ILC2s in PDAC. To perturb the ILC2-OX40L-Treg axis, ILC2-targeted OX40L conditional KO (cKO) mice (*Il7ra*$^{Cre/+}$*OX40L*$^{loxP/loxP}$)[272] were used to assess the effect of ILC2-targeted OX40L loss on PDAC tumour growth. OX40L deletion on ILC2s did not have an impact on tumour burden at 21 days post-implantation (**Figure 4.5a**). Immune profiling of tissue samples on day 21 showed that deletion of OX40L on ILC2s had the expected effect of reducing Th2 and GATA3^{+} Treg proportions in the pancreas, although the same effect was not observed in the tumour (**Figure 4.5b**). Results from a survival study confirmed the findings at day 21, showing no difference in survival between ILC2-targeted OX40L cKO and control mice (**Figure 4.5c**). An alternative way of perturbing the ILC2-OX40L-Treg axis was to delete OX40 expression on Tregs – the Foxp3-targeted OX40 cKO (*Foxp3*$^{YFP\text{-}iCre}$*; OX40*$^{loxP/loxP}$) mouse model was generated by other lab members, and 2838c3 tumours were orthotopically implanted into these mice. However, these mice did not show a significant difference in survival compared to controls (**Figure 4.5d**), and histological analysis of endpoint tumours did not show any difference in intratumoural Treg density (**Figure 4.5e**). This series of experiments therefore indicates that ILC2s do not promote PDAC tumour growth via OX40L-mediated Treg/Th2 expansion.

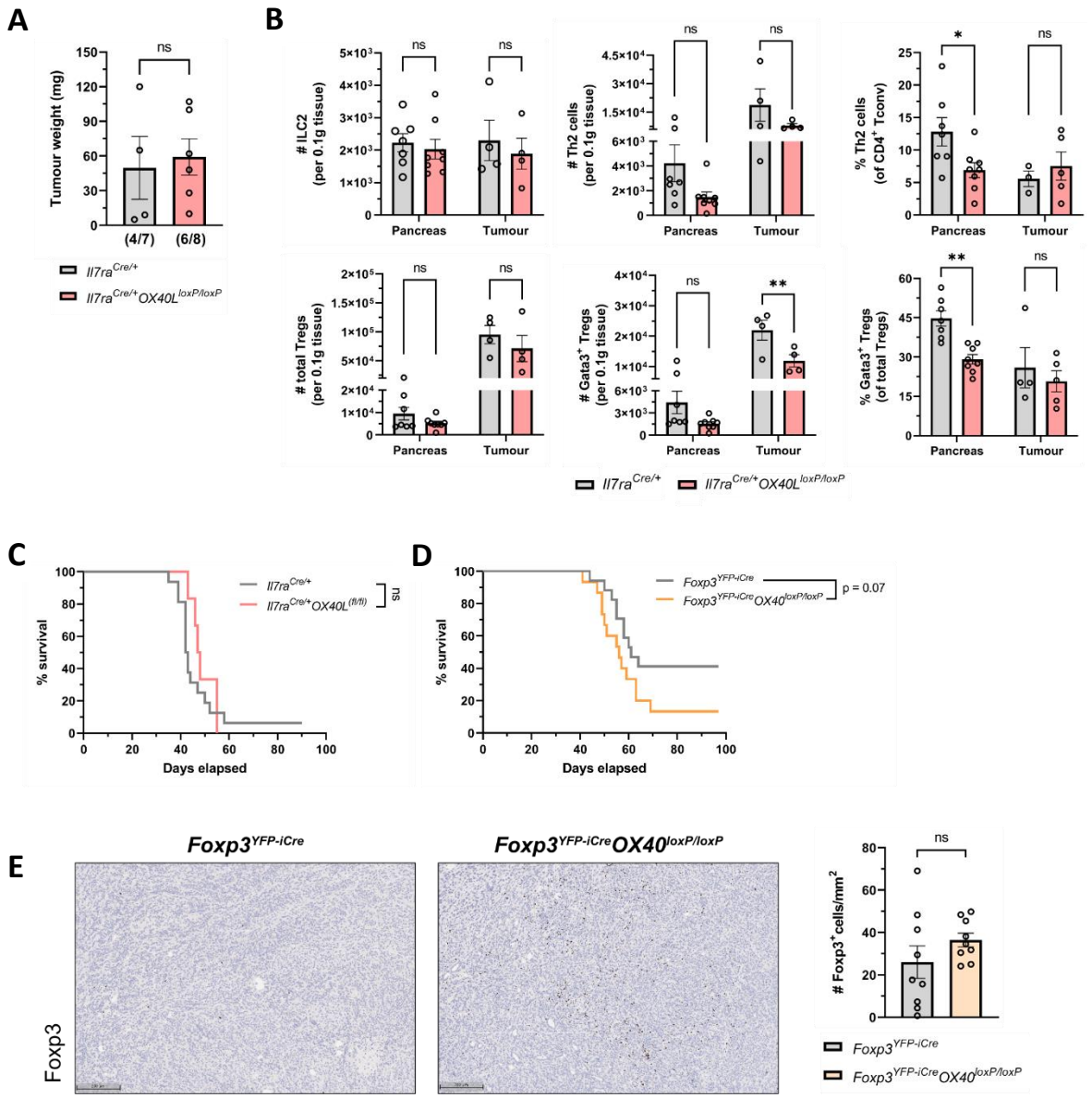

Figure 4.5. Perturbation of the ILC2-OX40L-Treg axis does not significantly influence PDAC tumour growth. (A) 2838c3 tumour weight at 21 days post-implantation in ILC2-targeted OX40L conditional KO (cKO) (*Il7ra*$^{Cre/+}$*OX40L*$^{loxP/loxP}$) and control (*Il7ra*$^{Cre/+}$) mice. Numbers in brackets indicate the number of mice with macroscopically visible tumours at endpoint/total number of mice in the group. (B) Frequency of ILC2, Th2 and Tregs in the tumour and adjacent pancreas of ILC2-targeted OX40L cKO (n = 8) and control (n = 7) mice 21 days post-implantation. (C) Survival of 2838c3-bearing ILC2-targeted OX40L cKO (n = 6) and control (n = 16) mice. (D) Survival of 2838c3-bearing Foxp3-targeted OX40 cKO (*Foxp3*$^{YFP\text{-}iCre}$*; OX40*$^{loxP/loxP}$, n = 15) and control (*Foxp3*$^{YFP\text{-}iCre}$, n = 17) mice. (E, left) Representative images and (right) quantification of intratumoural Foxp3$^+$ cells in Foxp3-targeted OX40 cKO (n = 9) and control (n = 9) mice. Data are pooled from two or more independent experiments, and error bars indicate mean ± SEM. The following tests were used to determine statistical significance: unpaired two-tailed t test in A and E, two-way ANOVA with Šídák's multiple comparison in B and log-rank test in C and D. * $P < 0.05$, ** $P < 0.01$.

4.7 ILC2s influence PDAC tumour growth via the adaptive immune system

To determine whether ILC2s promote tumour growth via the adaptive immune system, growth of orthotopic 2838c3 tumours was compared between Rag2KO (*Rag2*^{tm1Fwa}), Rag2-ILC2KO (*Rag2*^{tm1Fwa}*Il7ra*$^{cre/+}$*Rora*$^{loxP/loxP}$) and WT mice. At 21 days post-implantation, both Rag2KO groups had significantly larger tumours compared to WT mice, but there was no difference between the tumour burden of Rag2KO and Rag2-ILC2KO mice (**Figure 4.6a**). As ILC2 deficiency in a RagKO background no longer has a protective effect, it reasons that ILC2s influence PDAC tumour growth via an effect on adaptive immune cells. Given the decrease in intratumoural Treg infiltration in early-stage ILC2-deficient tumours, I then looked at the role of Tregs in 2838c3 PDAC growth. Foxp3^{+} Treg depletion (using the Foxp3^{DTR} model) significantly improved survival and clearance of 2838c3 PDAC tumours (**Figure 4.6b**), and no macroscopic tumours were visible in Foxp3^{DTR} mice 21 days post-tumour implantation (**Figure 4.6c**). Immune profiling of pancreas and pLN in these mice revealed extensive infiltration of immune cells upon Treg depletion, including CD8^{+} T cells, CD4^{+} conventional T cells and Tregs, cDC2s and eosinophils (**Figure 4.6d**). Systemic Treg depletion therefore induces a strong inflammatory response in the pancreas that suppresses PDAC tumour growth.

Among all adaptive immune cells, cytotoxic CD8^{+} T cells are best known for mediating strong anti-tumour responses, and their numbers in the pancreas were significantly increased in tumour-free pancreata of Treg-depleted mice. I therefore hypothesized that ILC2s may be promoting PDAC growth via suppression of CD8^{+} T cell function, either directly or indirectly via an effect on Tregs or Th2 cells. CD8^{+} T cell depletion in 2838c3-bearing WT mice led to significantly reduced survival, suggesting that CD8^{+} T cells play an important role in restraining tumour growth in this model (**Figure 4.7a**). CD8^{+} T cell depletion in 2838c3-bearing ILC2-deficient mice similarly led to a decrease in survival, to an extent that mimicked the survival of isotype-treated control mice (**Figure 4.7b**). CD8^{+} T cell depletion therefore abrogated the protection afforded in the absence of ILC2s, which strongly suggests that ILC2s influence tumour growth via CD8^{+} T cell suppression. Intriguingly, there was also a difference in survival between aCD8-treated ILC2-deficient and control mice – this indicates that ILC2s also influence tumour growth in a CD8^{+} T cell-independent manner.

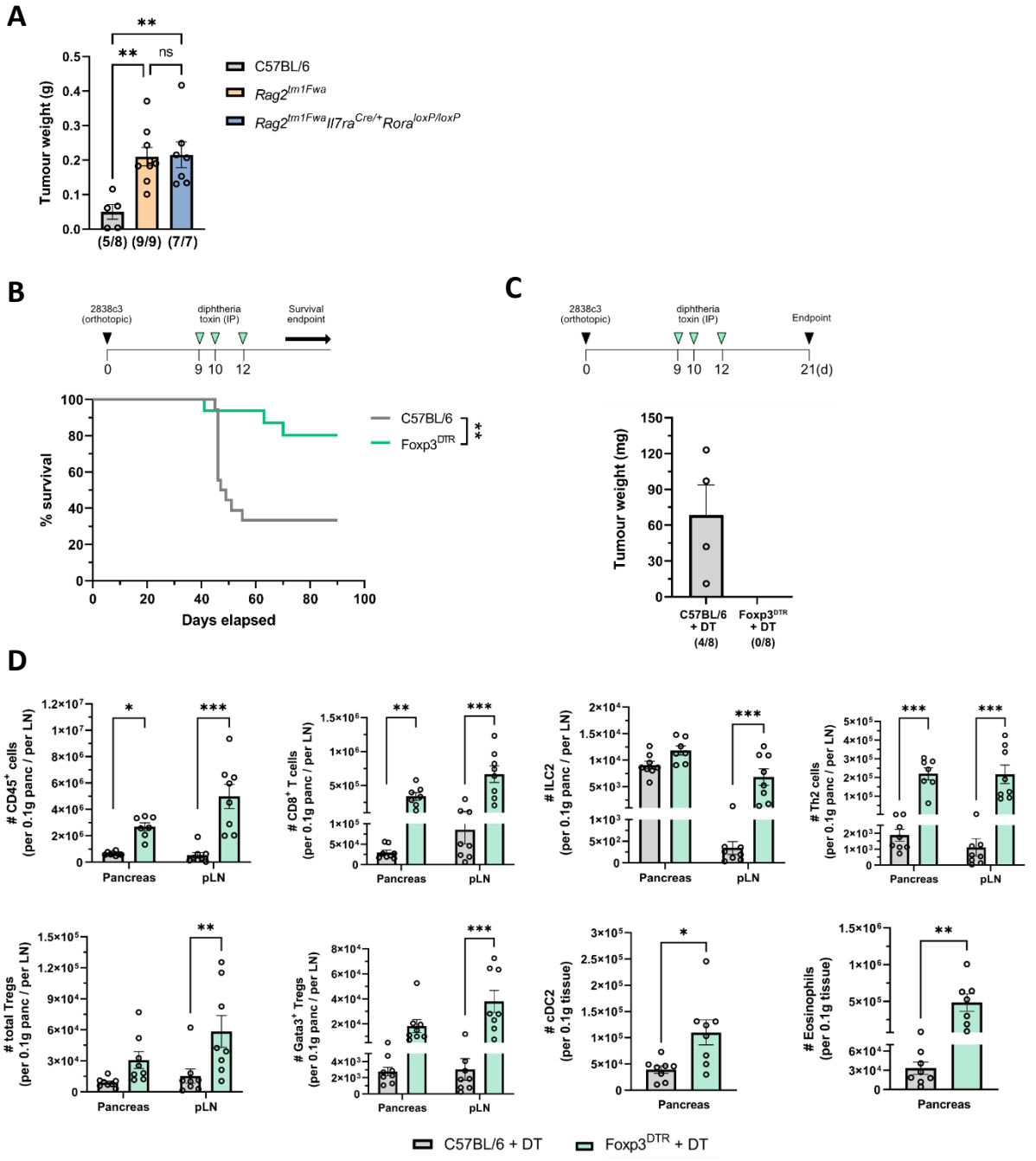

Figure 4.6. Foxp3⁺ Treg depletion induces a strong inflammatory response in the pancreas to suppress PDAC tumour growth. (A) Tumour weights at day 21 post-implantation of orthotopic 2838c3 tumours in C57BL/6, *Rag2*^{tm1Fwa} (Rag2KO) and *Rag2*^{tm1Fwa}*Il7ra*$^{cre/+}$*Rora*$^{loxP/loxP}$ (Rag2-ILC2KO) mice. Numbers in brackets indicate the number of mice with macroscopically visible tumours at endpoint/total number of mice in the group. (B, top) Schematic of diphtheria toxin (DT) dosing schedule and (bottom) survival of 2838c3-bearing Foxp3^{DTR} (n = 16) and C57BL/6 (n = 18) mice. Both experimental groups were dosed with DT. (C, top) Schematic of DT dosing schedule and (bottom) tumour weights at 21 days post-implantation in Foxp3^{DTR} and C57BL/6 mice. Numbers in brackets indicate the number of mice with macroscopically visible tumours at endpoint/total number of mice in the group. (D) Frequency of CD45⁺ cells, CD8⁺ T cells, ILC2, Th2 cells,

Tregs, cDC2 and eosinophils in the pancreas and pancreatic LN (pLN) of mice in C. Data are pooled from two or more independent experiments, and error bars indicate mean ± SEM. The following tests were used to determine statistical significance: one-way ANOVA with Tukey's multiple comparisons test in A, log-rank test in B, unpaired two-tailed t test in C, and two-way ANOVA with Šídák's multiple comparison in D (with the exception of cDC2 and eosinophil quantification, in which an unpaired two-tailed t test was used). * P < 0.05, ** P < 0.01, *** P < 0.001.

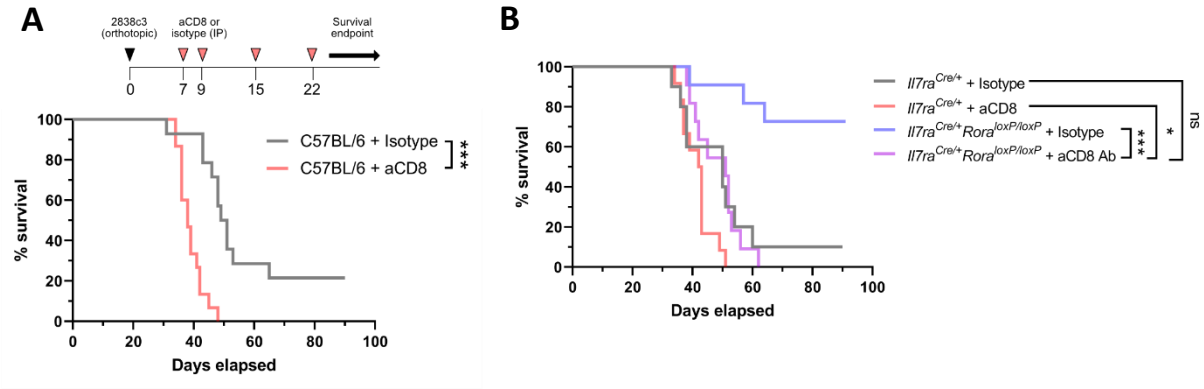

Figure 4.7. ILC2s promote PDAC tumour growth via both CD8⁺ T cell-dependent and independent mechanisms. (A, top) Dosing schedule and (bottom) survival of tumour-bearing C57BL/6 mice dosed with either CD8⁺ T cell depleting antibody (n = 17) or isotype antibody (n = 14). (B) Survival of tumour-bearing ILC2-deficient (*Il7ra*$^{Cre/+}$*Rora*$^{loxP/loxP}$) mice dosed with CD8⁺ T cell depleting antibody (n = 11) or isotype antibody (n = 11), and control (*Il7ra*$^{Cre/+}$) mice dosed with CD8⁺ T cell depleting antibody (n = 12) or isotype antibody (n = 10). Data are pooled from two independent experiments, and error bars indicate mean ± SEM. Log-rank tests were performed in B and C to determine statistical significance. * P < 0.05, *** P < 0.001.

4.8 Characterization of tumour-specific CD8$^+$ T cells using the 2838c3-OVA model

To explore the mechanism(s) by which ILC2s can influence CD8$^+$ T cell function, cytoplasmic OVA-expressing 2838c3 cells were generated by transducing the parental cell line with the pMIG-cytoOVA-IRES-tdTomato plasmid (kindly gifted by Maike de la Roche, University of Cambridge). Using this model, tumour-specific CD8$^+$ T cells can be identified and profiled via tetramer-mediated detection of OVA-specific endogenous or TCR-transgenic OT-I CD8$^+$ T cells. As the added expression of cytoplasmic OVA is likely to increase the immunogenicity of these tumour cells, I first characterized the growth and immune profile of 2838c3-OVA tumours compared to the parental cell line. Both tumour cell lines were orthotopically implanted in WT mice, followed by intravenous administration of OT-I cells on day 14. At 21 days post-implantation, no difference in tumour weight was observed between both cell lines (**Figure 4.8a**). Immunophenotyping revealed no striking differences in immune cell infiltration into the pancreas and tumour, with the exception of CD8$^+$ T cells (**Figure 4.8b**). Due to either the increased immunogenicity of 2838c3-OVA tumour cells or the transfusion of OT-I cells, 2838c3-OVA tumours were more highly infiltrated with CD8$^+$ T cells, a significant proportion of which (~40%) were OVA-specific CD8$^+$ T cells. In contrast, OT-I cells failed to accumulate in 2838c3 tumours. Intratumoural CD8$^+$ T cells between the two models also showed a difference in the expression of CD44 and PD-1 – namely, OT-I cells in 2838c3-OVA tumours showed lower expression of CD44 but higher expression of PD-1, whereas non-OT-I CD8$^+$ T cells in 2838c3-OVA tumours showed lower expression of PD-1 (**Figure 4.8c**). In the pLN, there was a similar number of CD8$^+$ T cells in both models but OT-I cells could only be detected in the draining LN of 2838c3-OVA tumours (**Figure 4.8d**). Strikingly, assessment of PD-1 and CD44 expression revealed that OT-I cells were specifically activated in the 2838c3-OVA model (**Figure 4.8d**). In summary, these results show that tumour-specific OT-I cells are able to expand and accumulate in 2838c3-OVA tumours and draining lymph nodes, although this was not associated with a lower tumour burden compared to parental 2838c3 tumours. As all mice received OT-I transfusion post-tumour implantation, it was unclear at this point if 2838c3-OVA tumours were able to elicit an endogenous OVA-specific CD8$^+$ T cell response.

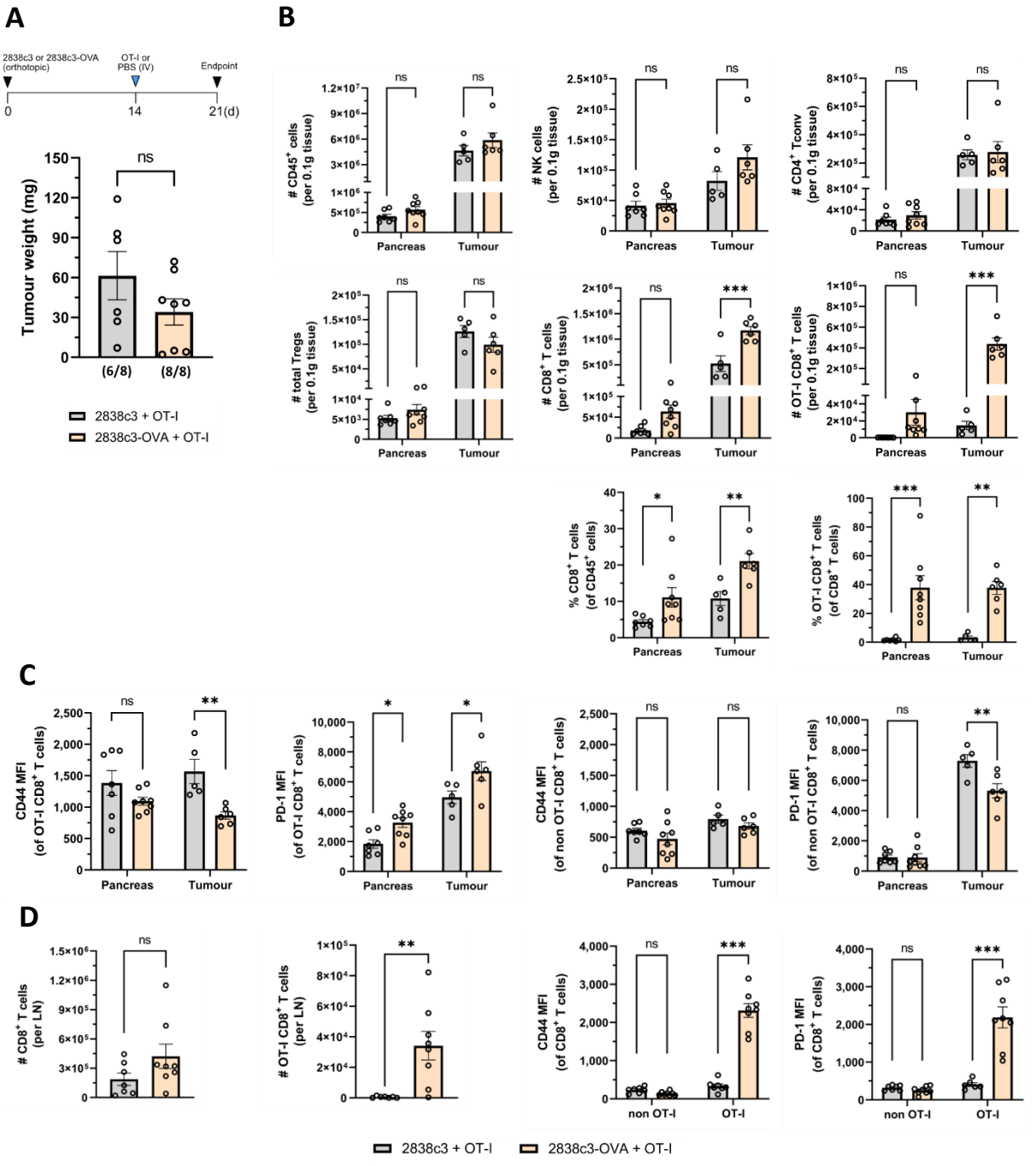

Figure 4.8. Characterization of the 2838c3-OVA tumour model. (A) Tumour weights at day 21 post-implantation of orthotopic 2838c3 and 2838c3-OVA tumours in C57BL/6 mice with adoptive transfer of 100k splenocytes from OT-I Rag2KO mice on day 14. Numbers in brackets indicate the number of mice with macroscopically visible tumours at endpoint/total number of mice in the group. (B) Frequency of $CD45^+$ cells, NK cells, $CD4^+$ Tconv cells, Tregs, total $CD8^+$ T cells and OVA-specific $CD8^+$ T cells in the tumour and adjacent pancreas of mice shown in A. (C) CD44 and PD-1 expression on OT-I $CD8^+$ T cells and non-OT-I $CD8^+$ T cells in the tumour and adjacent pancreas. (D) Quantification of total $CD8^+$ T cells and OVA-specific $CD8^+$ T cells and their expression of CD44 and PD-1 in the pancreatic LN. Error bars indicate mean ± SEM. The following tests were used to determine statistical significance: one-way ANOVA with Tukey's multiple

comparisons test in A and two-way ANOVA with Šídák's multiple comparison in B, C and D (with the exception of $CD8^+$ T cell and OT-I $CD8^+$ T cell quantification in D, in which an unpaired two-tailed t test was used) * $P < 0.05$, ** $P < 0.01$, *** $P < 0.001$.

To address the question of whether 2838c3-OVA tumours are able to elicit an endogenous OVA-specific $CD8^+$ T cell response and (if so) determine the kinetics of this process, $CD8^+$ T cells in the pancreatic LN and spleen were characterized 7, 14 and 21 days post-implantation of 2838c3-OVA tumours in WT mice. While total $CD45^+$ immune cell and $CD8^+$ T cell numbers in the pLN were similar between sham and day 7 post-implantation, there was a clear increase in these cells at day 14, which remained consistent until day 21 (**Figure 4.9a**). The same trend was observed with OVA-specific $CD8^+$ T cells, where there was a large increase from day 7 to day 14. OVA-specific $CD8^+$ T cells were also detected in the spleen, and there was similarly a significant increase in their numbers between day 7 and day 14 (**Figure 4.9b**). Histological analysis of tumour and adjacent pancreas from these mice show a clear increase in intratumoural $CD8^+$ T cells from day 7 to day 14 and 21 post-implantation, whereas there were no significant changes in intratumoural $Foxp3^+$ cell density across all timepoints (**Figure 4.9c**). These data therefore suggest that a $CD8^+$ T cell response to 2838c3-OVA tumours require more than a week to establish, and the kinetics of their appearance is synchronized across the tumour, pLN and spleen.

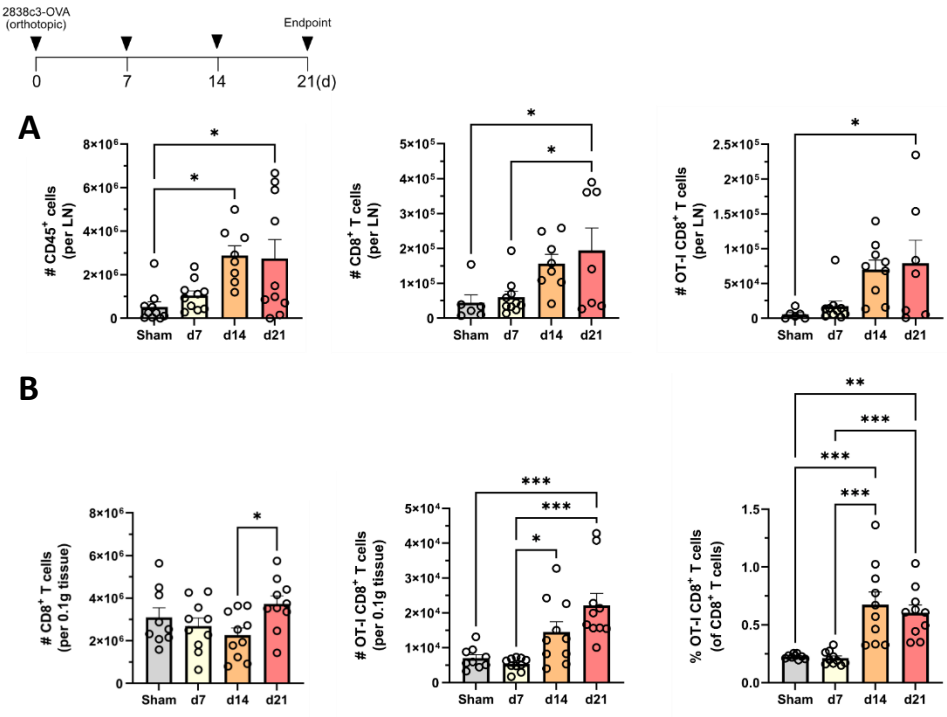

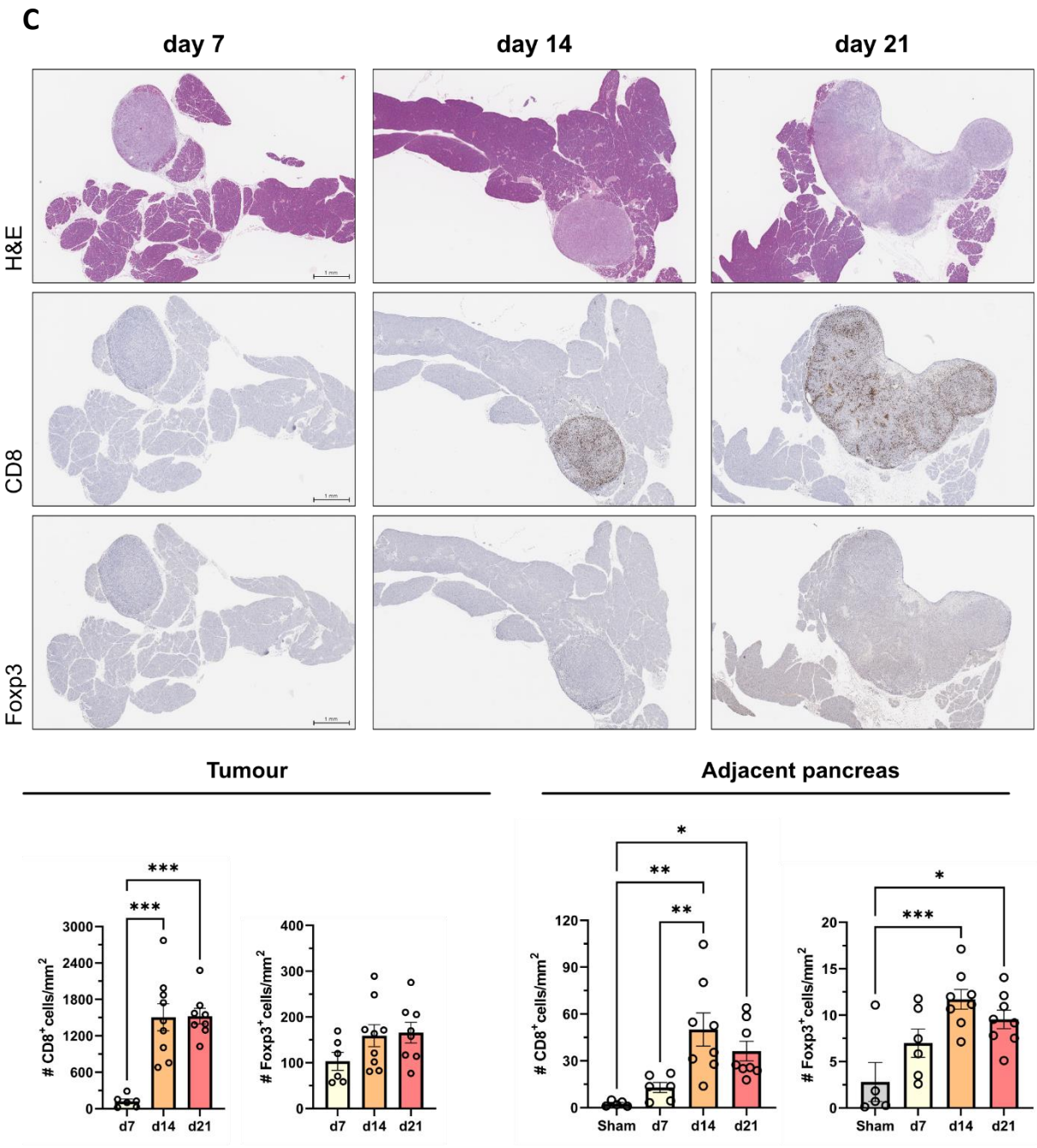

Figure 4.9. Characterizing the kinetics of tumour-specific CD8⁺ T cell development in the 2838c3-OVA model. Quantification of CD8⁺ T cells in the (A) pancreatic LN and (B) spleen of C57BL/6 mice at days 7, 14 and 21 post-implantation of 2838c3-OVA tumour cells. (C, top) Representative images showing H&E, CD8 IHC and Foxp3 IHC staining of tumour and adjacent pancreas in C57BL/6 mice at 7, 14 and 21 days post-implantation, (bottom) and quantification of CD8⁺ and Foxp3⁺ cells in these slides. Data are pooled from two independent experiments, and error bars indicate mean ± SEM. One-way ANOVA with Tukey's multiple comparisons test was used to determine statistical significance. * $P < 0.05$, ** $P < 0.01$, *** $P < 0.001$.

To determine if the absence of ILC2s has an impact on the development of an anti-tumour $CD8^+$ T cell response, 2838c3-OVA tumours were implanted in ILC2-deficient and control mice. As with the parental 2838c3 model, ILC2-deficient mice had a lower tumour burden compared to control mice at 21 days post-implantation (**Figure 4.10a**). However, given the exceedingly small tumours (~10 mg) and the low incidence of these tumours in ILC2-deficient mice, there was insufficient material for immunophenotyping. Flow cytometry analysis of $CD8^+$ T cells in the pancreatic LN at days 7 and 14 post-implantation revealed no differences in the abundance of total $CD8^+$ T cells or OVA-specific $CD8^+$ T cells between both timepoints, nor was there any difference between ILC2-deficient and control mice at each timepoint (**Figure 4.10b**). In the spleen, total $CD8^+$ T cell abundance was consistent across both timepoints and mouse models but there was an increase in OT-I $CD8^+$ T cells from day 7 to day 14 in both models, similar to that previously observed in C57BL/6 mice (**Figure 4.10c**). Several markers were used to assess the functional state of these $CD8^+$ T cells (e.g. CD44, PD-1, CD39, TCF-1 etc.) but none of these markers showed an ILC2-dependent shift (data not shown). Changes in $CD8^+$ T cell and $Foxp3^+$ Treg abundance within the tumour and adjacent pancreas were also similar to the trend observed in C57BL/6 mice - intratumoural $CD8^+$ T cells increased from day 7 to day 14 post-implantation, along with an increase in $CD8^+$ T cells and $Foxp3^+$ Tregs in the adjacent pancreas (**Figure 4.10d**). There was however no difference in the density of $CD8^+$ T cells or $Foxp3^+$ Tregs in the tumour or adjacent pancreas between both models. ILC2s therefore do not significantly modulate the rate at which an anti-tumour $CD8^+$ T cell response develops, nor does it change the abundance of tumour-specific $CD8^+$ T cells in the tumour, pLN and spleen within the first two weeks post-implantation.

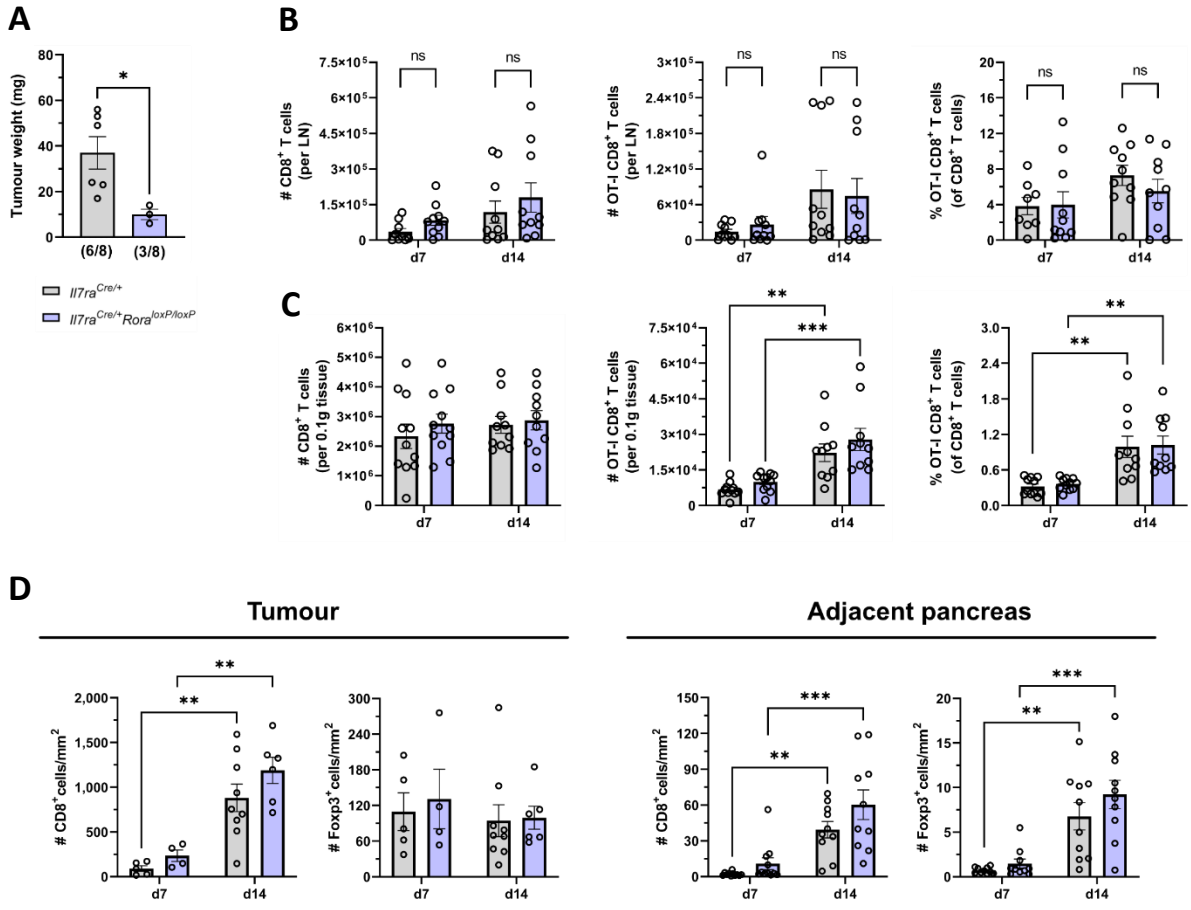

Figure 4.10. Kinetics of tumour-specific CD8⁺ T cell development are unaffected in the absence of ILC2s. (A) Tumour weights at day 21 post-implantation of orthotopic 2838c3-OVA tumours in ILC2-deficient (*Il7ra*$^{Cre/+}$*Rora*$^{loxP/loxP}$) and control (*Il7ra*$^{Cre/+}$) mice. Numbers in brackets indicate the number of mice with macroscopically visible tumours at endpoint/total number of mice in the group. Quantification of total CD8⁺ T cells and OVA-specific CD8⁺ T cells in the (B) pancreatic LN and (C) spleen of ILC2-deficient and control mice at days 7 and 14 post-implantation of 2838c3-OVA tumour cells. (D) Quantification of CD8⁺ cells and Foxp3⁺ cells in the tumour and adjacent pancreas of mice shown in B and C via immunohistochemistry. Data are pooled from two independent experiments, and error bars indicate mean ± SEM. The following tests were used to determine statistical significance: unpaired two-tailed t test in A and two-way ANOVA with Šídák's multiple comparison test in B, C and D. ** $P < 0.01$, *** $P < 0.001$.

4.9 Differential effect of ILC2 loss on different PDAC models

As 2838c3 tumours are known to have higher levels of intratumoural T cell infiltration compared to other mouse models of PDAC, another PDAC model (T69a PDAC organoids) was used to confirm the pro-tumourigenic role of ILC2s. However, the survival advantage of ILC2-deficient mice observed with the 2838c3 tumour model was not observed in the T69a tumour model (**Figure 4.11a**). Endpoint T69a tumours were taken for histological analysis, and H&E staining showed that T69a tumour cells were more differentiated and organized into duct-like structures compared to 2838c3 tumour cells (**Figure 4.11b**). Additionally, there was a significantly lower infiltration of $CD8^+$ and $Foxp3^+$ cells into T69a tumours compared to 2838c3 tumours. Given the potential of ILC2s to influence tumour growth via suppression of $CD8^+$ T cell responses, this 10-fold difference in $CD8^+$ T cell infiltration between tumour models may underlie the differential effect of ILC2 loss on tumour burden.

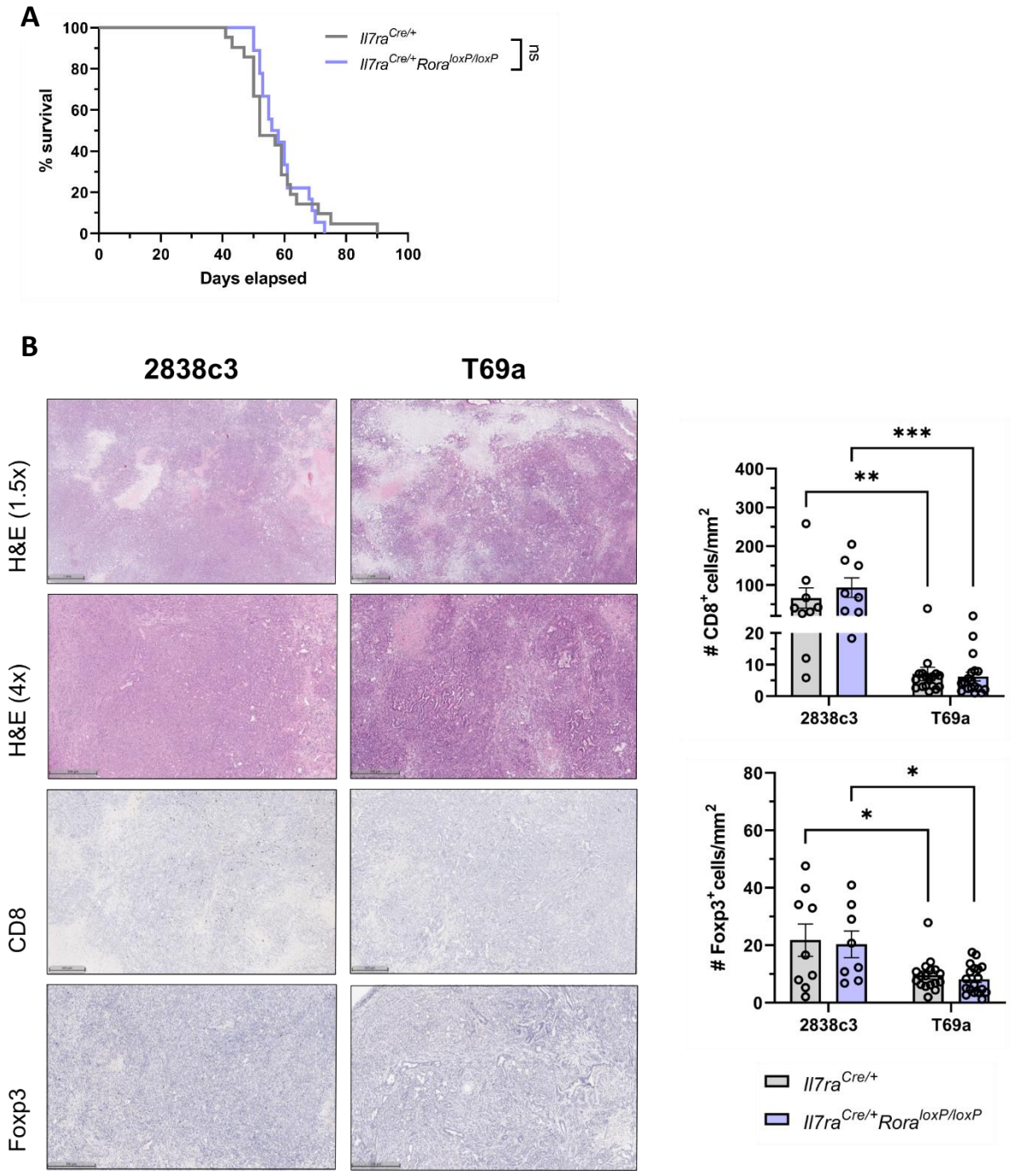

Figure 4.11. Genetic ablation of ILC2 does not affect survival of T69a-bearing mice. T69a tumour cells were orthotopically implanted into the mouse pancreas. (A) Survival of tumour-bearing ILC2-deficient (*Il7ra*$^{Cre/+}$*Rora*$^{loxP/loxP}$, n = 18) and control (*Il7ra*$^{Cre/+}$, n = 21) mice. (B, left) Representative images and (right) quantification of CD8$^+$ cells and Foxp3$^+$ cells in endpoint 2838c3 and T69a tumours. Data are pooled from two independent experiments, and error bars indicate mean ± SEM. The following tests were used to determine statistical significance: log-rank test in A and two-way ANOVA with Šídák's multiple comparison test in B. * P < 0.05, ** P < 0.01, *** P < 0.001.

Discussion

ILC2s are tissue-resident cells that act as key mediators of type 2 immunity, and previous studies have attributed ILC2s with both pro- and anti-tumourigenic roles in PDAC. My experiments in this chapter describes the pro-tumourigenic role of ILC2s in PDAC and my attempts to uncover the mechanism(s) underlying this observation.

4.10. Impact of ILC2 deletion on intratumoural and pancreatic immune cell infiltration

ILC2 deletion led to a reduction in total intratumoural immune infiltrate, including a reduced frequency of myeloid cells and total Tregs that is driven by the decrease of $GATA3^-$ Tregs. Given the known role of ILC2s in supporting Th2 and $GATA3^+$ Treg expansion[272], there was also an expected decrease in pancreatic Th2 and $GATA3^+$ Tregs, but this trend was surprisingly inverted in the tumour. ILC2 and Th2 cells are known to function cooperatively to promote type 2 inflammation, and to the best of my knowledge there are no previously characterized setting where ILC2s and Th2 cells are regulated in an opposite manner. One plausible explanation might be that the decrease of ILC2s and other ST2-expressing myeloid cells in the tumours of ILC2-deficient mice (e.g. macrophages[321], dendritic cells[322,323] and neutrophils[324]) resulted in an excess of tumour cell-derived IL-33 within the tumour microenvironment. As Th2 and $GATA3^+$ Tregs both express high levels of the IL-33 receptor ST2, upregulation of IL-33 signalling in these cells could promote their expansion within the tumour[325,326]. This paradoxical expansion of intratumoural type 2 immunity in ILC2-deficient mice could mean that the anti-tumour effect observed in ILC2-deficient mice is driven by type 2 immunity – however, prior studies that describe the anti-tumour functions of type 2 immunity are relatively sparse. In a mouse model of breast cancer, inhibition of TGF-β signalling in $CD4^+$ T cells led to IL-4-dependent vascular remodelling within the tumour, resulting in tumour cell hypoxia and death[327]. The authors noted a distinct, clustered pattern of tumour cell death that can be observed via histological cleaved caspase-3 (CC3) staining, but my ILC2-deficient tumour samples from both early and survival endpoints do not show a similar CC3 distribution pattern. Some studies cite IL-5-dependent eosinophilia as the primary mechanism of type 2 immunity-mediated anti-tumour response, but my experiments with PDAC-bearing eosinophil-deficient mice did not show any difference in survival compared to WT mice[304,328]. Type 2 inflammation is also known to induce the skewing of tumour-associated macrophages into an M2 phenotype, and M2 macrophages have been shown to induce tumour regression

via arginase production in a mouse model of myeloma[329]. However, this is unlikely to be applicable in PDAC as the pro-tumourigenic role of M2 macrophages in PDAC is well known and M2 macrophages are already the most abundant immune cell type in the PDAC TME[46].

Aside from the changes in Th2 and GATA3$^+$ Tregs, there was also a significant decrease in intratumoural myeloid cells in ILC2-deficient mice, including macrophages and neutrophils. ILC2-derived IL-13 is known to attract and activate intratumoural MDSCs in other cancer types[292], but the ILC2-IL13-MDSC axis is likely not the primary mechanism underlying the pro-tumourigenic role of ILC2s in my model as 2838c3-bearing IL-13-deficient mice did not show any difference in survival compared to WT mice. Neutrophils and macrophages are known to strongly suppress CD8$^+$ T cell responses in PDAC[46,59], and their decrease in ILC2-deficient tumours, combined with the decrease in GATA3$^-$ Tregs, could potentially result in a stronger CD8$^+$ T cell-mediated anti-tumour response. However, flow cytometry and histological analysis of tumour, adjacent pancreas and pancreatic LN did not show any increases in CD8$^+$ T cell abundance regardless of the timepoints assessed. Perhaps CD8$^+$ T cell function, rather than abundance, is enhanced in ILC2-deficient mice – in this regard, evaluating the functional status of intratumoural CD8$^+$ T cells in terms of cytokine production or gene expression would have been very informative. There was also a clear increase in NK1.1$^+$ cells within the pancreas and tumour of ILC2-deficient mice, but it is not known if these are NK cells or ILC1s as my panel did not include markers capable of separating the two (e.g. Eomes). Regardless, the increase in NK cells/ILC1 might contribute to the enhanced anti-tumour response in ILC2-deficient mice given that NK cell function is suppressed in PDAC and ILC2s have been shown to suppress NK cell function in the context of cancer[290,300,330]. Although NK cell depletion in tumour-bearing WT mice did not significantly extend survival, perhaps doing so in an ILC2-deficient setting would have had a bigger impact on survival.

4.11. Role of OX40-OX40L signalling in the regulation of pancreatic and intratumoural Tregs

Investigation into the ILC2-OX40L-Treg axis showed that ILC2s do not promote PDAC tumour growth via OX40L-mediated Treg/Th2 expansion. In ILC2-targeted OX40L cKO mice, changes in Th2 and GATA3$^+$ Treg frequency within the pancreas is similar to that observed in ILC2-deficient mice (which is a decrease in both subsets), but there was no inversion of this trend

in the tumour of ILC2-OX40L cKO mice. It is intriguing to consider if the observed increase in GATA3$^+$ Treg and Th2 in the tumour is related to, or indeed required for an effect on tumour growth. One caveat to consider is the deletion of OX40L on other *Il7ra*-expressing cells such as CD4$^+$ T cells, ILC3s and specific subsets of DCs in *Il7ra*^{Cre}*Tnfsf4*$^{fl/fl}$ mice. To control for the deletion of OX40L on these other subsets, other mouse models of OX40L deletion (more specifically, DCs: *Itgax*^{Cre}*Tnfsf4*$^{fl/fl}$, ILC3s: *Rorc*$^{Cre/+}$*Tnfsf4*$^{fl/fl}$ and CD4$^+$ T cells: *Cd4*$^{Cre/+}$*Tnfsf4*$^{fl/fl}$) could have been used. On the flip side, Foxp3-targeted deletion of OX40 also did not result in any changes in tumour burden. The role of OX40 on Tregs is highly multifaceted and context-dependent – OX40 signalling can either promote or suppress Treg responses depending on their origin (thymic/natural Tregs or peripheral/inducible Tregs), location (lymphoid or peripheral tissue-resident) and other signals present in their microenvironment[331–333]. OX40 is constitutively expressed on lymphoid-resident Tregs, whereas conventional CD4$^+$ and CD8$^+$ T cells only upregulate OX40 transiently upon TCR engagement[334]. Histological analysis of survival endpoint tumours in Foxp3-OX40 cKO mice did not show any difference in total Treg density, but perhaps similar to ILC2-deficient mice, any differences in Treg infiltration at an early timepoint is lost at a late timepoint. Given the crucial role of OX40 signalling in the expansion of tissue-resident GATA3$^+$ Tregs, it would be interesting to assess changes in the relative proportions of GATA3$^+$ and GATA3$^-$ Tregs in the tumour and adjacent pancreas in these mice at an early timepoint and determine if these changes mirror those observed in ILC2-deficient or ILC2-OX40L cKO mice. Regardless of GATA3 expression, Tregs as a whole clearly have a pro-tumourigenic role in the 2838c3 model as Treg depletion significantly decreased tumour burden. In light of the decrease of total Tregs in ILC2-deficient tumours, perhaps ILC2s are promoting tumour growth via the recruitment/expansion of intratumoural Tregs in an OX40L-independent manner.

4.12. Potential mechanisms underlying the pro-tumourigenic role of ILC2s in PDAC

Investigation into a wide range of potential cytokines and cell types underlying the pro-tumourigenic role of ILC2s (i.e. IL-33, IL-13, eosinophils, NK cells and the ILC2-OX40L-Treg axis) did not yield any positive results, although it is clear that they modulate tumour growth via adaptive immunity. CD8$^+$ T cell depletion abrogated the extended survival of tumour-bearing ILC2-deficient mice, indicating that ILC2s influence tumour growth via CD8$^+$ T cell suppression,

although comparison with $CD8^+$ T cell-depleted control mice also revealed a $CD8^+$ T cell-independent mechanism.

Given the pro-tumourigenic role of IL-33 in PDAC[291,313], it was surprising to see that 2838c3 tumour growth was unaffected in the absence (IL33KO) or excess (exogenous supplementation) of IL-33. It is possible that IL-33 was still present in the tumour microenvironment of IL-33-deficient mice given that tumour cells can be a source of IL-33[123,291]. Perhaps there would have been a reduction in tumour growth if IL-33 was also deleted from the implanted tumour cells, although unpublished data produced by a previous PhD student in the lab showed no difference in survival between KC and IL-33-deficient KC mice, which corroborate my results. On the other hand, the study by Moral et al described the anti-tumourigenic role of ILC2s in PDAC and suggested recombinant IL-33 injection as a potential treatment[73]. In this study, they show that IL-33-dependent activation of ILC2s promote intratumoural cDC1 recruitment via CCL5 production, and this results in a stronger $CD8^+$ T cell-dependent anti-tumour response. In my experiments, there was indeed a decrease in intratumoural cDC1 in ILC2-deficient tumours, although there was also a concurrent decrease in $CD8^+$ T cells. Exogenous IL-33 supplementation also failed to increase intratumoural $CD8^+$ T cell infiltration in WT mice, although the dose and schedule of IL-33 injections that I used is significantly different compared to those used in Moral et al's experiments.

Taken together, it seems that ILC2-mediated suppression of $CD8^+$ T cells is the most likely explanation for the pro-tumourigenic role of ILC2s in the 2838c3 model. If true, this would represent a novel mechanism by which $CD8^+$ T cell-dependent anti-tumour immunity is regulated by ILC2s. I have however been unable to obtain direct evidence to support this claim, primarily due to the difficulty of obtaining sufficient tumour material from early-stage tumours (21 days post-implantation) for downstream analysis. Although late-stage tumours would provide more material for analysis, early-stage tumours were used for two reasons: first, a difference in intratumoural $Foxp3^+$ Treg infiltration between ILC2-deficient and control mice was only observed at day 21 (**Figure 4.3b**). When allowed to progress to endpoint, there is no longer a difference in intratumoural Treg density between both groups (**Figure 4.11b**). Second, mice enrolled in survival studies are regularly checked for palpable tumours in the

abdomen, and when one is found (usually around 30 days for WT mice) they are then transferred onto a watchlist for enhanced monitoring of clinical signs. In all survival studies involving ILC2-deficient mice (or indeed, all studies presented in chapter 4), mice put on the watchlist are never taken off again – that is, tumours do not grow to a palpable size then regress. Instead, it is likely that ILC2s exert their effect early after tumour implantation to influence whether a palpable tumour will form and progress to endpoint, or if the tumour will be rejected before reaching a sizable mass. This suggests that important events are happening early after tumour implantation and waiting to sample tumours at a later stage might mean missing any significant observations. Indeed, a robust $CD8^+$ T cell response against 2838c3 tumours develops within 14 days, and tumours sampled at this timepoint are already highly infiltrated with $CD8^+$ T cells. To work with limited tumour material, techniques that allow for high-dimensional analysis of relatively low number of cells (e.g. scRNA-seq) would be useful to narrow down the scope of subsequent experiments and focus on relevant pathways.

At this point it is also important to consider the caveats of using *Il7ra*$^{Cre/+}$*Rora*$^{fl/fl}$ mice as an ILC2-deficient model. RORα plays a crucial role in ILC2 development and thus *Il7ra*-targeted deletion of RORα efficiently ablates ILC2s[335,336]. However, there is accumulating evidence to show that RORα also has important roles in other *Il7ra*-expressing immune cells. Among $CD4^+$ T cells, RORα was previously thought to be specifically expressed in RORγt$^+$ Th17 cells[337], but recent evidence now show that RORα expression can be detected in all subsets of activated T helper cells (i.e. GATA3$^+$ Th2 cells, T-bet$^+$ Th1 cells and RORγt$^+$ Th17 cells) and Foxp3$^+$ Tregs[338,339]. The function of RORα in Th17 cells is especially well characterized, where it is co-expressed with RORγt and they function synergistically to promote Th17 differentiation and effector function[337]. Loss of RORα in $CD4^+$ T cells therefore impairs Th17 differentiation and cytokine production, and these mice are protected from experimental colitis[340]. Additionally, RORα expression in $CD4^+$ T cells can be extrinsically regulated by cytokines and chemokines such as IL-33, IL-6 and SDF1a (CXCL12) – these mediators are known to be overexpressed in the PDAC TME, and the impact of these mediators on RORα expression and effector function in intratumoural T helper cells is lost in *Il7ra*$^{Cre/+}$*Rora*$^{fl/fl}$ mice[339]. Importantly, Th17 cells and IL-17A have clearly-defined, pro-tumourigenic roles in PDAC, and a decrease in tumour burden in *Il7ra*$^{Cre/+}$*Rora*$^{fl/fl}$ mice may simply be due to loss of Th17 function[72,88]. In addition to $CD4^+$ T cells, RORα is also expressed in all ILC subsets and has a role in regulating the

development and function of these cells[341–343]. Notably, RORα deletion in ILC3s led to impaired production of IL-17A and IL-22 in ILC3s, and this correlated with diminished pathology in a mouse model of Crohn's disease[344]. In a mouse model of CRC liver metastasis, Nkp46-targeted deletion of RORα impaired the effector function of liver-resident NK cells/ILC1s and accelerated tumour progression[345]. It is therefore clear that *Il7ra*-targeted deletion of RORα not only depletes ILC2s but also has far-reaching consequences on other immune cells. In light of this, additional experiments are necessary to control for this effect. The *Cd4*$^{Cre/+}$*Rora*$^{fl/fl}$ model can act as a control to exclude the impact of RORα loss on all CD4$^+$ T cells, whereas co-implantation of tumour cells and ILC2s in *Il7ra*$^{Cre/+}$*Rora*$^{fl/fl}$ mice helps determine if the anti-tumour effect is indeed ILC2-dependent. Having access to other ILC2-deficient mouse models would be useful, but there are no mouse models that specifically ablate ILC2 without affecting other cell types – for example, *Cd4*$^{Cre/+}$*Icos*$^{fl\text{-}Dtr/+}$ mice allows for the DT-mediated depletion of ICOS-expressing ILC2s, but ILC3s can also express ICOS[346]. There are also models that deplete ILC2s by targeting their effector cytokines (e.g. *Il5*$^{fl\text{-}DTR}$ *Lck*^{Cre} mice), but Th2 cells are also depleted in these models as they share expression of type 2 cytokines.

4.13. Differential effect of ILC2 deficiency in different PDAC models

Tumour cell-intrinsic factors play a critical role in determining intratumoural immune cell infiltration and function in PDAC, which consequently affects tumour growth kinetics and response to therapy[123,223,224]. The 2838c3 PDAC cell line is part of a library of PDAC cell clones generated by the Stanger lab, and it is one of the 'T cell high' clones, which, as its name suggests, is relatively highly infiltrated by CD3$^+$ T cells[123]. Together with the 'T cell low' clones in the library (e.g. 6419c5, described in chapter 3), they represent the heterogeneity of immune cell infiltration observed in human PDAC. While the loss of ILC2s in the 2838c3 model confers significant survival benefit, this was not observed in the T69a model. Given the strong possibility that ILC2s exert an effect on tumour growth by suppressing CD8$^+$ T cells, it is likely that the difference in intratumoural CD8$^+$ T cell infiltration between the two models underlies this differential effect of ILC2 loss. 2838c3 tumours elicit a strong CD8$^+$ T cell response at baseline, and this response is important in suppressing tumour growth as CD8$^+$ T cell depletion decreased the survival of 2838c3-bearing mice. However, this is not true for all PDAC models - KPC tumours are poorly infiltrated by CD8$^+$ T cells, and CD8$^+$ T cell depletion in

these mice do not have an impact on survival[347]. T69a tumours likely resemble KPC tumours in lacking a robust $CD8^+$ T cell response at baseline. Removal of ILC2-dependent suppression therefore becomes irrelevant in this model and would not have an impact on tumour burden.

In conclusion, ILC2 deletion significantly extends the survival of 2838c3-bearing mice and alters the intratumoural immune infiltrate, including changes in Treg subsets, Th2, $CD8^+$ T cell and myeloid cell populations. Attempts to pinpoint the mechanism(s) underlying the pro-tumourigenic role of ILC2s (i.e. IL-33, IL-13, eosinophils, NK cells and the ILC2-OX40L-Treg axis) did not yield any positive results, although it is clear that they modulate tumour growth via an effect on adaptive immunity. Further experiments involving $CD8^+$ T cell depletion in ILC2-deficient mice revealed that ILC2s influence tumour growth via both $CD8^+$ T cell-dependent and independent mechanisms. Using the 2838c3-OVA model, an anti-tumour $CD8^+$ T cell response was found to be established within 14 days post-implantation, although ILC2 deletion did not change the abundance of tumour-specific $CD8^+$ T cells in the tumour, pLN and spleen in this timeframe. Finally, the impact of ILC2 deletion on PDAC tumour growth was found to be dependent on tumour cell-intrinsic factors, possibly on those that dictate the strength of the baseline anti-tumour $CD8^+$ T cell response.

CHAPTER FIVE: Conclusion

In summary, results in chapter 3 show that Gem/ATRi has an imunostimulatory effect on DCs in PDAC but the extent of activation is dependent on multiple factors, including the specific DC subset and PDAC model in question. Gem/ATRi also depletes intratumoural $CD8^+$ T cells, but of the remaining population there is a smaller proportion of exhausted cells and a larger population of proliferating cells. The abundance of intratumoural $CD4^+$ T cells are however unchanged by Gem/ATRi therapy – this might reflect a fundamental difference in the way that $CD8^+$ and $CD4^+$ T cell populations are regulated in the tumour, be it through intratumoural proliferation or extratumoural recruitment. The initial aim of this project was to determine whether Gem/ATRi can potentially be combined with ICPI for enhanced preclinical efficacy – with currently available data, it is difficult to provide a conclusive answer as Gem/ATRi has shown contrasting effects on the PDAC TME. While it has an immunostimulatory effect on DCs, data regarding the downstream impact of DC activation on adaptive anti-tumour immunity is lacking. As the ATRiUM trial is currently ongoing, analysis of matched pre- and post-treatment tumour samples will provide invaluable insight on the impact of Gem/ATRi on anti-tumour immunity in PDAC.

In chapter 4, I demonstrated the pro-tumourigenic role of ILC2s in PDAC and investigated multiple mechanisms that potentially underlie this observation. ILC2 deletion significantly alters the intratumoural immune infiltrate, including changes in Treg, Th2, $CD8^+$ T cell and myeloid cell populations. Each of these cell types have been shown in different settings to modulate PDAC tumour growth, which makes it difficult to pin down the driving mechanism underlying the pro-tumourigenic role of ILC2s. ILC2-mediated suppression of $CD8^+$ T cells seems to be the most likely candidate, although more experiments are required to substantiate this hypothesis. Results from both chapters also showcased the powerful influence of tumour-intrinsic factors in modulating anti-tumour immunity in PDAC - these factors determined if intratumoural cDC1s will be rendered dysfunctional and unresponsive to stimulation, and if the presence (or absence) of ILC2s will have a significant impact on tumour growth.

There are currently no approved anticancer therapies that specifically target helper ILCs in the clinic, although their shared expression of co-inhibitory molecules with T cells could render them susceptible to modulation by ICPI[304,306]. Given that there are no known agents that can specifically ablate ILC2s *in vivo*, potential therapies that inhibit the pro-tumourigenic role of ILC2s will have to block their effector function (e.g. anti-IL-5 antibodies). There are small molecules that selectively inhibit RORα activity, but the safety profile of these molecules are not known and they are likely to have many off target effects, given the broad expression pattern of RORα[340,348]. Strategies that disrupt ILC2 function in PDAC will likely have to be used in combination with other therapies that enhance the $CD8^+$ T cell response, given the lack of effect of ILC2 deletion on a PDAC model with low $CD8^+$ T cell infiltration. Stratification of patients may also be required to identify patients that have higher $CD8^+$ T cell infiltration at baseline – however, the boundaries that define a 'high' level of $CD8^+$ T cell remains to be established.

Given the key role of ILCs in modulating anti-tumour immunity in a wide range of cancers, therapeutic targeting of ILCs may represent the next generation of immunotherapies. Much of the research on helper ILCs in the past 2 decades have been performed in academia, but recent insights into the novel mechanisms by which ILCs can shape anticancer immunity are starting to garner interest in the pharmaceutical industry - hopefully this will accelerate the development of novel therapeutic modalities that exploit ILC biology for cancer therapy.

REFERENCES

1. Hackeng, W. M., Hruban, R. H., Offerhaus, G. J. A. & Brosens, L. A. A. Surgical and molecular pathology of pancreatic neoplasms. *Diagn. Pathol.* **11**, 47 (2016).
2. Siegel, R. L., Miller, K. D. & Jemal, A. Cancer statistics, 2019. *CA Cancer J. Clin.* **69**, 7–34 (2019).
3. Rahib, L. *et al.* Projecting cancer incidence and deaths to 2030: the unexpected burden of thyroid, liver, and pancreas cancers in the United States. *Cancer Res.* **74**, 2913–2921 (2014).
4. Hruban, R. H., Canto, M. I., Goggins, M., Schulick, R. & Klein, A. P. Update on familial pancreatic cancer. *Adv. Surg.* **44**, 293–311 (2010).
5. Quaresma, M., Coleman, M. P. & Rachet, B. 40-year trends in an index of survival for all cancers combined and survival adjusted for age and sex for each cancer in England and Wales, 1971-2011: a population-based study. *Lancet* **385**, 1206–1218 (2015).
6. Kleeff, J. *et al.* Pancreatic cancer. *Nat Rev Dis Primers* **2**, 16022 (2016).
7. Dal Molin, M. *et al.* Very Long-term Survival Following Resection for Pancreatic Cancer Is Not Explained by Commonly Mutated Genes: Results of Whole-Exome Sequencing Analysis. *Clin. Cancer Res.* **21**, 1944–1950 (2015).
8. Burris, H. A., 3rd *et al.* Improvements in survival and clinical benefit with gemcitabine as first-line therapy for patients with advanced pancreas cancer: a randomized trial. *J. Clin. Oncol.* **15**, 2403–2413 (1997).
9. Conroy, T. *et al.* FOLFIRINOX versus gemcitabine for metastatic pancreatic cancer. *N. Engl. J. Med.* **364**, 1817–1825 (2011).
10. Von Hoff, D. D. *et al.* Increased Survival in Pancreatic Cancer with nab-Paclitaxel plus Gemcitabine. *N. Engl. J. Med.* **369**, 1691–1703 (2013).
11. Hruban, R. H., Goggins, M., Parsons, J. & Kern, S. E. Progression Model for Pancreatic Cancer. *Clin. Cancer Res.* **6**, 2969–2972 (2000).

12. Yachida, S. *et al.* Distant metastasis occurs late during the genetic evolution of pancreatic cancer. *Nature* **467**, 1114–1117 (2010).
13. Notta, F. *et al.* A renewed model of pancreatic cancer evolution based on genomic rearrangement patterns. *Nature* **538**, 378–382 (2016).
14. Witkiewicz, A. K. *et al.* Whole-exome sequencing of pancreatic cancer defines genetic diversity and therapeutic targets. *Nat. Commun.* **6**, 6744 (2015).
15. Forbes, S. A. *et al.* COSMIC: somatic cancer genetics at high-resolution. *Nucleic Acids Res.* **45**, D777–D783 (2017).
16. Hunter, J. C. *et al.* Biochemical and structural analysis of common cancer-associated KRAS mutations. *Mol. Cancer Res.* **13**, 1325–1335 (2015).
17. Alvarado-Ortiz, E. *et al.* Mutant p53 Gain-of-Function: Role in Cancer Development, Progression, and Therapeutic Approaches. *Front Cell Dev Biol* **8**, 607670 (2020).
18. Kim, M. P. & Lozano, G. Mutant p53 partners in crime. *Cell Death Differ.* **25**, 161–168 (2018).
19. Ghosh, M. *et al.* Mutant p53 suppresses innate immune signaling to promote tumorigenesis. *Cancer Cell* **39**, 494-508.e5 (2021).
20. Doyle, A. *et al.* The impact of CDKN2A mutations on overall survival in pancreatic adenocarcinoma. *J. Clin. Orthod.* **37**, 278–278 (2019).
21. Schutte, M. *et al.* Abrogation of the Rb/p16 tumor-suppressive pathway in virtually all pancreatic carcinomas. *Cancer Res.* **57**, 3126–3130 (1997).
22. Xia, X. *et al.* SMAD4 and its role in pancreatic cancer. *Tumour Biol.* **36**, 111–119 (2015).
23. Jones, S. *et al.* Core signaling pathways in human pancreatic cancers revealed by global genomic analyses. *Science* **321**, 1801–1806 (2008).
24. Collisson, E. A. *et al.* Subtypes of pancreatic ductal adenocarcinoma and their differing responses to therapy. *Nat. Med.* **17**, 500–503 (2011).
25. Moffitt, R. A. *et al.* Virtual microdissection identifies distinct tumor- and stroma-specific subtypes of pancreatic ductal adenocarcinoma. *Nat. Genet.* **47**, 1168–1178 (2015).

26. Bailey, P. *et al.* Genomic analyses identify molecular subtypes of pancreatic cancer. *Nature* **531**, 47–52 (2016).

27. Linder, S., Castaños-Velez, E., von Rosen, A. & Biberfeld, P. Immunohistochemical expression of extracellular matrix proteins and adhesion molecules in pancreatic carcinoma. *Hepatogastroenterology* **48**, 1321–1327 (2001).

28. Biffi, G. & Tuveson, D. A. Diversity and Biology of Cancer-Associated Fibroblasts. *Physiol. Rev.* **101**, 147–176 (2021).

29. Du, W., Pasca di Magliano, M. & Zhang, Y. Therapeutic Potential of Targeting Stromal Crosstalk-Mediated Immune Suppression in Pancreatic Cancer. *Front. Oncol.* **11**, 682217 (2021).

30. Elyada, E. *et al.* Cross-Species Single-Cell Analysis of Pancreatic Ductal Adenocarcinoma Reveals Antigen-Presenting Cancer-Associated Fibroblasts. *Cancer Discov.* **9**, 1102–1123 (2019).

31. Feig, C. *et al.* Targeting CXCL12 from FAP-expressing carcinoma-associated fibroblasts synergizes with anti-PD-L1 immunotherapy in pancreatic cancer. *Proc. Natl. Acad. Sci. U. S. A.* **110**, 20212–20217 (2013).

32. Wang, Z. *et al.* Carcinomas assemble a filamentous CXCL12-keratin-19 coating that suppresses T cell-mediated immune attack. *Proc. Natl. Acad. Sci. U. S. A.* **119**, (2022).

33. Biasci, D. *et al.* CXCR4 inhibition in human pancreatic and colorectal cancers induces an integrated immune response. *Proc. Natl. Acad. Sci. U. S. A.* **117**, 28960–28970 (2020).

34. Rhim, A. D. *et al.* Stromal elements act to restrain, rather than support, pancreatic ductal adenocarcinoma. *Cancer Cell* **25**, 735–747 (2014).

35. Özdemir, B. C. *et al.* Depletion of carcinoma-associated fibroblasts and fibrosis induces immunosuppression and accelerates pancreas cancer with reduced survival. *Cancer Cell* **25**, 719–734 (2014).

36. Biffi, G. *et al.* IL1-Induced JAK/STAT Signaling Is Antagonized by TGFβ to Shape CAF Heterogeneity in Pancreatic Ductal Adenocarcinoma. *Cancer Discov.* **9**, 282–301 (2019).

37. Huang, H. *et al.* Mesothelial cell-derived antigen-presenting cancer-associated fibroblasts induce expansion of regulatory T cells in pancreatic cancer. *Cancer Cell* **0**, (2022).

38. Ramanathan, R. K. *et al.* Phase IB/II Randomized Study of FOLFIRINOX Plus Pegylated Recombinant Human Hyaluronidase Versus FOLFIRINOX Alone in Patients With Metastatic Pancreatic Adenocarcinoma: SWOG S1313. *J. Clin. Oncol.* **37**, 1062–1069 (2019).

39. Van Cutsem, E. *et al.* Randomized Phase III Trial of Pegvorhyaluronidase Alfa With Nab-Paclitaxel Plus Gemcitabine for Patients With Hyaluronan-High Metastatic Pancreatic Adenocarcinoma. *J. Clin. Oncol.* **38**, 3185–3194 (2020).

40. Kindler, H. L. *et al.* Gemcitabine plus bevacizumab compared with gemcitabine plus placebo in patients with advanced pancreatic cancer: phase III trial of the Cancer and Leukemia Group B (CALGB 80303). *J. Clin. Oncol.* **28**, 3617–3622 (2010).

41. Kindler, H. L. *et al.* Axitinib plus gemcitabine versus placebo plus gemcitabine in patients with advanced pancreatic adenocarcinoma: a double-blind randomised phase 3 study. *Lancet Oncol.* **12**, 256–262 (2011).

42. Catenacci, D. V. T. *et al.* Randomized Phase Ib/II Study of Gemcitabine Plus Placebo or Vismodegib, a Hedgehog Pathway Inhibitor, in Patients With Metastatic Pancreatic Cancer. *J. Clin. Oncol.* **33**, 4284–4292 (2015).

43. De Jesus-Acosta, A. *et al.* Phase 2 study of vismodegib, a hedgehog inhibitor, combined with gemcitabine and nab-paclitaxel in patients with untreated metastatic pancreatic adenocarcinoma. *Br. J. Cancer* **122**, 498–505 (2020).

44. Hosein, A. N., Brekken, R. A. & Maitra, A. Pancreatic cancer stroma: an update on therapeutic targeting strategies. *Nat. Rev. Gastroenterol. Hepatol.* **17**, 487–505 (2020).

45. Joyce, J. A. & Fearon, D. T. T cell exclusion, immune privilege, and the tumor microenvironment. *Science* **348**, 74–80 (2015).

46. Poh, A. R. & Ernst, M. Tumor-Associated Macrophages in Pancreatic Ductal Adenocarcinoma: Therapeutic Opportunities and Clinical Challenges. *Cancers* **13**, (2021).

47. Yu, M. *et al.* Prognostic value of tumor-associated macrophages in pancreatic cancer: a meta-analysis. *Cancer Manag. Res.* **11**, 4041–4058 (2019).

48. Zhu, Y. *et al.* Tissue-Resident Macrophages in Pancreatic Ductal Adenocarcinoma Originate from Embryonic Hematopoiesis and Promote Tumor Progression. *Immunity* **47**, 323-338 e6 (2017).

49. Sanford, D. E. *et al.* Inflammatory monocyte mobilization decreases patient survival in pancreatic cancer: a role for targeting the CCL2/CCR2 axis. *Clin. Cancer Res.* **19**, 3404–3415 (2013).

50. Murray, P. J. *et al.* Macrophage activation and polarization: nomenclature and experimental guidelines. *Immunity* **41**, 14–20 (2014).

51. Beatty, G. L. *et al.* CD40 agonists alter tumor stroma and show efficacy against pancreatic carcinoma in mice and humans. *Science* **331**, 1612–1616 (2011).

52. Mitchem, J. B. *et al.* Targeting tumor-infiltrating macrophages decreases tumor-initiating cells, relieves immunosuppression, and improves chemotherapeutic responses. *Cancer Res.* **73**, 1128–1141 (2013).

53. Zhu, Y. *et al.* CSF1/CSF1R blockade reprograms tumor-infiltrating macrophages and improves response to T-cell checkpoint immunotherapy in pancreatic cancer models. *Cancer Res.* **74**, 5057–5069 (2014).

54. Papadopoulos, K. P. *et al.* First-in-Human Study of AMG 820, a Monoclonal Anti-Colony-Stimulating Factor 1 Receptor Antibody, in Patients with Advanced Solid Tumors. *Clin. Cancer Res.* **23**, 5703–5710 (2017).

55. Machiels, J.-P. *et al.* Phase Ib study of anti-CSF-1R antibody emactuzumab in combination with CD40 agonist selicrelumab in advanced solid tumor patients. *J Immunother Cancer* **8**, (2020).

56. Bayne, L. J. *et al.* Tumor-derived granulocyte-macrophage colony-stimulating factor regulates myeloid inflammation and T cell immunity in pancreatic cancer. *Cancer Cell* **21**, 822–835 (2012).

57. Pylayeva-Gupta, Y., Lee, K. E., Hajdu, C. H., Miller, G. & Bar-Sagi, D. Oncogenic Kras-induced GM-CSF production promotes the development of pancreatic neoplasia. *Cancer Cell* **21**, 836–847 (2012).

58. Steele, C. W. *et al.* CXCR2 Inhibition Profoundly Suppresses Metastases and Augments Immunotherapy in Pancreatic Ductal Adenocarcinoma. *Cancer Cell* **29**, 832–845 (2016).

59. Chao, T., Furth, E. E. & Vonderheide, R. H. CXCR2-Dependent Accumulation of Tumor-Associated Neutrophils Regulates T-cell Immunity in Pancreatic Ductal Adenocarcinoma. *Cancer Immunol Res* **4**, 968–982 (2016).

60. Dunne, R. F. *et al.* A phase I study to evaluate the safety and tolerability of SX-682 in combination with PD-1 inhibitor as maintenance therapy for unresectable pancreatic adenocarcinoma. *J. Clin. Orthod.* **40**, TPS631–TPS631 (2022).

61. Panni, R. Z. *et al.* Agonism of CD11b reprograms innate immunity to sensitize pancreatic cancer to immunotherapies. *Sci. Transl. Med.* **11**, (2019).

62. DeNardo, D. G., Galkin, A., Dupont, J., Zhou, L. & Bendell, J. GB1275, a first-in-class CD11b modulator: rationale for immunotherapeutic combinations in solid tumors. *J Immunother Cancer* **9**, (2021).

63. Plesca, I. *et al.* Clinical Significance of Tumor-Infiltrating Conventional and Plasmacytoid Dendritic Cells in Pancreatic Ductal Adenocarcinoma. *Cancers* **14**, (2022).

64. Allen, B. M. *et al.* Systemic dysfunction and plasticity of the immune macroenvironment in cancer models. *Nat. Med.* **26**, 1125–1134 (2020).

65. Tjomsland, V. *et al.* Semi mature blood dendritic cells exist in patients with ductal pancreatic adenocarcinoma owing to inflammatory factors released from the tumor. *PLoS One* **5**, e13441 (2010).

66. Meyer, M. A. *et al.* Breast and pancreatic cancer interrupt IRF8-dependent dendritic cell development to overcome immune surveillance. *Nat. Commun.* **9**, 1250 (2018).

67. Lin, J. H. *et al.* Type 1 conventional dendritic cells are systemically dysregulated early in pancreatic carcinogenesis. *J. Exp. Med.* **217**, (2020).

68. Barilla, R. M. *et al.* Specialized dendritic cells induce tumor-promoting IL-10(+)IL-17(+) FoxP3(neg) regulatory CD4(+) T cells in pancreatic carcinoma. *Nat. Commun.* **10**, 1424 (2019).

69. Bellone, G. *et al.* Cooperative induction of a tolerogenic dendritic cell phenotype by cytokines secreted by pancreatic carcinoma cells. *J. Immunol.* **177**, 3448–3460 (2006).

70. Jang, J.-E. *et al.* Crosstalk between Regulatory T Cells and Tumor-Associated Dendritic Cells Negates Anti-tumor Immunity in Pancreatic Cancer. *Cell Rep.* **20**, 558–571 (2017).

71. Kenkel, J. A. *et al.* An Immunosuppressive Dendritic Cell Subset Accumulates at Secondary Sites and Promotes Metastasis in Pancreatic Cancer. *Cancer Res.* **77**, 4158–4170 (2017).

72. Hegde, S. *et al.* Dendritic Cell Paucity Leads to Dysfunctional Immune Surveillance in Pancreatic Cancer. *Cancer Cell* **37**, 289-307.e9 (2020).

73. Moral, J. A. *et al.* ILC2s amplify PD-1 blockade by activating tissue-specific cancer immunity. *Nature* **579**, 130–135 (2020).

74. Ma, D. Y. & Clark, E. A. The role of CD40 and CD154/CD40L in dendritic cells. *Semin. Immunol.* **21**, 265–272 (2009).

75. Ghislat, G. *et al.* NF-κB-dependent IRF1 activation programs cDC1 dendritic cells to drive antitumor immunity. *Sci Immunol* **6**, (2021).

76. Beatty, G. L. *et al.* A phase I study of an agonist CD40 monoclonal antibody (CP-870,893) in combination with gemcitabine in patients with advanced pancreatic ductal adenocarcinoma. *Clin. Cancer Res.* **19**, 6286–6295 (2013).

77. Winograd, R. *et al.* Induction of T-cell Immunity Overcomes Complete Resistance to PD-1 and CTLA-4 Blockade and Improves Survival in Pancreatic Carcinoma. *Cancer Immunol Res* **3**, 399–411 (2015).

78. Byrne, K. T., Leisenring, N. H., Bajor, D. L. & Vonderheide, R. H. CSF-1R-Dependent Lethal Hepatotoxicity When Agonistic CD40 Antibody Is Given before but Not after Chemotherapy. *J. Immunol.* **197**, 179–187 (2016).

79. Byrne, K. T. & Vonderheide, R. H. CD40 Stimulation Obviates Innate Sensors and Drives T Cell Immunity in Cancer. *Cell Rep.* **15**, 2719–2732 (2016).

80. Morrison, A. H., Diamond, M. S., Hay, C. A., Byrne, K. T. & Vonderheide, R. H. Sufficiency of CD40 activation and immune checkpoint blockade for T cell priming and tumor immunity. *Proc. Natl. Acad. Sci. U. S. A.* **117**, 8022–8031 (2020).

81. Byrne, K. T. *et al.* Neoadjuvant Selicrelumab, an Agonist CD40 Antibody, Induces Changes in the Tumor Microenvironment in Patients with Resectable Pancreatic Cancer. *Clin. Cancer Res.* **27**, 4574–4586 (2021).

82. O'Hara, M. H. *et al.* CD40 agonistic monoclonal antibody APX005M (sotigalimab) and chemotherapy, with or without nivolumab, for the treatment of metastatic pancreatic adenocarcinoma: an open-label, multicentre, phase 1b study. *Lancet Oncol.* **22**, 118–131 (2021).

83. Padrón, L. J. *et al.* Sotigalimab and/or nivolumab with chemotherapy in first-line metastatic pancreatic cancer: clinical and immunologic analyses from the randomized phase 2 PRINCE trial. *Nat. Med.* **28**, 1167–1177 (2022).

84. Togashi, Y., Shitara, K. & Nishikawa, H. Regulatory T cells in cancer immunosuppression - implications for anticancer therapy. *Nat. Rev. Clin. Oncol.* **16**, 356–371 (2019).

85. Orhan, A. *et al.* The prognostic value of tumour-infiltrating lymphocytes in pancreatic cancer: a systematic review and meta-analysis. *Eur. J. Cancer* **132**, 71–84 (2020).

86. Tan, M. C. B. *et al.* Disruption of CCR5-dependent homing of regulatory T cells inhibits tumor growth in a murine model of pancreatic cancer. *J. Immunol.* **182**, 1746–1755 (2009).

87. Zhang, Y. *et al.* Regulatory T-cell Depletion Alters the Tumor Microenvironment and Accelerates Pancreatic Carcinogenesis. *Cancer Discov.* **10**, 422–439 (2020).

88. McAllister, F. *et al.* Oncogenic Kras activates a hematopoietic-to-epithelial IL-17 signaling axis in preinvasive pancreatic neoplasia. *Cancer Cell* **25**, 621–637 (2014).

89. Zhang, Y. *et al.* Immune Cell Production of Interleukin 17 Induces Stem Cell Features of Pancreatic Intraepithelial Neoplasia Cells. *Gastroenterology* **155**, 210-223.e3 (2018).

90. Zhang, Y. *et al.* Interleukin-17-induced neutrophil extracellular traps mediate resistance to checkpoint blockade in pancreatic cancer. *J. Exp. Med.* **217**, (2020).

91. Mucciolo, G. *et al.* IL17A critically shapes the transcriptional program of fibroblasts in pancreatic cancer and switches on their protumorigenic functions. *Proc. Natl. Acad. Sci. U. S. A.* **118**, (2021).

92. Vannucci, L. Stroma as an Active Player in the Development of the Tumor Microenvironment. *Cancer Microenviron.* **8**, 159–166 (2015).

93. Klose, C. S. & Artis, D. Innate lymphoid cells as regulators of immunity, inflammation and tissue homeostasis. *Nat. Immunol.* **17**, 765–774 (2016).

94. Brouwer, T. P. *et al.* Local and systemic immune profiles of human pancreatic ductal adenocarcinoma revealed by single-cell mass cytometry. *J Immunother Cancer* **10**, (2022).

95. Xuan, X. *et al.* ILC3 cells promote the proliferation and invasion of pancreatic cancer cells through IL-22/AKT signaling. *Clin. Transl. Oncol.* **22**, 563–575 (2020).

96. Masugi, Y. *et al.* Characterization of spatial distribution of tumor-infiltrating CD8+ T cells refines their prognostic utility for pancreatic cancer survival. *Mod. Pathol.* **32**, 1495–1507 (2019).

97. Liudahl, S. M. *et al.* Leukocyte Heterogeneity in Pancreatic Ductal Adenocarcinoma: Phenotypic and Spatial Features Associated with Clinical Outcome. *Cancer Discov.* **11**, 2014–2031 (2021).

98. Fukunaga, A. *et al.* CD8+ tumor-infiltrating lymphocytes together with CD4+ tumor-infiltrating lymphocytes and dendritic cells improve the prognosis of patients with pancreatic adenocarcinoma. *Pancreas* **28**, e26-31 (2004).

99. Carstens, J. L. *et al.* Spatial computation of intratumoral T cells correlates with survival of patients with pancreatic cancer. *Nat. Commun.* **8**, 15095 (2017).

100. Hodi, F. S. *et al.* Improved survival with ipilimumab in patients with metastatic melanoma. *N. Engl. J. Med.* **363**, 711–723 (2010).

101. Royal, R. E. *et al.* Phase 2 trial of single agent Ipilimumab (anti-CTLA-4) for locally advanced or metastatic pancreatic adenocarcinoma. *J. Immunother.* **33**, 828–833 (2010).

102. Le, D. T. *et al.* Mismatch repair deficiency predicts response of solid tumors to PD-1 blockade. *Science* **357**, 409–413 (2017).

103. Daud, A. I. *et al.* Tumor immune profiling predicts response to anti-PD-1 therapy in human melanoma. *J. Clin. Invest.* **126**, 3447–3452 (2016).

104. Banchereau, R. *et al.* Intratumoral CD103+ CD8+ T cells predict response to PD-L1 blockade. *J Immunother Cancer* **9**, (2021).

105. Watson, R. A. *et al.* Immune checkpoint blockade sensitivity and progression-free survival associates with baseline $CD8^+$ T cell clone size and cytotoxicity. *Sci Immunol* **6**, eabj8825 (2021).

106. Huang, T. *et al.* Prognostic Role of Tumor Mutational Burden in Cancer Patients Treated With Immune Checkpoint Inhibitors: A Systematic Review and Meta-Analysis. *Front. Oncol.* **11**, 706652 (2021).

107. Samstein, R. M. *et al.* Tumor mutational load predicts survival after immunotherapy across multiple cancer types. *Nat. Genet.* **51**, 202–206 (2019).

108. Yarchoan, M., Hopkins, A. & Jaffee, E. M. Tumor Mutational Burden and Response Rate to PD-1 Inhibition. *N. Engl. J. Med.* **377**, 2500–2501 (2017).

109. McGranahan, N. *et al.* Clonal neoantigens elicit T cell immunoreactivity and sensitivity to immune checkpoint blockade. *Science* **351**, 1463–1469 (2016).

110. Alexandrov, L. B. *et al.* Signatures of mutational processes in human cancer. *Nature* **500**, 415–421 (2013).

111. Bailey, P. *et al.* Exploiting the neoantigen landscape for immunotherapy of pancreatic ductal adenocarcinoma. *Sci. Rep.* **6**, 35848 (2016).

112. Hingorani, S. R. *et al.* Trp53R172H and KrasG12D cooperate to promote chromosomal instability and widely metastatic pancreatic ductal adenocarcinoma in mice. *Cancer Cell* **7**, 469–483 (2005).

113. Pan, F. C. & Wright, C. Pancreas organogenesis: from bud to plexus to gland. *Dev. Dyn.* **240**, 530–565 (2011).

114. Westphalen, C. B. & Olive, K. P. Genetically engineered mouse models of pancreatic cancer. *Cancer J.* **18**, 502–510 (2012).

115. Mazur, P. K. *et al.* Identification of epidermal Pdx1 expression discloses different roles of Notch1 and Notch2 in murine Kras(G12D)-induced skin carcinogenesis in vivo. *PLoS One* **5**, e13578 (2010).

116. Hingorani, S. R. *et al.* Preinvasive and invasive ductal pancreatic cancer and its early detection in the mouse. *Cancer Cell* **4**, 437–450 (2003).

117. Yang, J. *et al.* Dynamic profiling of immune microenvironment during pancreatic cancer development suggests early intervention and combination strategy of immunotherapy. *EBioMedicine* **78**, 103958 (2022).

118. D'Costa, Z. *et al.* Gemcitabine-Induced TIMP1 Attenuates Therapy Response and Promotes Tumor Growth and Liver Metastasis in Pancreatic Cancer. *Cancer Res.* **77**, 5952–5962 (2017).

119. Mazur, P. K. & Siveke, J. T. Genetically engineered mouse models of pancreatic cancer: unravelling tumour biology and progressing translational oncology. *Gut* **61**, 1488–1500 (2012).

120. Zhan, B. *et al.* Identification and causes of metabonomic difference between orthotopic and subcutaneous xenograft of pancreatic cancer. *Oncotarget* **8**, 61264–61281 (2017).

121. Erstad, D. J. *et al.* Orthotopic and heterotopic murine models of pancreatic cancer and their different responses to FOLFIRINOX chemotherapy. *Dis. Model. Mech.* **11**, (2018).

122. Kettler, B., Trauzold, A., Röder, C., Egberts, J.-H. & Kalthoff, H. Topology impacts TRAIL therapy: Differences in primary cancer growth and liver metastasis between orthotopic and

subcutaneous xenotransplants of pancreatic ductal adenocarcinoma cells. *Hepatobiliary Pancreat. Dis. Int* **20**, 279–284 (2021).

123. Li, J. *et al.* Tumor Cell-Intrinsic Factors Underlie Heterogeneity of Immune Cell Infiltration and Response to Immunotherapy. *Immunity* **49**, 178-193.e7 (2018).
124. Olive, K. P. *et al.* Inhibition of Hedgehog signaling enhances delivery of chemotherapy in a mouse model of pancreatic cancer. *Science* **324**, 1457–1461 (2009).
125. Oni, T. E. *et al.* SOAT1 promotes mevalonate pathway dependency in pancreatic cancer. *J. Exp. Med.* **217**, (2020).
126. Mayer, C. T. *et al.* Selective and efficient generation of functional Batf3-dependent CD103+ dendritic cells from mouse bone marrow. *Blood* **124**, 3081–3091 (2014).
127. Naviaux, R. K., Costanzi, E., Haas, M. & Verma, I. M. The pCL vector system: rapid production of helper-free, high-titer, recombinant retroviruses. *J. Virol.* **70**, 5701–5705 (1996).
128. Dobin, A. *et al.* STAR: ultrafast universal RNA-seq aligner. *Bioinformatics* **29**, 15–21 (2013).
129. Liao, Y., Smyth, G. K. & Shi, W. The Subread aligner: fast, accurate and scalable read mapping by seed-and-vote. *Nucleic Acids Res.* **41**, e108 (2013).
130. Love, M. I., Huber, W. & Anders, S. Moderated estimation of fold change and dispersion for RNA-seq data with DESeq2. *Genome Biol.* **15**, 550 (2014).
131. Subramanian, A. *et al.* Gene set enrichment analysis: a knowledge-based approach for interpreting genome-wide expression profiles. *Proc. Natl. Acad. Sci. U. S. A.* **102**, 15545–15550 (2005).
132. Pishesha, N., Harmand, T. J. & Ploegh, H. L. A guide to antigen processing and presentation. *Nat. Rev. Immunol.* 1–14 (2022).
133. Lafferty, K. J. & Cunningham, A. J. A new analysis of allogeneic interactions. *Aust. J. Exp. Biol. Med. Sci.* **53**, 27–42 (1975).
134. Steinman, R. M. & Cohn, Z. A. Identification of a novel cell type in peripheral lymphoid organs of mice. I. Morphology, quantitation, tissue distribution. *J. Exp. Med.* **137**, 1142–1162 (1973).

135. Segura, E. & Amigorena, S. Inflammatory dendritic cells in mice and humans. *Trends Immunol.* **34**, 440–445 (2013).

136. León, B., López-Bravo, M. & Ardavín, C. Monocyte-derived dendritic cells formed at the infection site control the induction of protective T helper 1 responses against Leishmania. *Immunity* **26**, 519–531 (2007).

137. Cisse, B. *et al.* Transcription factor E2-2 is an essential and specific regulator of plasmacytoid dendritic cell development. *Cell* **135**, 37–48 (2008).

138. Gilliet, M., Cao, W. & Liu, Y.-J. Plasmacytoid dendritic cells: sensing nucleic acids in viral infection and autoimmune diseases. *Nat. Rev. Immunol.* **8**, 594–606 (2008).

139. Treilleux, I. *et al.* Dendritic cell infiltration and prognosis of early stage breast cancer. *Clin. Cancer Res.* **10**, 7466–7474 (2004).

140. Munn, D. H. *et al.* Expression of indoleamine 2,3-dioxygenase by plasmacytoid dendritic cells in tumor-draining lymph nodes. *J. Clin. Invest.* **114**, 280–290 (2004).

141. Conrad, C. *et al.* Plasmacytoid dendritic cells promote immunosuppression in ovarian cancer via ICOS costimulation of Foxp3+ T-regulatory cells. *Cancer Res.* **72**, 5240–5249 (2012).

142. Sisirak, V. *et al.* Breast cancer-derived transforming growth factor-β and tumor necrosis factor-α compromise interferon-α production by tumor-associated plasmacytoid dendritic cells. *Int. J. Cancer* **133**, 771–778 (2013).

143. Le Mercier, I. *et al.* Tumor promotion by intratumoral plasmacytoid dendritic cells is reversed by TLR7 ligand treatment. *Cancer Res.* **73**, 4629–4640 (2013).

144. Gardner, A. & Ruffell, B. Dendritic Cells and Cancer Immunity. *Trends Immunol.* **37**, 855–865 (2016).

145. Broz, M. L. *et al.* Dissecting the tumor myeloid compartment reveals rare activating antigen-presenting cells critical for T cell immunity. *Cancer Cell* **26**, 638–652 (2014).

146. Ahrens, S. *et al.* F-actin is an evolutionarily conserved damage-associated molecular pattern recognized by DNGR-1, a receptor for dead cells. *Immunity* **36**, 635–645 (2012).

147. Canton, J. *et al.* The receptor DNGR-1 signals for phagosomal rupture to promote cross-presentation of dead-cell-associated antigens. *Nat. Immunol.* **22**, 140–153 (2021).

148. Brown, C. C. *et al.* Transcriptional Basis of Mouse and Human Dendritic Cell Heterogeneity. *Cell* **179**, 846-863 e24 (2019).

149. Förster, R. *et al.* CCR7 coordinates the primary immune response by establishing functional microenvironments in secondary lymphoid organs. *Cell* **99**, 23–33 (1999).

150. Chen, D. S. & Mellman, I. Oncology meets immunology: the cancer-immunity cycle. *Immunity* **39**, 1–10 (2013).

151. Laoui, D. *et al.* The tumour microenvironment harbours ontogenically distinct dendritic cell populations with opposing effects on tumour immunity. *Nat. Commun.* **7**, 13720 (2016).

152. Gerhard, G. M., Bill, R., Messemaker, M., Klein, A. M. & Pittet, M. J. Tumor-infiltrating dendritic cell states are conserved across solid human cancers. *J. Exp. Med.* **218**, (2021).

153. Roberts, E. W. *et al.* Critical Role for CD103(+)/CD141(+) Dendritic Cells Bearing CCR7 for Tumor Antigen Trafficking and Priming of T Cell Immunity in Melanoma. *Cancer Cell* **30**, 324–336 (2016).

154. Salmon, H. *et al.* Expansion and Activation of CD103(+) Dendritic Cell Progenitors at the Tumor Site Enhances Tumor Responses to Therapeutic PD-L1 and BRAF Inhibition. *Immunity* **44**, 924–938 (2016).

155. Spranger, S., Dai, D., Horton, B. & Gajewski, T. F. Tumor-Residing Batf3 Dendritic Cells Are Required for Effector T Cell Trafficking and Adoptive T Cell Therapy. *Cancer Cell* **31**, 711-723 e4 (2017).

156. Mikucki, M. E. *et al.* Non-redundant requirement for CXCR3 signalling during tumoricidal T-cell trafficking across tumour vascular checkpoints. *Nat. Commun.* **6**, 7458 (2015).

157. Chow, M. T. *et al.* Intratumoral Activity of the CXCR3 Chemokine System Is Required for the Efficacy of Anti-PD-1 Therapy. *Immunity* **50**, 1498-1512.e5 (2019).

158. Sánchez-Paulete, A. R. *et al.* Cancer Immunotherapy with Immunomodulatory Anti-CD137 and Anti–PD-1 Monoclonal Antibodies Requires BATF3-Dependent Dendritic Cells. *Cancer Discov.* **6**, 71–79 (2016).

159. Garris, C. S. *et al.* Successful Anti-PD-1 Cancer Immunotherapy Requires T Cell-Dendritic Cell Crosstalk Involving the Cytokines IFN-gamma and IL-12. *Immunity* (2018) doi:10.1016/j.immuni.2018.09.024.

160. Barry, K. C. *et al.* A natural killer-dendritic cell axis defines checkpoint therapy-responsive tumor microenvironments. *Nat. Med.* **24**, 1178–1191 (2018).

161. Bottcher, J. P. & Reis, E. S. C. The Role of Type 1 Conventional Dendritic Cells in Cancer Immunity. *Trends Cancer Res.* **4**, 784–792 (2018).

162. Saxena, M. & Bhardwaj, N. Re-Emergence of Dendritic Cell Vaccines for Cancer Treatment. *Trends Cancer Res.* **4**, 119–137 (2018).

163. Galluzzi, L., Buque, A., Kepp, O., Zitvogel, L. & Kroemer, G. Immunological Effects of Conventional Chemotherapy and Targeted Anticancer Agents. *Cancer Cell* **28**, 690–714 (2015).

164. Tanaka, H., Matsushima, H., Mizumoto, N. & Takashima, A. Classification of chemotherapeutic agents based on their differential in vitro effects on dendritic cells. *Cancer Res.* **69**, 6978–6986 (2009).

165. Tanaka, H., Matsushima, H., Nishibu, A., Clausen, B. E. & Takashima, A. Dual therapeutic efficacy of vinblastine as a unique chemotherapeutic agent capable of inducing dendritic cell maturation. *Cancer Res.* **69**, 6987–6994 (2009).

166. Shurin, G. V., Tourkova, I. L., Kaneno, R. & Shurin, M. R. Chemotherapeutic agents in noncytotoxic concentrations increase antigen presentation by dendritic cells via an IL-12-dependent mechanism. *J. Immunol.* **183**, 137–144 (2009).

167. Kroemer, G., Galassi, C., Zitvogel, L. & Galluzzi, L. Immunogenic cell stress and death. *Nat. Immunol.* **23**, 487–500 (2022).

168. Menger, L. *et al.* Cardiac Glycosides Exert Anticancer Effects by Inducing Immunogenic Cell Death. *Sci. Transl. Med.* **4**, 143ra99-143ra99 (2012).

169. Fumet, J.-D., Limagne, E., Thibaudin, M. & Ghiringhelli, F. Immunogenic Cell Death and Elimination of Immunosuppressive Cells: A Double-Edged Sword of Chemotherapy. *Cancers* **12**, (2020).

170. Fucikova, J. *et al.* Detection of immunogenic cell death and its relevance for cancer therapy. *Cell Death Dis.* **11**, 1013 (2020).

171. Ma, Y. *et al.* Anticancer Chemotherapy-Induced Intratumoral Recruitment and Differentiation of Antigen-Presenting Cells. *Immunity* **38**, 729–741 (2013).

172. McDonnell, A. M. *et al.* Tumor-infiltrating dendritic cells exhibit defective cross-presentation of tumor antigens, but is reversed by chemotherapy. *Eur. J. Immunol.* **45**, 49–59 (2015).

173. Liu, W. M., Fowler, D. W., Smith, P. & Dalgleish, A. G. Pre-treatment with chemotherapy can enhance the antigenicity and immunogenicity of tumours by promoting adaptive immune responses. *Br. J. Cancer* **102**, 115–123 (2010).

174. Zhou, Y. *et al.* Activation of NF-κB and p300/CBP potentiates cancer chemoimmunotherapy through induction of MHC-I antigen presentation. *Proc. Natl. Acad. Sci. U. S. A.* **118**, (2021).

175. Plate, J. M., Plate, A. E., Shott, S., Bograd, S. & Harris, J. E. Effect of gemcitabine on immune cells in subjects with adenocarcinoma of the pancreas. *Cancer Immunol. Immunother.* **54**, 915–925 (2005).

176. Eriksson, E., Wenthe, J., Irenaeus, S., Loskog, A. & Ullenhag, G. Gemcitabine reduces MDSCs, tregs and TGFβ-1 while restoring the teff/treg ratio in patients with pancreatic cancer. *J. Transl. Med.* **14**, 282 (2016).

177. Suzuki, E., Kapoor, V., Jassar, A. S., Kaiser, L. R. & Albelda, S. M. Gemcitabine selectively eliminates splenic Gr-1+/CD11b+ myeloid suppressor cells in tumor-bearing animals and enhances antitumor immune activity. *Clin. Cancer Res.* **11**, 6713–6721 (2005).

178. Kan, S. *et al.* Suppressive effects of cyclophosphamide and gemcitabine on regulatory T-cell induction in vitro. *Anticancer Res.* **32**, 5363–5369 (2012).

179. Shevchenko, I. *et al.* Low-dose gemcitabine depletes regulatory T cells and improves survival in the orthotopic Panc02 model of pancreatic cancer. *Int. J. Cancer* **133**, 98–107 (2013).

180. Hartlova, A. *et al.* DNA damage primes the type I interferon system via the cytosolic DNA sensor STING to promote anti-microbial innate immunity. *Immunity* **42**, 332–343 (2015).

181. Parkes, E. E. *et al.* Activation of STING-Dependent Innate Immune Signaling By S-Phase-Specific DNA Damage in Breast Cancer. *J. Natl. Cancer Inst.* **109**, (2017).

182. Sen, T. *et al.* Targeting DNA Damage Response Promotes Antitumor Immunity through STING-Mediated T-cell Activation in Small Cell Lung Cancer. *Cancer Discov.* **9**, 646–661 (2019).

183. Zhang, Q. *et al.* Inhibition of ATM increases interferon signaling and sensitizes pancreatic cancer to immune checkpoint blockade therapy. *Cancer Res.* canres.0761.2019 (2019).

184. Chen, J. *et al.* Cell Cycle Checkpoints Cooperate to Suppress DNA- and RNA-Associated Molecular Pattern Recognition and Anti-Tumor Immune Responses. *Cell Rep.* **32**, 108080 (2020).

185. Okude, H., Ori, D. & Kawai, T. Signaling Through Nucleic Acid Sensors and Their Roles in Inflammatory Diseases. *Front. Immunol.* **11**, 625833 (2020).

186. Barber, G. N. STING: infection, inflammation and cancer. *Nat. Rev. Immunol.* **15**, 760–770 (2015).

187. Dunphy, G. *et al.* Non-canonical Activation of the DNA Sensing Adaptor STING by ATM and IFI16 Mediates NF-kappaB Signaling after Nuclear DNA Damage. *Mol. Cell* **71**, 745-760 e5 (2018).

188. Kwon, J. & Bakhoum, S. F. The Cytosolic DNA-Sensing cGAS-STING Pathway in Cancer. *Cancer Discov.* **10**, 26–39 (2020).

189. Woo, S.-R. *et al.* STING-dependent cytosolic DNA sensing mediates innate immune recognition of immunogenic tumors. *Immunity* **41**, 830–842 (2014).

190. Corrales, L. *et al.* Direct Activation of STING in the Tumor Microenvironment Leads to Potent and Systemic Tumor Regression and Immunity. *Cell Rep.* **11**, 1018–1030 (2015).

191. Takashima, K. *et al.* STING in tumor and host cells cooperatively work for NK cell-mediated tumor growth retardation. *Biochem. Biophys. Res. Commun.* **478**, 1764–1771 (2016).

192. Wang, F. *et al.* Tumour sensitization via the extended intratumoural release of a STING agonist and camptothecin from a self-assembled hydrogel. *Nat Biomed Eng* **4**, 1090–1101 (2020).

193. Jing, W. *et al.* STING agonist inflames the pancreatic cancer immune microenvironment and reduces tumor burden in mouse models. *J Immunother Cancer* **7**, 115 (2019).

194. Vonderhaar, E. P. *et al.* STING Activated Tumor-Intrinsic Type I Interferon Signaling Promotes CXCR3 Dependent Antitumor Immunity in Pancreatic Cancer. *Cell Mol Gastroenterol Hepatol* **12**, 41–58 (2021).

195. Ager, C. R. *et al.* High potency STING agonists engage unique myeloid pathways to reverse pancreatic cancer immune privilege. *J Immunother Cancer* **9**, (2021).

196. Montoya, M. *et al.* Type I interferons produced by dendritic cells promote their phenotypic and functional activation. *Blood* **99**, 3263–3271 (2002).

197. Cauwels, A. *et al.* Delivering Type I Interferon to Dendritic Cells Empowers Tumor Eradication and Immune Combination Treatments. *Cancer Res.* **78**, 463–474 (2018).

198. Zitvogel, L., Apetoh, L., Ghiringhelli, F. & Kroemer, G. Immunological aspects of cancer chemotherapy. *Nat. Rev. Immunol.* **8**, 59–73 (2008).

199. Langer, C. J. *et al.* Carboplatin and pemetrexed with or without pembrolizumab for advanced, non-squamous non-small-cell lung cancer: a randomised, phase 2 cohort of the open-label KEYNOTE-021 study. *Lancet Oncol.* **17**, 1497–1508 (2016).

200. Galluzzi, L., Humeau, J., Buqué, A., Zitvogel, L. & Kroemer, G. Immunostimulation with chemotherapy in the era of immune checkpoint inhibitors. *Nat. Rev. Clin. Oncol.* **17**, 725–741 (2020).

201. Wallez, Y. *et al.* The ATR Inhibitor AZD6738 Synergizes with Gemcitabine In Vitro and In Vivo to Induce Pancreatic Ductal Adenocarcinoma Regression. *Mol. Cancer Ther.* **17**, 1670–1682 (2018).

202. Dunlop, C. R. *et al.* Complete loss of ATM function augments replication catastrophe induced by ATR inhibition and gemcitabine in pancreatic cancer models. *Br. J. Cancer* **123**, 1424–1436 (2020).

203. Bain, C. C. *et al.* TGFβR signalling controls CD103+CD11b+ dendritic cell development in the intestine. *Nat. Commun.* **8**, 620 (2017).

204. Yum, S., Li, M. & Chen, Z. J. Old dogs, new trick: classic cancer therapies activate cGAS. *Cell Res.* **30**, 639–648 (2020).

205. Conlon, J. *et al.* Mouse, but not human STING, binds and signals in response to the vascular disrupting agent 5,6-dimethylxanthenone-4-acetic acid. *J. Immunol.* **190**, 5216–5225 (2013).

206. Schadt, L. *et al.* Cancer-Cell-Intrinsic cGAS Expression Mediates Tumor Immunogenicity. *Cell Rep.* **29**, 1236-1248.e7 (2019).

207. Brown, J. S., Sundar, R. & Lopez, J. Combining DNA damaging therapeutics with immunotherapy: more haste, less speed. *Br. J. Cancer* **118**, 312–324 (2018).

208. Hong, X. *et al.* Impact of 5-Fu/oxaliplatin on mouse dendritic cells and synergetic effect with a colon cancer vaccine. *Chin. J. Cancer Res.* **30**, 197–208 (2018).

209. Dudek, A. M., Martin, S., Garg, A. D. & Agostinis, P. Immature, Semi-Mature, and Fully Mature Dendritic Cells: Toward a DC-Cancer Cells Interface That Augments Anticancer Immunity. *Front. Immunol.* **4**, 438 (2013).

210. Schiavoni, G. *et al.* Cyclophosphamide synergizes with type I interferons through systemic dendritic cell reactivation and induction of immunogenic tumor apoptosis. *Cancer Res.* **71**, 768–778 (2011).

211. Fuertes Marraco, S. A. *et al.* Type I interferon drives dendritic cell apoptosis via multiple BH3-only proteins following activation by PolyIC in vivo. *PLoS One* **6**, e20189 (2011).

212. Pang, E. S. *et al.* Discordance in STING-Induced Activation and Cell Death Between Mouse and Human Dendritic Cell Populations. *Front. Immunol.* **13**, 794776 (2022).

213. Egelston, C. *et al.* Complex phenotyping of PD-1+ CD39+ exhausted CD8+ T cells in human carcinomas. *The Journal of Immunology* **200**, 57.23-57.23 (2018).

214. Leem, G. *et al.* 4-1BB co-stimulation further enhances anti-PD-1-mediated reinvigoration of exhausted CD39+ CD8 T cells from primary and metastatic sites of epithelial ovarian cancers. *J Immunother Cancer* **8**, (2020).

215. Turtle, C. J., Swanson, H. M., Fujii, N., Estey, E. H. & Riddell, S. R. A distinct subset of self-renewing human memory CD8+ T cells survives cytotoxic chemotherapy. *Immunity* **31**, 834–844 (2009).

216. Shibayama, Y. *et al.* Implication of chemo-resistant memory T cells for immune surveillance in patients with sarcoma receiving chemotherapy. *Cancer Sci.* **108**, 1739–1745 (2017).

217. Hildner, K. *et al.* Batf3 deficiency reveals a critical role for CD8alpha+ dendritic cells in cytotoxic T cell immunity. *Science* **322**, 1097–1100 (2008).

218. Jung, S. *et al.* In vivo depletion of CD11c+ dendritic cells abrogates priming of CD8+ T cells by exogenous cell-associated antigens. *Immunity* **17**, 211–220 (2002).

219. Graziano, V. *et al.* The heterogeneous distribution of extracellular adenosine reveals a myeloid-dependent axis, shaping the immunosuppressive microenvironment in pancreatic ductal adenocarcinoma. *bioRxiv* 2022.05.24.493238 (2022) doi:10.1101/2022.05.24.493238.

220. Sanchez, P. J., McWilliams, J. A., Haluszczak, C., Yagita, H. & Kedl, R. M. Combined TLR/CD40 Stimulation Mediates Potent Cellular Immunity by Regulating Dendritic Cell Expression of CD70 In Vivo. *The Journal of Immunology* **178**, 1564–1572 (2007).

221. Schenkel, J. M. *et al.* Conventional type I dendritic cells maintain a reservoir of proliferative tumor-antigen specific TCF-1+ CD8+ T cells in tumor-draining lymph nodes. *Immunity* **54**, 2338-2353.e6 (2021).

222. Wculek, S. K. *et al.* Dendritic cells in cancer immunology and immunotherapy. *Nat. Rev. Immunol.* (2019) doi:10.1038/s41577-019-0210-z.

223. Markosyan, N. *et al.* Tumor cell-intrinsic EPHA2 suppresses anti-tumor immunity by regulating PTGS2 (COX-2). *J. Clin. Invest.* **129**, 3594–3609 (2019).

224. Li, J. *et al.* Tumor Cell-Intrinsic USP22 Suppresses Antitumor Immunity in Pancreatic Cancer. *Cancer Immunol Res* **8**, 282–291 (2020).

225. Li, J. *et al.* Epigenetic and Transcriptional Control of the Epidermal Growth Factor Receptor Regulates the Tumor Immune Microenvironment in Pancreatic Cancer. *Cancer Discov.* **11**, 736–753 (2021).

226. Barbie, D. A. *et al.* Systematic RNA interference reveals that oncogenic KRAS-driven cancers require TBK1. *Nature* **462**, 108–112 (2009).

227. Cooper, J. M. *et al.* TBK1 Provides Context-Selective Support of the Activated AKT/mTOR Pathway in Lung Cancer. *Cancer Res.* **77**, 5077–5094 (2017).

228. Ludwig, K. F. *et al.* Small-Molecule Inhibition of Axl Targets Tumor Immune Suppression and Enhances Chemotherapy in Pancreatic Cancer. *Cancer Res.* **78**, 246–255 (2018).

229. Casares, N. *et al.* Caspase-dependent immunogenicity of doxorubicin-induced tumor cell death. *J. Exp. Med.* **202**, 1691–1701 (2005).

230. Apetoh, L. *et al.* Toll-like receptor 4-dependent contribution of the immune system to anticancer chemotherapy and radiotherapy. *Nat. Med.* **13**, 1050–1059 (2007).

231. Delvecchio, F. R. *et al.* Pancreatic Cancer Chemotherapy Is Potentiated by Induction of Tertiary Lymphoid Structures in Mice. *Cell Mol Gastroenterol Hepatol* **12**, 1543–1565 (2021).

232. Shin, S. B. & McNagny, K. M. ILC-You in the Thymus: A Fresh Look at Innate Lymphoid Cell Development. *Front. Immunol.* **12**, 681110 (2021).

233. Kiessling, R., Klein, E., Pross, H. & Wigzell, H. 'Natural' killer cells in the mouse. II. Cytotoxic cells with specificity for mouse Moloney leukemia cells. Characteristics of the killer cell. *Eur. J. Immunol.* **5**, 117–121 (1975).

234. Mebius, R. E., Rennert, P. & Weissman, I. L. Developing lymph nodes collect CD4+CD3- LTbeta+ cells that can differentiate to APC, NK cells, and follicular cells but not T or B cells. *Immunity* **7**, 493–504 (1997).

235. Spits, H. & Di Santo, J. P. The expanding family of innate lymphoid cells: regulators and effectors of immunity and tissue remodeling. *Nat. Immunol.* **12**, 21–27 (2011).

236. Spits, H. *et al.* Innate lymphoid cells--a proposal for uniform nomenclature. *Nat. Rev. Immunol.* **13**, 145–149 (2013).

237. Wang, S. *et al.* Regulatory Innate Lymphoid Cells Control Innate Intestinal Inflammation. *Cell* **171**, 201-216.e18 (2017).

238. Bando, J. K. *et al.* ILC2s are the predominant source of intestinal ILC-derived IL-10. *J. Exp. Med.* **217**, (2020).

239. Seehus, C. R. *et al.* Alternative activation generates IL-10 producing type 2 innate lymphoid cells. *Nat. Commun.* **8**, 1900 (2017).

240. Morita, H. *et al.* Induction of human regulatory innate lymphoid cells from group 2 innate lymphoid cells by retinoic acid. *J. Allergy Clin. Immunol.* **143**, 2190-2201.e9 (2019).

241. Artis, D. & Spits, H. The biology of innate lymphoid cells. *Nature* **517**, 293–301 (2015).

242. Lim, A. I. *et al.* Systemic Human ILC Precursors Provide a Substrate for Tissue ILC Differentiation. *Cell* **168**, 1086-1100.e10 (2017).

243. Gasteiger, G., Fan, X., Dikiy, S., Lee, S. Y. & Rudensky, A. Y. Tissue residency of innate lymphoid cells in lymphoid and nonlymphoid organs. *Science* **350**, 981–985 (2015).

244. Robinette, M. L. *et al.* Transcriptional programs define molecular characteristics of innate lymphoid cell classes and subsets. *Nat. Immunol.* **16**, 306–317 (2015).

245. Ricardo-Gonzalez, R. R. *et al.* Tissue signals imprint ILC2 identity with anticipatory function. *Nat. Immunol.* **19**, 1093–1099 (2018).

246. Simoni, Y. *et al.* Human Innate Lymphoid Cell Subsets Possess Tissue-Type Based Heterogeneity in Phenotype and Frequency. *Immunity* **46**, 148–161 (2017).

247. Mazzurana, L. *et al.* Tissue-specific transcriptional imprinting and heterogeneity in human innate lymphoid cells revealed by full-length single-cell RNA-sequencing. *Cell Res.* **31**, 554–568 (2021).

248. Dutton, E. E. *et al.* Peripheral lymph nodes contain migratory and resident innate lymphoid cell populations. *Sci Immunol* **4**, (2019).

249. Huang, Y. *et al.* IL-25-responsive, lineage-negative KLRG1(hi) cells are multipotential 'inflammatory' type 2 innate lymphoid cells. *Nat. Immunol.* **16**, 161–169 (2015).

250. Huang, Y. *et al.* S1P-dependent interorgan trafficking of group 2 innate lymphoid cells supports host defense. *Science* **359**, 114–119 (2018).

251. Ricardo-Gonzalez, R. R. *et al.* Tissue-specific pathways extrude activated ILC2s to disseminate type 2 immunity. *J. Exp. Med.* **217**, (2020).

252. Bal, S. M., Golebski, K. & Spits, H. Plasticity of innate lymphoid cell subsets. *Nat. Rev. Immunol.* **20**, 552–565 (2020).

253. Cortez, V. S. *et al.* Transforming Growth Factor-β Signaling Guides the Differentiation of Innate Lymphoid Cells in Salivary Glands. *Immunity* **44**, 1127–1139 (2016).

254. Gao, Y. *et al.* Tumor immunoevasion by the conversion of effector NK cells into type 1 innate lymphoid cells. *Nat. Immunol.* **18**, 1004–1015 (2017).

255. Koh, J. *et al.* IL23-Producing Human Lung Cancer Cells Promote Tumor Growth via Conversion of Innate Lymphoid Cell 1 (ILC1) into ILC3. *Clin. Cancer Res.* **25**, 4026–4037 (2019).

256. Wang, S. *et al.* Transdifferentiation of tumor infiltrating innate lymphoid cells during progression of colorectal cancer. *Cell Res.* **30**, 610–622 (2020).

257. Hurst, S. D. *et al.* New IL-17 family members promote Th1 or Th2 responses in the lung: in vivo function of the novel cytokine IL-25. *J. Immunol.* **169**, 443–453 (2002).

258. Fallon, P. G. *et al.* Identification of an interleukin (IL)-25-dependent cell population that provides IL-4, IL-5, and IL-13 at the onset of helminth expulsion. *J. Exp. Med.* **203**, 1105–1116 (2006).

259. Owyang, A. M. *et al.* Interleukin 25 regulates type 2 cytokine-dependent immunity and limits chronic inflammation in the gastrointestinal tract. *J. Exp. Med.* **203**, 843–849 (2006).

260. Price, A. E. *et al.* Systemically dispersed innate IL-13-expressing cells in type 2 immunity. *Proc. Natl. Acad. Sci. U. S. A.* **107**, 11489–11494 (2010).

261. Moro, K. *et al.* Innate production of T(H)2 cytokines by adipose tissue-associated c-Kit(+)Sca-1(+) lymphoid cells. *Nature* **463**, 540–544 (2010).

262. Neill, D. R. *et al.* Nuocytes represent a new innate effector leukocyte that mediates type-2 immunity. *Nature* **464**, 1367–1370 (2010).

263. Halim, T. Y. F., Krauss, R. H., Sun, A. C. & Takei, F. Lung natural helper cells are a critical source of Th2 cell-type cytokines in protease allergen-induced airway inflammation. *Immunity* **36**, 451–463 (2012).

264. Cavagnero, K. & Doherty, T. A. Cytokine and Lipid Mediator Regulation of Group 2 Innate Lymphoid Cells (ILC2s) in Human Allergic Airway Disease. *J Cytokine Biol* **2**, (2017).

265. Schuijs, M. J. & Halim, T. Y. F. Group 2 innate lymphocytes at the interface between innate and adaptive immunity. *Ann. N. Y. Acad. Sci.* **1417**, 87–103 (2018).

266. Irie, M., Sasahara, K., Artis, D. & Kabata, H. Current overview of the role of neuropeptides in ILC2s and future directions. *Allergol. Int.* **71**, 294–300 (2022).

267. Monticelli, L. A. *et al.* Innate lymphoid cells promote lung-tissue homeostasis after infection with influenza virus. *Nat. Immunol.* **12**, 1045–1054 (2011).

268. Brestoff, J. R. *et al.* Group 2 innate lymphoid cells promote beiging of white adipose tissue and limit obesity. *Nature* **519**, 242–246 (2015).

269. Golebski, K. *et al.* Induction of IL-10-producing type 2 innate lymphoid cells by allergen immunotherapy is associated with clinical response. *Immunity* **54**, 291-307.e7 (2021).

270. Oliphant, C. J. *et al.* MHCII-mediated dialog between group 2 innate lymphoid cells and CD4(+) T cells potentiates type 2 immunity and promotes parasitic helminth expulsion. *Immunity* **41**, 283–295 (2014).

271. Maazi, H. *et al.* ICOS:ICOS-ligand interaction is required for type 2 innate lymphoid cell function, homeostasis, and induction of airway hyperreactivity. *Immunity* **42**, 538–551 (2015).

272. Halim, T. Y. F. *et al.* Tissue-Restricted Adaptive Type 2 Immunity Is Orchestrated by Expression of the Costimulatory Molecule OX40L on Group 2 Innate Lymphoid Cells. *Immunity* **48**, 1195-1207.e6 (2018).

273. León, B. & Ballesteros-Tato, A. Modulating Th2 Cell Immunity for the Treatment of Asthma. *Front. Immunol.* **12**, 637948 (2021).

274. Bartemes, K. R. *et al.* IL-33-responsive lineage- CD25+ CD44(hi) lymphoid cells mediate innate type 2 immunity and allergic inflammation in the lungs. *J. Immunol.* **188**, 1503–1513 (2012).

275. Halim, T. Y. F. *et al.* Group 2 innate lymphoid cells are critical for the initiation of adaptive T helper 2 cell-mediated allergic lung inflammation. *Immunity* **40**, 425–435 (2014).

276. Halim, T. Y. F. *et al.* Group 2 innate lymphoid cells license dendritic cells to potentiate memory TH2 cell responses. *Nat. Immunol.* **17**, 57–64 (2016).

277. Mirchandani, A. S. *et al.* Type 2 innate lymphoid cells drive CD4+ Th2 cell responses. *J. Immunol.* **192**, 2442–2448 (2014).

278. Molofsky, A. B. *et al.* Innate lymphoid type 2 cells sustain visceral adipose tissue eosinophils and alternatively activated macrophages. *J. Exp. Med.* **210**, 535–549 (2013).

279. Wu, D. *et al.* Eosinophils sustain adipose alternatively activated macrophages associated with glucose homeostasis. *Science* **332**, 243–247 (2011).

280. Lee, M.-W. *et al.* Activated type 2 innate lymphoid cells regulate beige fat biogenesis. *Cell* **160**, 74–87 (2015).

281. Rana, B. M. J. *et al.* A stromal cell niche sustains ILC2-mediated type-2 conditioning in adipose tissue. *J. Exp. Med.* **216**, 1999–2009 (2019).

282. Zaiss, D. M. W., Gause, W. C., Osborne, L. C. & Artis, D. Emerging functions of amphiregulin in orchestrating immunity, inflammation, and tissue repair. *Immunity* **42**, 216–226 (2015).

283. Turner, J.-E. *et al.* IL-9-mediated survival of type 2 innate lymphoid cells promotes damage control in helminth-induced lung inflammation. *J. Exp. Med.* **210**, 2951–2965 (2013).

284. Monticelli, L. A. *et al.* IL-33 promotes an innate immune pathway of intestinal tissue protection dependent on amphiregulin-EGFR interactions. *Proc. Natl. Acad. Sci. U. S. A.* **112**, 10762–10767 (2015).

285. Cao, Q. *et al.* Potentiating Tissue-Resident Type 2 Innate Lymphoid Cells by IL-33 to Prevent Renal Ischemia-Reperfusion Injury. *J. Am. Soc. Nephrol.* **29**, 961–976 (2018).

286. Wu, J. & Lanier, L. L. Natural Killer Cells and Cancer. in *Advances in Cancer Research* vol. 90 127–156 (Academic Press, 2003).

287. Jacquelot, N., Seillet, C., Vivier, E. & Belz, G. T. Innate lymphoid cells and cancer. *Nat. Immunol.* (2022) doi:10.1038/s41590-022-01127-z.

288. Mattner, J. & Wirtz, S. Friend or Foe? The Ambiguous Role of Innate Lymphoid Cells in Cancer Development. *Trends Immunol.* **38**, 29–38 (2017).

289. Jovanovic, I. P. *et al.* Interleukin-33/ST2 axis promotes breast cancer growth and metastases by facilitating intratumoral accumulation of immunosuppressive and innate lymphoid cells. *Int. J. Cancer* **134**, 1669–1682 (2014).

290. Schuijs, M. J. *et al.* ILC2-driven innate immune checkpoint mechanism antagonizes NK cell antimetastatic function in the lung. *Nat. Immunol.* **21**, 998–1009 (2020).

291. Alam, A. *et al.* Fungal mycobiome drives IL-33 secretion and type 2 immunity in pancreatic cancer. *Cancer Cell* **40**, 153-167.e11 (2022).

292. Jou, E. *et al.* An innate IL-25–ILC2–MDSC axis creates a cancer-permissive microenvironment for *Apc* mutation–driven intestinal tumorigenesis. *Science Immunology* **7**, eabn0175 (2022).

293. Trabanelli, S. *et al.* Tumour-derived PGD2 and NKp30-B7H6 engagement drives an immunosuppressive ILC2-MDSC axis. *Nat. Commun.* **8**, 593 (2017).

294. Wu, L. *et al.* Mesenchymal PGD2 activates an ILC2-Treg axis to promote proliferation of normal and malignant HSPCs. *Leukemia* **34**, 3028–3041 (2020).

295. Ercolano, G., Falquet, M., Vanoni, G., Trabanelli, S. & Jandus, C. ILC2s: New Actors in Tumor Immunity. *Front. Immunol.* **10**, 2801 (2019).

296. Xu, X. *et al.* Group-2 Innate Lymphoid Cells Promote HCC Progression Through CXCL2-Neutrophil-Induced Immunosuppression. *Hepatology* **74**, 2526–2543 (2021).

297. Trabanelli, S. *et al.* CD127+ innate lymphoid cells are dysregulated in treatment naïve acute myeloid leukemia patients at diagnosis. *Haematologica* **100**, e257-60 (2015).

298. Chevalier, M. F. *et al.* ILC2-modulated T cell-to-MDSC balance is associated with bladder cancer recurrence. *J. Clin. Invest.* **127**, 2916–2929 (2017).

299. Pan, Y., Yu, Y., Wang, X. & Zhang, T. Tumor-Associated Macrophages in Tumor Immunity. *Front. Immunol.* **11**, 583084 (2020).

300. Long, A. *et al.* Type 2 Innate Lymphoid Cells Impede IL-33-Mediated Tumor Suppression. *J. Immunol.* **201**, 3456–3464 (2018).

301. Cao, H. *et al.* IL-13/STAT6 signaling plays a critical role in the epithelial-mesenchymal transition of colorectal cancer cells. *Oncotarget* **7**, 61183–61198 (2016).

302. Ercolano, G. *et al.* PPARɣ drives IL-33-dependent ILC2 pro-tumoral functions. *Nat. Commun.* **12**, 2538 (2021).

303. Dey, P. *et al.* Oncogenic KRAS-Driven Metabolic Reprogramming in Pancreatic Cancer Cells Utilizes Cytokines from the Tumor Microenvironment. *Cancer Discov.* **10**, 608–625 (2020).

304. Jacquelot, N. *et al.* Blockade of the co-inhibitory molecule PD-1 unleashes ILC2-dependent antitumor immunity in melanoma. *Nat. Immunol.* **22**, 851–864 (2021).

305. Wagner, M. *et al.* Tumor-Derived Lactic Acid Contributes to the Paucity of Intratumoral ILC2s. *Cell Rep.* **30**, 2743-2757.e5 (2020).

306. Howard, E. *et al.* PD-1 Blockade on Tumor Microenvironment-Resident ILC2s Promotes TNF-α Production and Restricts Progression of Metastatic Melanoma. *Front. Immunol.* **12**, 733136 (2021).

307. Kim, J. *et al.* Intratumorally Establishing Type 2 Innate Lymphoid Cells Blocks Tumor Growth. *J. Immunol.* **196**, 2410–2423 (2016).

308. Saranchova, I. *et al.* Type 2 Innate Lymphocytes Actuate Immunity Against Tumours and Limit Cancer Metastasis. *Sci. Rep.* **8**, 2924 (2018).

309. Bonilla, W. V. *et al.* The alarmin interleukin-33 drives protective antiviral $CD8^+$ T cell responses. *Science* **335**, 984–989 (2012).

310. Huang, Q. *et al.* Type 2 Innate Lymphoid Cells Protect against Colorectal Cancer Progression and Predict Improved Patient Survival. *Cancers* **13**, (2021).

311. Carrière, C., Young, A. L., Gunn, J. R., Longnecker, D. S. & Korc, M. Acute pancreatitis markedly accelerates pancreatic cancer progression in mice expressing oncogenic Kras. *Biochem. Biophys. Res. Commun.* **382**, 561–565 (2009).

312. Kempuraj, D. *et al.* The novel cytokine interleukin-33 activates acinar cell proinflammatory pathways and induces acute pancreatic inflammation in mice. *PLoS One* **8**, e56866 (2013).

313. Alonso-Curbelo, D. *et al.* A gene-environment-induced epigenetic program initiates tumorigenesis. *Nature* **590**, 642–648 (2021).

314. Donahue, K. *et al.* Abstract PO-102: Fibroblast-derived interleukin-33 promotes pancreatic ductal adenocarcinoma as a result of tumor cell KRASG12D. *Cancer Res.* **81**, PO-102 (2021).

315. Fang, Y. *et al.* IL-33 acts as a foe to MIA PaCa-2 pancreatic cancer. *Med. Oncol.* **34**, 23 (2017).

316. Takenaga, K., Akimoto, M., Koshikawa, N. & Nagase, H. Cancer cell-derived interleukin-33 decoy receptor sST2 enhances orthotopic tumor growth in a murine pancreatic cancer model. *PLoS One* **15**, e0232230 (2020).

317. Ye, L. *et al.* Hypoxia-reprogrammed regulatory group 2 innate lymphoid cells promote immunosuppression in pancreatic cancer. *EBioMedicine* **79**, 104016 (2022).

318. Riquelme, E. *et al.* Tumor Microbiome Diversity and Composition Influence Pancreatic Cancer Outcomes. *Cell* **178**, 795-806.e12 (2019).

319. Aykut, B. *et al.* The fungal mycobiome promotes pancreatic oncogenesis via activation of MBL. *Nature* **574**, 264–267 (2019).

320. Wohlfert, E. A. *et al.* GATA3 controls Foxp3^{+} regulatory T cell fate during inflammation in mice. *J. Clin. Invest.* **121**, 4503–4515 (2011).

321. Kurowska-Stolarska, M. *et al.* IL-33 amplifies the polarization of alternatively activated macrophages that contribute to airway inflammation. *J. Immunol.* **183**, 6469–6477 (2009).

322. Matta, B. M. *et al.* IL-33 is an unconventional Alarmin that stimulates IL-2 secretion by dendritic cells to selectively expand IL-33R/ST2+ regulatory T cells. *J. Immunol.* **193**, 4010–4020 (2014).

323. Rank, M. A. *et al.* IL-33-activated dendritic cells induce an atypical TH2-type response. *J. Allergy Clin. Immunol.* **123**, 1047–1054 (2009).

324. Alves-Filho, J. C. *et al.* Interleukin-33 attenuates sepsis by enhancing neutrophil influx to the site of infection. *Nat. Med.* **16**, 708–712 (2010).

325. Schiering, C. *et al.* The alarmin IL-33 promotes regulatory T-cell function in the intestine. *Nature* **513**, 564–568 (2014).

326. Alvarez, F., Fritz, J. H. & Piccirillo, C. A. Pleiotropic Effects of IL-33 on CD4+ T Cell Differentiation and Effector Functions. *Front. Immunol.* **10**, 522 (2019).

327. Liu, M. *et al.* TGF-β suppresses type 2 immunity to cancer. *Nature* **587**, 115–120 (2020).

328. Mattes, J. *et al.* Immunotherapy of cytotoxic T cell-resistant tumors by T helper 2 cells: an eotaxin and STAT6-dependent process. *J. Exp. Med.* **197**, 387–393 (2003).

329. Lorvik, K. B. *et al.* Adoptive Transfer of Tumor-Specific Th2 Cells Eradicates Tumors by Triggering an In Situ Inflammatory Immune Response. *Cancer Res.* **76**, 6864–6876 (2016).

330. Jeon, S. *et al.* Multiple defects in NK cells of surgically resectable pancreatic cancer patients can be reversed by ex-vivo stimulation. *The Journal of Immunology* **200**, 124.10-124.10 (2018).

331. Takeda, I. *et al.* Distinct roles for the OX40-OX40 ligand interaction in regulatory and nonregulatory T cells. *J. Immunol.* **172**, 3580–3589 (2004).

332. Kumar, P. *et al.* Soluble OX40L and JAG1 Induce Selective Proliferation of Functional Regulatory T-Cells Independent of canonical TCR signaling. *Sci. Rep.* **7**, 39751 (2017).

333. Zhang, X. *et al.* OX40 Costimulation Inhibits Foxp3 Expression and Treg Induction via BATF3-Dependent and Independent Mechanisms. *Cell Rep.* **24**, 607–618 (2018).

334. Vu, M. D. *et al.* OX40 costimulation turns off Foxp3+ Tregs. *Blood* **110**, 2501–2510 (2007).

335. Halim, T. Y. F. *et al.* Retinoic-acid-receptor-related orphan nuclear receptor alpha is required for natural helper cell development and allergic inflammation. *Immunity* **37**, 463–474 (2012).

336. Wong, S. H. *et al.* Transcription factor RORα is critical for nuocyte development. *Nat. Immunol.* **13**, 229–236 (2012).

337. Yang, X. O. *et al.* T helper 17 lineage differentiation is programmed by orphan nuclear receptors ROR alpha and ROR gamma. *Immunity* **28**, 29–39 (2008).

338. Malhotra, N. *et al.* RORα-expressing T regulatory cells restrain allergic skin inflammation. *Sci Immunol* **3**, (2018).

339. Haim-Vilmovsky, L. *et al.* Mapping Rora expression in resting and activated CD4+ T cells. *PLoS One* **16**, e0251233 (2021).

340. Wang, R. *et al.* Genetic and pharmacological inhibition of the nuclear receptor RORα regulates TH17 driven inflammatory disorders. *Nat. Commun.* **12**, 76 (2021).

341. Walker, J. A. *et al.* Polychromic Reporter Mice Reveal Unappreciated Innate Lymphoid Cell Progenitor Heterogeneity and Elusive ILC3 Progenitors in Bone Marrow. *Immunity* **51**, 104-118.e7 (2019).

342. Fiancette, R. *et al.* Reciprocal transcription factor networks govern tissue-resident ILC3 subset function and identity. *Nat. Immunol.* **22**, 1245–1255 (2021).

343. Stehle, C. *et al.* T-bet and RORα control lymph node formation by regulating embryonic innate lymphoid cell differentiation. *Nat. Immunol.* **22**, 1231–1244 (2021).

344. Lo, B. C. *et al.* The orphan nuclear receptor RORα and group 3 innate lymphoid cells drive fibrosis in a mouse model of Crohn's disease. *Sci Immunol* **1**, eaaf8864 (2016).

345. Song, J. *et al.* Requirement of RORα for Maintenance and Anti-Tumor Immunity of Liver-Resident Natural Killer Cells/ILC1s. *Hepatology* (2021) doi:10.1002/hep.32147.

346. Dutton, E. E. *et al.* Characterisation of innate lymphoid cell populations at different sites in mice with defective T cell immunity. *Wellcome Open Res* **2**, 117 (2017).

347. Evans, R. A. *et al.* Lack of immunoediting in murine pancreatic cancer reversed with neoantigen. *JCI Insight* **1**, (2016).

348. Kumar, N. *et al.* Identification of SR3335 (ML-176): a synthetic RORα selective inverse agonist. *ACS Chem. Biol.* **6**, 218–222 (2011).